3-26-2012

Multiuser Detection in Multiple Input Multiple Output Orthogonal Frequency Division Multiplexing Systems by Blind Signal Separation Techniques

Yu Du
Florida International University, dyu002@fiu.edu

FLORIDA INTERNATIONAL UNIVERSITY

Miami, Florida

MULTIUSER DETECTION IN MULTPLE INPUT MULTPLE OUTPUT

ORTHOGONAL FREQUENCY DIVISION MULTIPLEXING SYSTEMS BY BLIND

SIGNAL SEPARATION TECHNIQUES

A dissertation submitted in partial fulfillment of the

requirements for the degree of

DOCTOR OF PHILOSOPHY

in

ELECTRICAL ENGINEERING

by

Yu Du

2012

To: Dean Amir Mirmiran
    College of Engineering and Computing

This dissertation, written by Yu Du, and entitled Multiuser Detection in Multiple Input Multiple Output Orthogonal Frequency Division Multiplexing Systems by Blind Signal Separation Techniques, having been approved in respect to style and intellectual content, is referred to you for judgment.

We have read this dissertation and recommend that it be approved.

_____
Yimin Zhu

_____
Deng Pan

_____
Jean H. Andrian

_____
Kang K. Yen, Major Professor

Date of Defense: March 26, 2012

The dissertation of Yu Du is approved.

_____
Dean Amir Mirmiran
College of Engineering and Computing

_____
Dean Lakshmi N. Reddi
University Graduate School

Florida International University, 2012

ii

DEDICATION

I dedicate this thesis to my parents, who give me confidence and unlimited love to finish my degree.

I dedicate this thesis to my wife, who takes care of my life, loves my family and me, and supports my research.

I dedicate this thesis to my parents-in-law, who give me a beautiful and smart wife.

I dedicate this thesis to all of my relatives and friends.

The completion of this work will not be possible if I do not have support from all of you.

ACKNOWLEDGMENTS

ABSTRACT OF THE DISSERTATION

MULTIUSER DETECTION IN MULTPLE INPUT MULTPLE OUTPUT

ORTHOGONAL FREQUENCY DIVISION MULTIPLEXING SYSTEMS BY BLIND

SIGNAL SEPARATION TECHNIQUES

by

Yu Du

Florida International University, 2012

Miami, Florida

Professor Kang K. Yen, Major Professor

This dissertation introduces three novel multiuser detection approaches in
Multiple Input Multiple Output (MIMO) Orthogonal Frequency Division Multiplexing
(OFDM) systems by blind signal separation (BSS) techniques. The conventional
methodologies for multiuser detection have to retransmit channel state information (CSI)
constantly from the transmitter in MIMO ODFM systems at the cost of economic
efficiency, because they require more channel resources to improve the communication
quality. Compared with the traditional methodologies, the proposed BSS methods are
relatively efficient approaches without the unnecessary retransmission of channel state
information.

The current methodologies apply the space-time coding or the spatial
multiplexing to implement an MIMO OFDM system, which requires relatively complex
antenna design and allocation in the transmitter. The proposed Spatial Division Multiple
Access (SDMA) method enables different mobile users to share the same bandwidth
simultaneously in different geographical locations, and this scheme requires only one

antenna for each mobile user. Therefore, it greatly simplifies the antenna design and allocation.

The goal of this dissertation is to design and implement three blind multiuser detection schemes without knowing the channel state information or the channel transfer function in the SDMA-based uplink MIMO OFDM system. The proposed scenarios include: (a) the BSS-only scheme, (b) the BSS-Minimum Mean Square Error (MMSE) scheme, and (c) the BSS-Minimum Bit Error Ratio (MBER) scheme.

The major contributions of the dissertation include: (a) the three proposed schemes save the commercially expensive cost of channel resources; (b) the proposed SDMA-based uplink MIMO OFDM system simplifies the requirements of antennas for mobile users; (c) the three proposed schemes obtain high parallel computing efficiency through paralleled subcarriers; (d) the proposed BSS-MBER scheme gains the best BER performance; (e) the proposed BSS-MMSE method yields the best computational efficiency; and (f) the proposed BSS-only scenario balances the BER performance and computational complexity.

TABLE OF CONTENTS

LIST OF TABLES

LIST OF FIGURES

LIST OF ABBREVIATIONS

AM	Amplitude Modulation
AWGN	Additive White Gaussian Noise
BER	Bit Error Rate/Ratio
BPSK	Binary Phase Shift Keying
BSS	Blind Signal Separation
CIR	Channel Impulse Response
CP	Cyclic Prefix
CSI	Channel State Information
DAB	Digital Audio Broadcasting
DS-CDMA	Direct-Sequence Code Division Multiple Access
DSP	Digital Signal Processing
DFT	Discrete Fourier Transform
FastICA	Fast Independent Component Analysis
FDM	Frequency-Division Multiplexing
FDMA	Frequency Division Multiple Access
FFT	Fast Fourier Transform
FPGA	Field Programmable Gate Array
FM	Frequency Modulation
GSM	Global System for Mobile Communications
HOS	Higher-Order Statistics
ICA	Independent Component Analysis
IDFT	Inverse Discrete Fourier Transform

IEEE	Institute of Electrical and Electronics Engineers
IFFT	Inverse Fast Fourier Transform
IS-95	Interim Standard 95
ISI	Inter Symbol Interference
JADE	Joint Approximate Diagonalization of Eigenmatrices
LOS	Line of Sight
MBER	Minimum Bit Error Ratio
MIMO	Multiple Input Multiple Output
MISO	Multiple Input Single Output
MMSE	Minimum Mean Square Error
MSE	Mean Square Error
OFDM	Orthogonal Frequency Division Multiplexing
pdf	Probability Density Function
PCA	Principal Component Analysis
PLL	Phase-Locked Loop
PSK	Phase Shift Keying
QAM	Quadrature Amplitude Modulation
QPSK	Quad Phase Shift Keying
RF	Radio Frequency
SDMA	Spatial Division Multiple Access
SER	Symbol Error Rate
SIMO	Single Input Multiple Output
SISO	Single Input Single Output

SNR	Signal Noise Ratio
SOS	Second-Order Statistics
SSE	Sum of Square Errors
TDMA	Time Division Multiple Access
UWB	Ultra-Wideband
Wi-Fi	Wireless Fidelity
WiMAX	Worldwide Interoperability for Microwave Access

LIST OF SYMBOLS

$(\cdot)^+$	Pseudo-inverse
$(\cdot)^*$	Complex conjugation
$\|\cdot\|$	Euclidean norm
α	Arbitrary positive constant
$\arg(\cdot)$	Argument on a complex value
β	Large-scale fading parameter
$\mathbb{C}$	Complex space
$\overline{C}$	Channel capacity
$\gamma^{(k)(r)}$	Inverted diagonal matrix for $\mathbf{P}^{(k)(r)}$
D	Peak amplitude of the LOS signal
d_0	Reference distance
$\mathbf{d}^{(k)}$	Binary bit vectors in the subcarrier k
$\hat{d}_i^{(k)}$	Estimated data bit sequences in the subcarrier k
$\mathbf{D}^{(k)}$	Unknown scaling in the subcarrier k
$E(\cdot)$	Expectation
$\mathbf{e}^{(k)}$	Error vector in the subcarrier k
$\mathbf{E}_x$	Energy of the transmitted signals
Δf	Difference between subchannels
$f(\cdot)$	Non-linear sigmoid function for the complex domain
f_c	Carrier frequency

$f_{Rayleigh}(r)$	Probability density of the Rayleigh distribution
$f_{Rician}(r)$	Probability density of the Rician distribution
$G(\cdot)$	Smooth even function
$g(\cdot)$	Derivative of $G(\cdot)$
$g'(\cdot)$	Derivative of $g(\cdot)$
$\mathbf{H}$	Channel transfer matrix
$(\cdot)^H$	Hermitian transpose
$\hat{\mathbf{H}}^{(k)}$	Estimated channel matrix in the subcarrier k
$H(f)$	Channel response in the frequency domain
$h(t)$	Channel response in the time domain
$\mathbf{I}$	Unit matrix
$I(\cdot)$	Modified Bessel function of the first kind
$Im(\cdot)$	Imaginary part of a complex value
$J(\mathbf{W})$	Objective function
K	Rician factor
k	Subcarrier index number
l	Number of transmitting antennas
M	Modulation order
μ	Step size for MBER
$\mathbf{n}$	Vector for the AWGN noise
N	Number of subcarriers
$\mathbf{N}_0$	Power spectral density of the additive noise

$N_{cross-correlation}$	Total numbers of the cross-correlation
N_d	Number of binary bit vectors $\mathbf{d}^{(k)}$
p	Number of elements for an antenna array in the receiver
P_{BER}	Bit error probability
P_d	Average power at a distance d
P_e_AWGN	Probability of error for the AWGN channel
$P_e\_Rayleigh$	Probability of error for the Rayleigh channel
$\mathbf{P}^{(k)}$	Unknown permutation at the subcarrier k
P_{SER}	Symbol error probability
P_t	Average transmitted power
$Q(\cdot)$	Standard Q-function
r	Magnitude of the received signal
$R(f)$	Received signals in the frequency domain
$Re(\cdot)$	Real part of a complex value
$\mathbf{R}_{\mathbf{S}^{(r)},\hat{\mathbf{X}}^{(r)}}$	Cross-correlation matrix between $\mathbf{S}^{(k)}$ and $\hat{\mathbf{X}}^{(r)}$
$r(t)$	Received signals in the time domain
$\mathbf{R}_{xx}$	Autocorrelation of the transmitted signal vector
$\mathbf{R}_{\hat{\mathbf{X}}^{(r)},\hat{\mathbf{X}}^{(r)}}$	Autocorrelation matrix $\hat{\mathbf{X}}^{(r)}$ in the subcarrier r
$\mathbf{s}$	Vector for the source signals
$s(t)$	Source signals in the time domain
$S(f)$	Source signals in the frequency domain
$\{S_n\}$	Data symbols

$\hat{\mathbf{S}}^{(k)}$	Estimated vector of the source vector $\mathbf{S}^{(k)}$ in the subcarrier k
sgn($\cdot$)	Sign function
σ^2	Average power
σ_n	Standard deviation for the variance of $\sigma_n{}^2$
$\sigma_n{}^2$	Variance for the AWGN noise
T	Symbol time
$1/T$	Frequency of subcarriers
$(\cdot)^T$	Transpose
T_g	Length of the guard interval
$Tr(\cdot)$	Squared Frobenius norm
v	Path loss exponent
$\mathbf{V}$	Whitened mixed matrix $\mathbf{H}$
v_j	Unknown phase for each source s_j
$\overline{\mathbf{V}}^{(k)}$	Noise free signal vector in the subcarrier k
W	OFMD bandwidth
$\mathbf{W}$	Separation matrix for mixed real source signals
$\mathbf{W}^H$	Separation matrix for mixed complex source signals
$\mathbf{W}_{MMSE}{}^{(k)}$	MMSE separation matrix in the subcarrier k
$\mathbf{W}_{MBER}{}^{(k)}$	MBER separation matrix in the subcarrier k
$\mathbf{x}$	Vector for the received signals
$\overline{\mathbf{x}}^{(k)}$	Noiseless component for $\mathbf{x}^{(k)}$
$\mathbf{z}$	Whitened mixed vector

$\Phi_{\text{JADE}}[\cdot]$ Contrast function for the JADE algorithm

ξ Simple formula of $\dfrac{\mathbf{w}_i^{H(k)}\overline{\mathbf{V}}^{(k)}}{\sqrt{\mathbf{w}_i^{H(k)}\mathbf{w}_i^{(k)}}\sigma_n}$ in the subcarrier k

CHAPTER 1

INTRODUCTION

1.1 Research Background

In recent years, the techniques of MIMO OFDM systems, which are the leading trends of future wireless communication, have been adopted by the fourth generation of wireless communication standards [1], [2].

For any receiver of MIMO OFDM systems, the channel state information or some priori parameters, which normally include the characteristics of users and noise, the timing information of users and noise, the relative amplitude and the training sequences, are regularly required for the conventional multiuser detection methods containing matched filter detection, optimum detection, decorrelation detection and adaptive detection [3]. It is obvious that those priori parameters occupy expensive communication resources, and the conventional multiuser detection methods are undoubtedly inefficient ways of wireless communication.

In addition, there are some disadvantages of the conventional detection methods. Firstly, the CSI is typically difficult to be obtained in MIMO OFDM systems. Secondly, the transmission of the CSI is not often effective for the fast time-varying channel of MIMO OFDM systems. Furthermore, the attenuation of the CSI may cause a wrong multiuser detection in MIMO OFDM systems [4]. At last, the conventional methods reduce the channel capacity in MIMO OFDM systems.

One of the attractive solutions is whether we can find a method to separate or recover multiusers without the CSI or priori parameters in MIMO OFDM systems. Multiuser detection by blind signal/source separation [5-8] techniques, which is also called blind multiuser detection, is chosen as a novel and efficient approach without priori parameters in MIMO OFDM systems.

According to the literature review, there are some researchers [9-14] who have applied BSS techniques in the space-time coding [15], [16] or spatial multiplexing [17-22] MIMO OFDM systems. However, for an uplink transmission from mobile devices to a base station, either the space-time coding scheme or the spatial multiplexing scheme requests two or more antennas for every mobile device to transmit their source signals. In other words, each mobile device has to be equipped with at least two antennas in the space-time coding or spatial multiplexing MIMO OFDM systems.

The antenna elements must be separated from each other roughly between 10 λ and 40 λ for the purpose of a low spatial correlation [23]. Table 1-1 shows the minimum distance between two adjacent antennas under different frequencies. It is obvious that there is almost no possibility for a mobile device with a limited size to be equipped with two or more antennas under those frequencies. Even for a 5 GHz frequency band, the minimum distance between two adjacent antennas is at least 0.6 meters in this case. A useful solution for the uplink transmission from mobile users to the base station in an MIMO OFDM system is that one mobile device should be equipped with only one antenna. Otherwise, to design and allocate two or more antennas for every mobile device will be very complex.

Table 1-1 Minimum distance between two adjacent antennas

Frequency	$10\,\lambda$	$40\,\lambda$
900 MHz	3.33 m	13.32 m
1800 MHz	1.67 m	6.68 m
5 GHz	0.60 m	2.40 m

Currently, to achieve an MIMO OFDM system, we also have other techniques, such as beamforming, SDMA, and network [1]. From those candidate schemes, the SDMA-based MIMO OFDM systems are chosen for uplink MIMO OFDM systems in this dissertation. The SDMA techniques can greatly simplify the design and allocation of antennas for mobile devices, because each mobile device only needs to be employed by one antenna.

Compared with other types of MIMO OFDM systems, there are some benefits of the SDMA-based MIMO OFDM systems [24-28]. First, the coverage area by a base station can be extended by the SDMA techniques. Second, the SDMA techniques are able to reduce the interference in MIMO OFDM systems. Another merit is that the multipath propagation can often be mitigated by the SDMA techniques. The channel capacity increment is another advantage of the SDMA techniques. Finally, the SDMA techniques are capable of working with almost any modulation method, bandwidth, frequency band including Global System for Mobile Communications (GSM), Interim Standard 95 (IS-95), OFDM, et al. Therefore, the SDMA techniques are a suitable choice for uplink MIMO OFDM systems with many advantages.

To evaluate the performance for multiuser detection in MIMO OFDM systems, there are two important aspects, which contain the Bit Error Rate/Ratio (BER) performance and the computational complexity. However, the current BSS approaches [9-14] in MIMO OFDM systems not only cannot find the best BER performance but also cannot find the best computational efficiency.

In all, the current research has four problems: (1) the conventional multiuser detection schemes have drawbacks of the transmission of the CSI and waste channel resources; (2) the current blind multiuser detection methods in space-time coding or spatial multiplexing MIMO OFDM systems are not suitable for the uplink transmission from mobile users to the base station; (3) the existing BSS schemes [9-14] cannot provide the best BER performance in MIMO OFDM systems; (4) the current BSS approaches [9-14] cannot gain the best computational efficiency in MIMO OFDM systems.

1.2 Objective of the Dissertation

According to the research background, the objective of this dissertation mainly consists of four aspects. (1) Apply blind multiuser detection techniques to have higher channel utilization and save the channel resources, compared with the conventional detection schemes in MIMO OFDM systems. (2) Propose a SDMA-based uplink MIMO OFDM system to solve the transmission problems from mobile devices to the base station. (3) Propose a BSS only method, which is referred to as BSS-only, to compromise on both the BER performance and the computational complexity. (4) Propose a BSS scheme combined with a linear Minimum Mean Square Error scheme, which is referred to as

BSS-MMSE, to minimize the computational complexity. (5) Propose a BSS joined with a linear Minimum Bit Error Rate algorithm, which is referred to as BSS-MBER, to obtain the best BER performance.

To display the performance of all proposed schemes, the implementation, simulation and performance analysis are developed by MATLAB and the software version is R2008a. Various conditions of the proposed SDMA-based uplink MIMO OFDM system are considered to simulate the three proposed blind multiuser detection schemes for their BER performance or computational complexity.

1.3 Dissertation Outline

In Chapter 1, four problems of the current research are revealed about multiuser detection in MIMO OFDM systems. The objective of this dissertation is introduced according to those current problems. Three proposed blind multiuser detection schemes promise three different performance goals in the proposed SDMA-based uplink MIMO OFDM system.

The proposed SDMA-based uplink MIMO OFDM system is introduced in Chapter 2. To achieve a suitable system with our different design goals, some important aspects including the wireless channel, the MIMO techniques and the OFDM techniques, need to be analyzed, discussed and considered in this chapter. In addition, the fading channels, the capacity analysis of MIMO systems, and OFDM base band signals are also simulated and analyzed.

Chapter 3 illustrates the blind signal separation techniques. The development of BSS and independent component analysis (ICA) techniques is demonstrated first, and then significant BSS algorithms are introduced. According to our analysis, the Fast Independent Component Analysis (FastICA) algorithm is selected and modified for three proposed blind multiuser detection schemes in the SDMA-based uplink MIMO OFDM system. Several types of complex FastICA algorithms are also simulated in this chapter.

Chapter 4 proposes BSS-only, BSS-MMSE, BSS-MBER schemes for different design goals, in which the merits for all of the schemes are provided and discussed. With these schemes, the researchers are able to decide which one should be chosen for a special design objective. The discussion focuses on their BER performance and computational complexity.

The simulation results are discussed and analyzed in Chapter 5. It provides how to set up the simulation environment and shows the simulation results about the BER performance for three proposed methods. In addition, the influence by a different number of frames is also discussed. Finally, the computational complexity is simulated through the running time.

Chapter 6 summarizes the major outcomes of this dissertation and proposes new endeavors for researchers to extend the prospects for industrial applications further. In retrospect, this research establishes three new schemes for the SDMA-based uplink MIMO OFDM system with a variety of performances.

CHAPTER 2

SDMA-BASED UPLINK MIMO OFDM SYSTEMS

The research of MIMO OFDM was started in the early 2000s [1]. The MIMO based OFDM schemes may simultaneously improve the transmission rate, the transmission range and the transmission reliability of a wireless system. Because MIMO OFDM is more efficient than MIMO combined with other modulations [1], a combination of both MIMO and OFDM can tap their potentials at the same time. The MIMO OFDM techniques have been applied in the Institute of Electrical and Electronics Engineers (IEEE) 802.11n or Wireless Fidelity (Wi-Fi) networks [29], [30].

User 2

User 1

User l

Element 1   Element 2 $\bullet \bullet \bullet \bullet \bullet \bullet$ Element p

Base Station with p-element antenna array
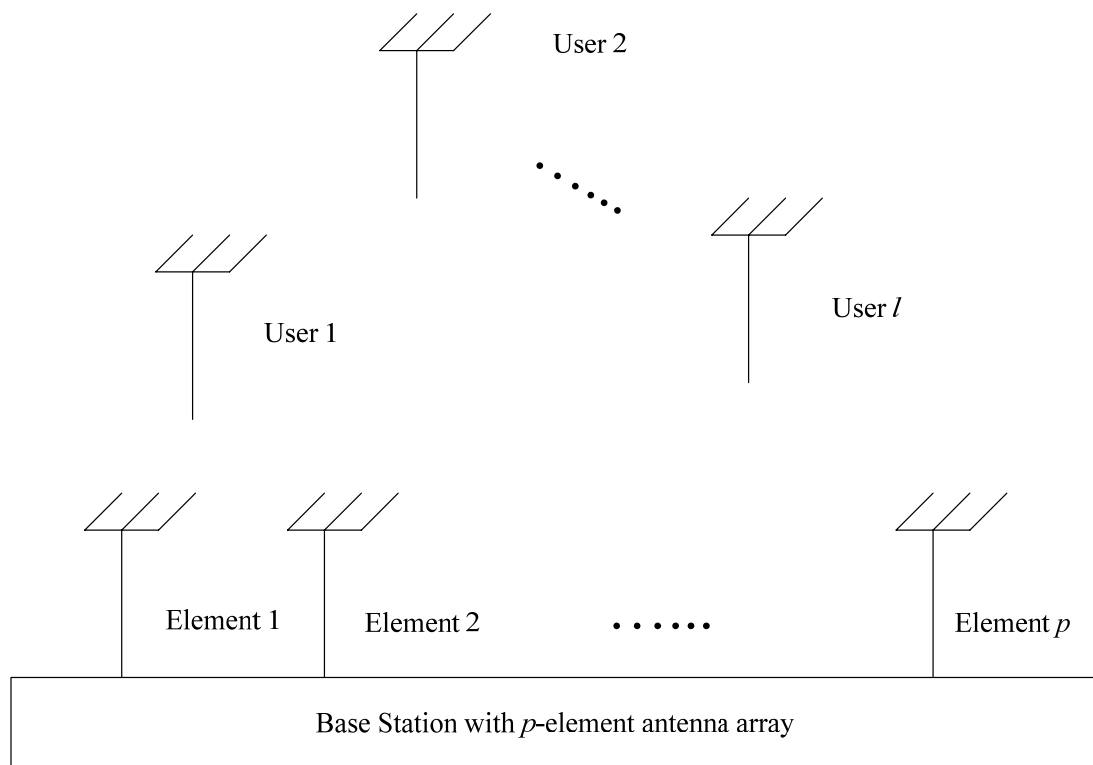
Figure 2-1 Mobile Users in Different Geographical Locations

The SDMA-based MIMO OFDM system is a specific subclass of MIMO OFDM systems that should be able to enable different mobile users to share the same bandwidth simultaneously in different geographical locations. Figure 2-1 illustrates the block diagram of mobile users in different places. We assume that there are l transmitting antennas for l users' signals and a p-element antenna array is installed in the receiver. Although the transmitters are equipped with multiple antennas, the uniqueness of the SDMA techniques is that these transmission antennas cannot be shared by different mobile users and each of them belongs to one user only. In other words, because of the limited space of mobile devices, each mobile user can only be equipped with one antenna. The transmission of OFDM signals cannot be coordinated or allocated, compared with the special multiplexing or space-time coding scheme in which all of users are capable of sharing every antenna in the transmitters.

2.1 Proposed SDMA-based Uplink MIMO OFDM Systems

The proposed SDMA-based uplink MIMO OFDM system can be included in all kinds of existing multiple-access standards with some enhancements of system capacity. There are two types of SDMA-based MIMO OFDM systems: the SDMA-FDMA (Frequency Division Multiple Access) scheme and the SDMA-TDMA (Time Division Multiple Access) scheme. If the SDMA-based MIMO OFDM scheme is combined with a conventional FDMA scheme in Figure 2-2, n mobile users' OFDM signals will share the same time slot. The other case in Figure 2-3 illustrates n mobile users' OFDM signals share the same frequency band. It is clear that both of them boost up the system capacity. Generally, the SDMA-TDMA scheme is more popular, because it only employs one

single carrier frequency, which saves limited and expensive frequency resources. Moreover, the SDMA-TDMA scheme is able to maximize the number of users supported. If there is no special mention, the following SDMA scheme refers to the SDMA-TDMA scheme in this dissertation. Therefore, this scheme will be applied to the proposed SDMA-based uplink MIMO OFDM system for three proposed blind multiuser detection schemes.
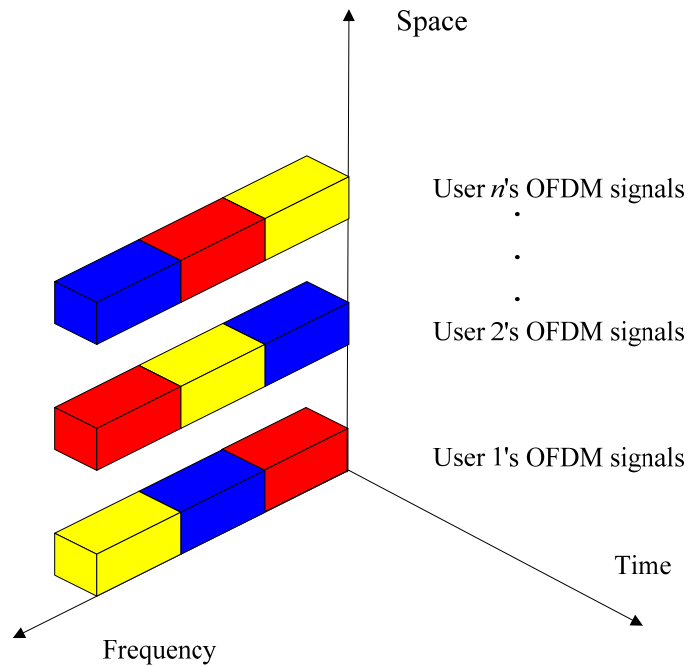
Figure 2-2 SDMA-FDMA-based MIMO OFDM System

There are mainly two parts for the proposed SDMA-based uplink MIMO OFDM system, which are the transmitter and the receiver. Figure 2-4 shows the schematic diagram of the proposed SDMA-based uplink MIMO OFDM system. We assume there are l users and each user transfers its source bit sequences into OFDM signals through an

OFDM transmitter module. After this procedure, l antennas simultaneously transmit the OFDM signals to the receiver. The receiver, which is equipped with a p-element antenna array, is to receive the linearly mixed complex OFDM signals. Finally, the OFDM receiver modules demodulate the mixed OFDM signals into the mixed bit sequences of l users.
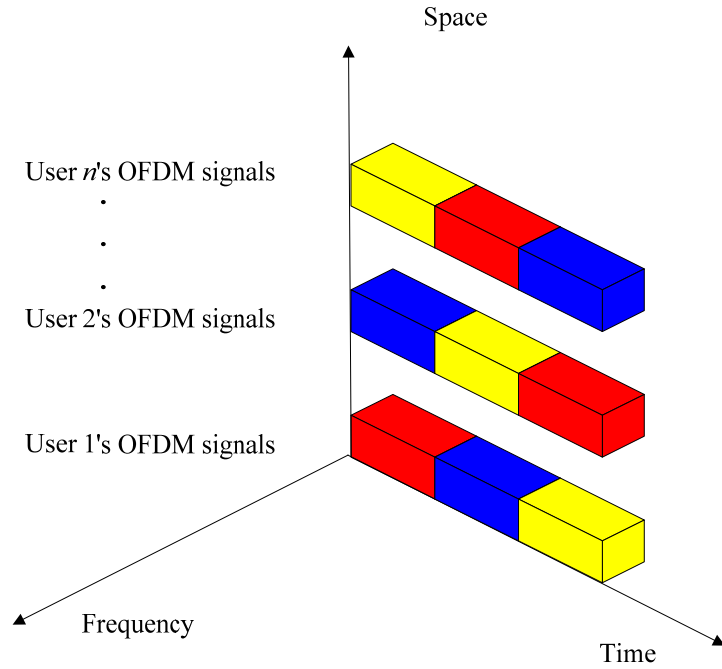
Figure 2-3 SDMA-TDMA-based MIMO OFDM System

The transmitter and receiver relationship of the proposed SDMA-based uplink MIMO OFDM system in one of OFDM subcarriers k can be described by [1]

$$\begin{bmatrix} x_1^{(k)} \\ \vdots \\ x_p^{(k)} \end{bmatrix} = \begin{bmatrix} H_{11}^{(k)} & \cdots & H_{l1}^{(k)} \\ \vdots & \ddots & \vdots \\ H_{1p}^{(k)} & \cdots & H_{lp}^{(k)} \end{bmatrix} \begin{bmatrix} s_1^{(k)} \\ \vdots \\ s_l^{(k)} \end{bmatrix} + \begin{bmatrix} n_1^{(k)} \\ \vdots \\ n_p^{(k)} \end{bmatrix} \quad (2.1)$$

where x_i are mixed source signals at the receiver, s_i are independent source signals at the transmitter, n_i are additive white Gaussian noises (AWGN) that are added at the receiver, and H_{ij} denote the elements of the frequency domain channel transfer matrix **H** with $p \times l$ dimension. If k is omitted for the sake of notational convenience and the vectors **x**, **s**, and **n** are given by

$$\mathbf{x} = [x_1, x_2, \cdots, x_p]^\mathrm{T} \tag{2.2}$$

$$\mathbf{s} = [s_1, s_2, \cdots, s_l]^\mathrm{T} \tag{2.3}$$

$$\mathbf{n} = [n_1, n_2, \cdots, n_p]^\mathrm{T} \tag{2.4}$$

where T denotes transpose. The frequency domain channel transfer matrix **H** with $p \times l$ dimension is given by

$$\mathbf{H} = [\mathbf{H}_1, \mathbf{H}_2, \ldots, \mathbf{H}_l]^\mathrm{T} \tag{2.5}$$

where $\mathbf{H}_i$ ($i = 1, 2, \cdots, l$) are the set of the channel transfer function vectors of the l users to each element of the p-element receiver, which is express as

$$\mathbf{H}_i = [H_{i1}, H_{i2}, \ldots, H_{ip}]^\mathrm{T}, \quad i = 1, 2, \cdots, l. \tag{2.6}$$

The compact expression of the proposed SDMA-based uplink MIMO OFDM system in the subcarrier k can be expressed by the following equation

$$\mathbf{x}^{(k)} = \mathbf{H}^{(k)}\mathbf{s}^{(k)} + \mathbf{n}^{(k)} = \overline{\mathbf{x}}^{(k)} + \mathbf{n}^{(k)} \tag{2.7}$$

where $\overline{\mathbf{x}}^{(k)}$ denotes the noiseless component for $\mathbf{x}^{(k)}$ in the subcarrier k. It is easy to understand that the number of antennas can decide the dimension of the channel transfer matrix. The higher the number of antennas is increased, the more the number of dimensions of transfer matrix is estimated.
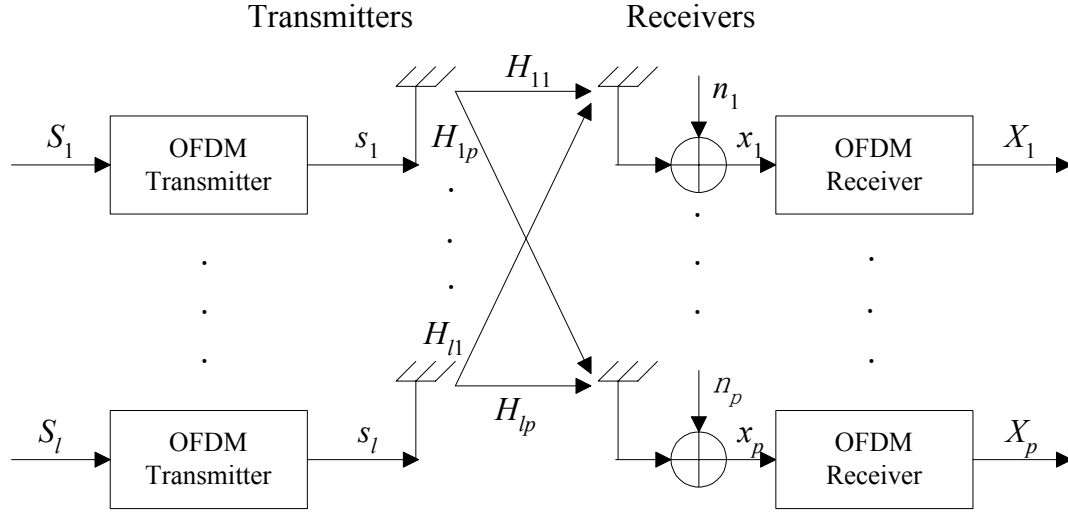
Figure 2-4 Schematic Diagram of the Proposed SDMA-based Uplink MIMO OFDM System

There are some assumptions in the designed SDMA-based uplink MIMO OFDM system. We assume that it is an instantaneous linear mixture model. The complex source signals are independent and have non-Gaussian distribution, and AWGN noises have zero mean and a variance of σ_n^2. In addition, the frequency channel transfer function $\mathbf{H}$ is stationary and has Gaussian distribution.

To design a suitable SDMA-based uplink MIMO OFDM system for the proposed multiuser detection schemes, some significant specifics should be considered, and they

include: the fading analysis of the wireless channel, the selection and capacity analysis of MIMO techniques, and the implementation of the OFDM transmitter module and the OFDM receiver module. The following of this chapter focuses on these important aspects to implement a proposed SDMA-based uplink MIMO OFDM system.

2.2 Wireless Channel

The term "wireless" is a generic word, which illustrates that electromagnetic waves or radio frequencies (RF) transmit information through a part of or the whole communication paths. Wireless communication is able to transfer information over both short distances and long distances. Furthermore, it is commonly employed in telecommunication with an impractical or impossible use of wires. The users in the next generation wireless communication need higher information transmission rate and better transmission quality, however, wireless resources are correspondingly limited. Therefore, it is very significant to analyze the properties of the wireless modes and the wireless fading channel models, which are able to support us to design the proposed uplink MIMO OFDM system with such limited and expensive telecommunication resources.

The wireless modes include point-to-point communication, point-to-multipoint communication, multipoint-to-multipoint communication, broadcasting, and others. Figure 2-5 shows several wireless modes. The wireless devices, such as a cellphone, a wireless router, a laptop with Wi-Fi, an amplitude modulation (AM) or Frequency Modulation (FM) radio, and so on, utilize the electromagnetic spectrum from 9 kHz to 300 GHz in wireless communication. However, the frequencies are considered as a public

resource by most of countries and different ranges can be used for different purposes. For example, the frequency band of a common GSM cellphone is 900 MHz or 1800 MHz. The regular frequency band for a pilot to communicate with the control tower of an airport is around 900 MHz as well. If a passenger is using a cellphone during takeoff or landing, the passenger's phone call may interfere with pilot's communication with the control tower. Therefore, the efficient utilization of the limited channel resources is very meaningful.
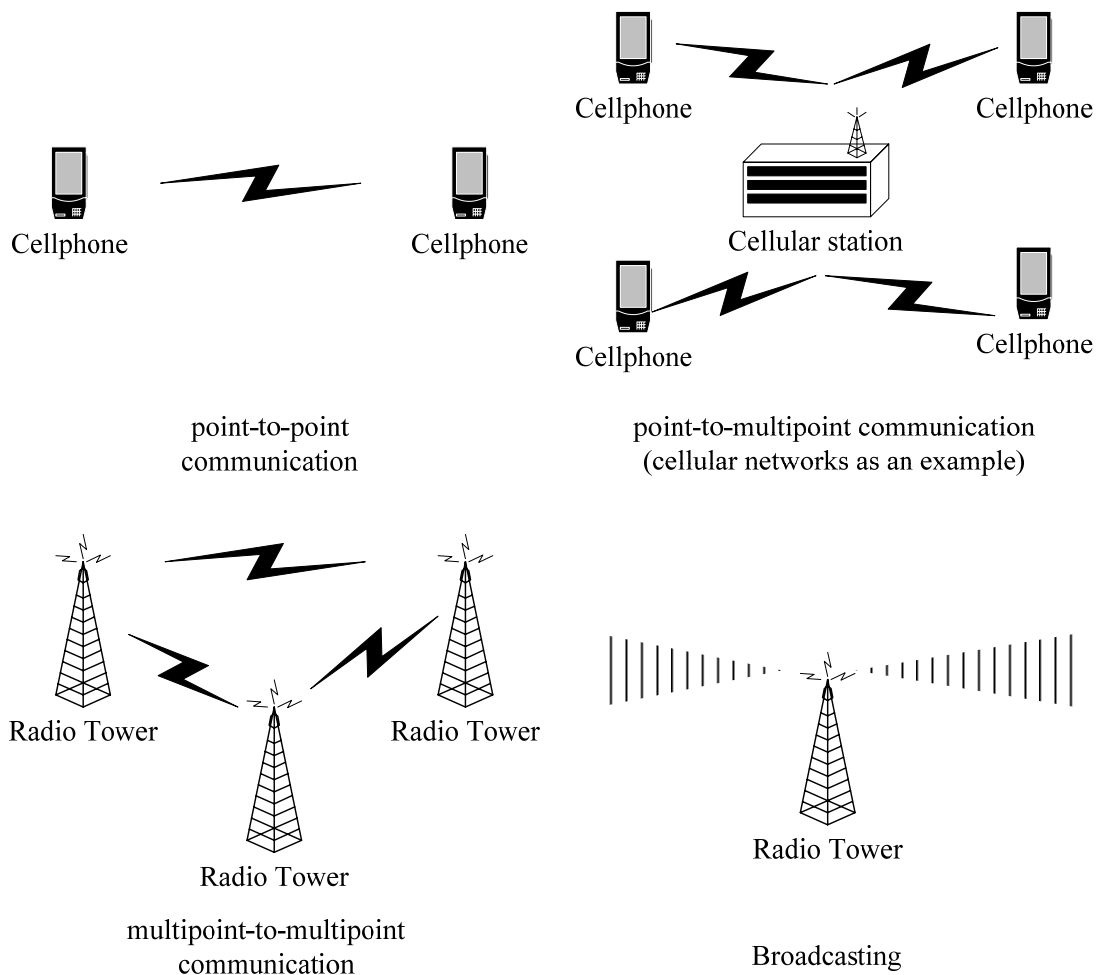
Figure 2-5 Wireless Modes

Several important types of wireless fading channels related to the proposed SDMA-based MIMO OFDM channels need to be considered. Fading means a kind of attenuation and it may possibly happen when transmitting modulated signals over some propagation media. In wireless communication, fading may be due to either multipath propagation or shadowing.
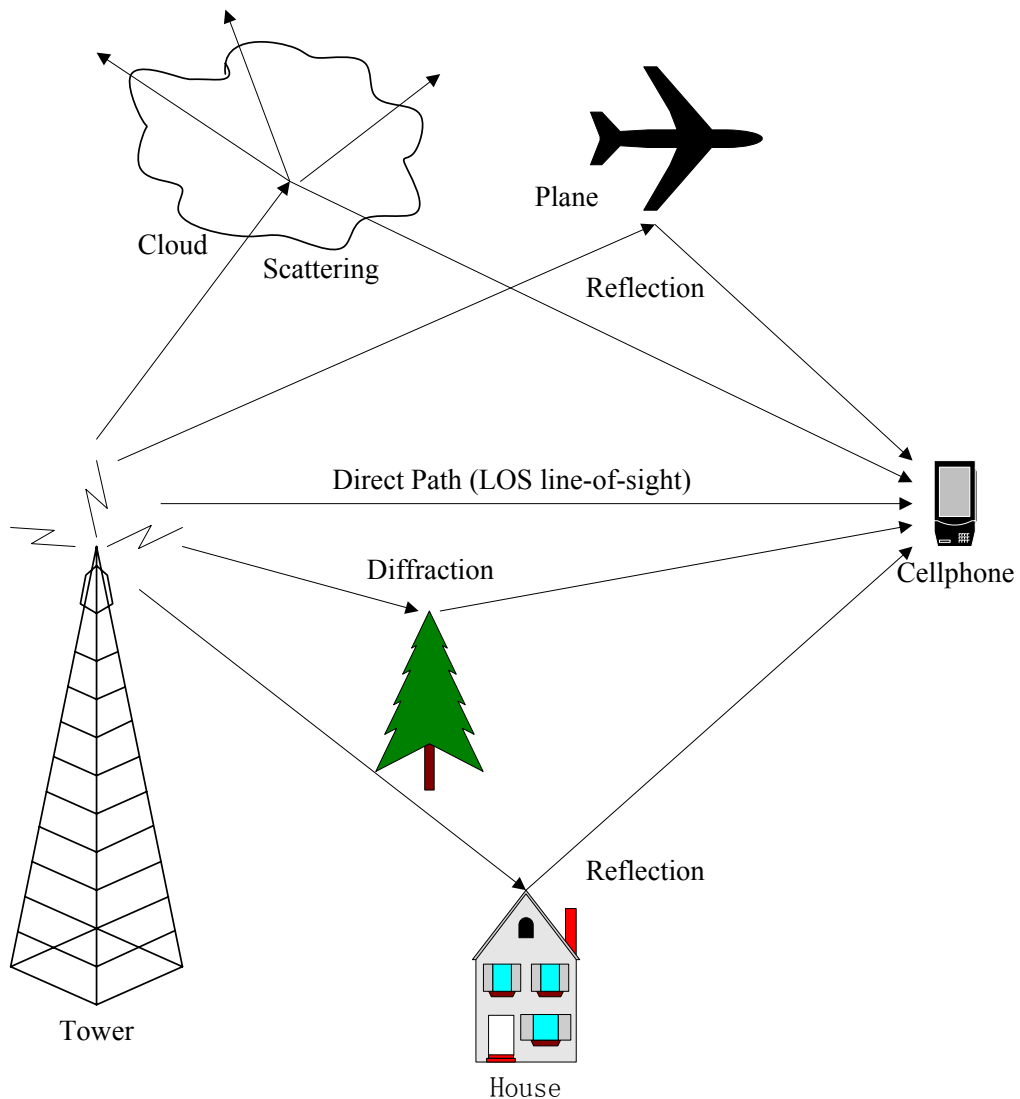
Figure 2-6 Fading and Multipath

Figure 2-6 shows that the obstacles such as building, cloud, tress or plane can reflect, scatter, or diffract the transmitted waves. The direct path for the transmitted waves between the transmitter and the receiver is called line of sight (LOS). The transmitted waves by none-LOS paths are usually destructed by those obstacles. Therefore, the received signals through the LOS are generally stronger than others from none-LOS paths.

Different time, frequency or location could change the fading, and common fading channel models include two aspects: large-scale fading and small-scale fading [31]. The large-scale fading, which is also called attenuation or path loss, relates to large distances or time-average characteristics of transmitted signals. On the contrary, small-scale fading, which means fading for short, is the fast fluctuation of the amplitude or power of the transmitted signals corresponds to short distances or short time intervals. Attenuation and several fading channels containing flat fading, frequency-selective fading, slow fading, fast fading, Rayleigh fading, Rician fading, et al should be considered.

2.2.1 Large-scale Fading Model

Large-scale fading, or attenuation, illustrates the path loss by propagation including reflection, scattering and diffraction in an open space environment. The average power at a distance d from the transmitter is given as

$$P_d = \beta \, (d/d_0)^{-v} \, P_t \tag{2.8}$$

where β is a large-scale fading parameter depending on antenna gain, frequency, wavelength, and other factors, d_0 is the reference distance, P_t is the average transmitted power, and v is the path loss exponent.

Large-scale Fading Model, f_c=1800MHz,
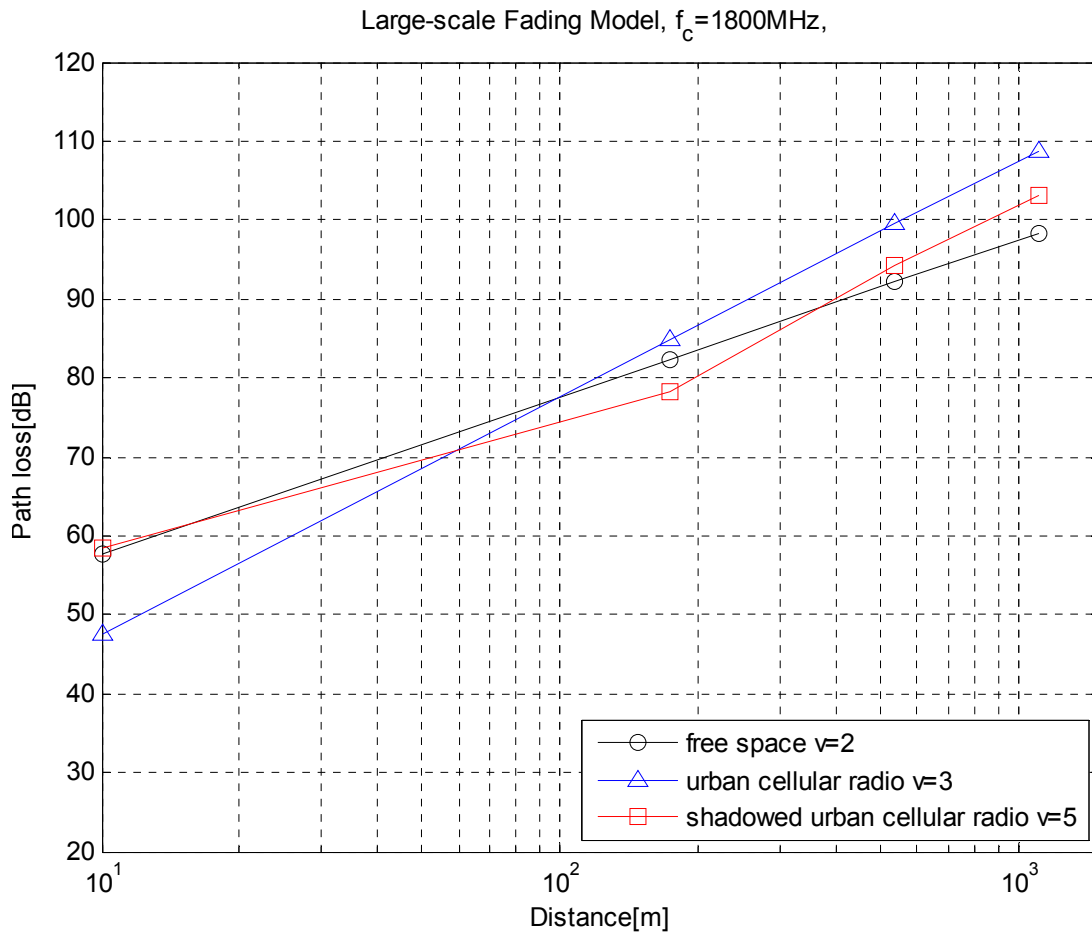
Figure 2-7 Large Scale Fading Model

The path loss exponent is usually equal to 2 in an open space environment and is greater than 2 in an environment with obstacles as shown in Figure 2-6. In a practical or empirical situation like the cellphone in Figure 2-6, the measurement for P_d of the phone may not be the same value in different places at the same distance from the transmitting

tower or the base station, because these obstacles can randomly influence the path loss. It is so called shadowing. The probability density function (pdf) of the average power for a large-scale fading will submit to Gaussian distribution [31].

Figure 2-7 illustrates the large scale fading model by Equation 2.8. The carrier frequency is set to 1800 MHz and the reference distance d_0 is 100 m. There are three types of situations considered in this model: v is 2 for an open space cellular radio, 3 for an urban cellular radio, and 5 for a shadowed urban cellular radio, respectively. The horizontal axis is log-distance, and the vertical one is path loss measured by dB. When there is no shadow, it is obvious that the path loss increases with the v. However, the random shadow may make an impact on the path lose. Thus, we can see it is not a straight line in this figure compared with the environment without shadow, and it varies with the random shadowing effect.

2.2.2 Small-scale Fading Model

Small-scale fading, or fading, illustrates a fast fluctuation of the power of the transmitted signals when the receivers are moved within a slightly small area. It is caused by the multipath waves of the transmitted signals and these waves reach the receivers at moderate different times. As mentioned before, scattering, diffraction, and reflection can generate the multipath waves and this is known as multipath fading. In order to research the behavior of different fading channels, a general channel model is depicted in Figure 2-8. In the time or frequency domain, the source signals, the channel response, and the received signals are $s(t)$ or $S(f)$, $h(t)$ or $H(f)$, and $r(t)$ or $R(f)$, respectively.
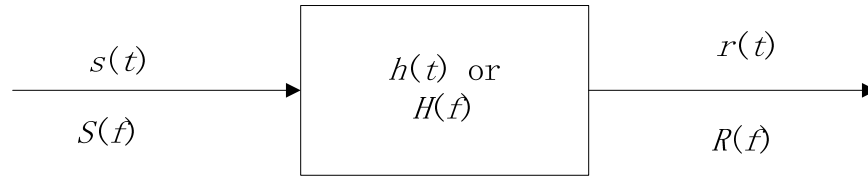
Figure 2-8 General Channel Model

Figure 2-9 shows two types of wireless channels that are flat fading channel and frequency-selective fading channel. Flat fading channel means the coherence bandwidth of the channel is larger than the bandwidth of the source signal, which is depicted in the frequency domain on the left side of the figure. Here the coherence means the minimum frequency or time required for the magnitude change of the channel. On the other hand, if the opposite assumption with a larger bandwidth of the source signal compared with a smaller coherence channel bandwidth in the frequency domain as shown on the right side of the figure, the received signals will be distorted. If we consider $S(f)$ as a symbol bandwidth in the frequency domain for the proposed SDMA-based uplink MIMO OFDM system, it indicates that Inter Symbol Interference (ISI) exists. Therefore, the channel bandwidth $H(f)$ in the frequency domain should be equal to or larger than the coherence channel bandwidth in the frequency domain to avoid ISI.

Compared with the delay restriction of the transmission channel, slow fading will happen if the coherence time of this channel is not small. The shadowing mentioned above can lead to slow fading. The rate of the channel will be much slower than that of the transmitted signal. Then the variations of amplitude and phase can be considered static over one or several bandwidth intervals. On the other hand, if the coherence time of

the channel is relatively less than the delay restriction of the transmission channel, the fast fading will take place. In this case, it is worthy to notice that the change of the amplitude and phase is not static anymore, and the channel response alters fast inside the symbol period.

$S(f)$ $S(f)$

$H(f)$ $H(f)$

$R(f)$ $R(f)$
Flat fading   Frequency-selective fading
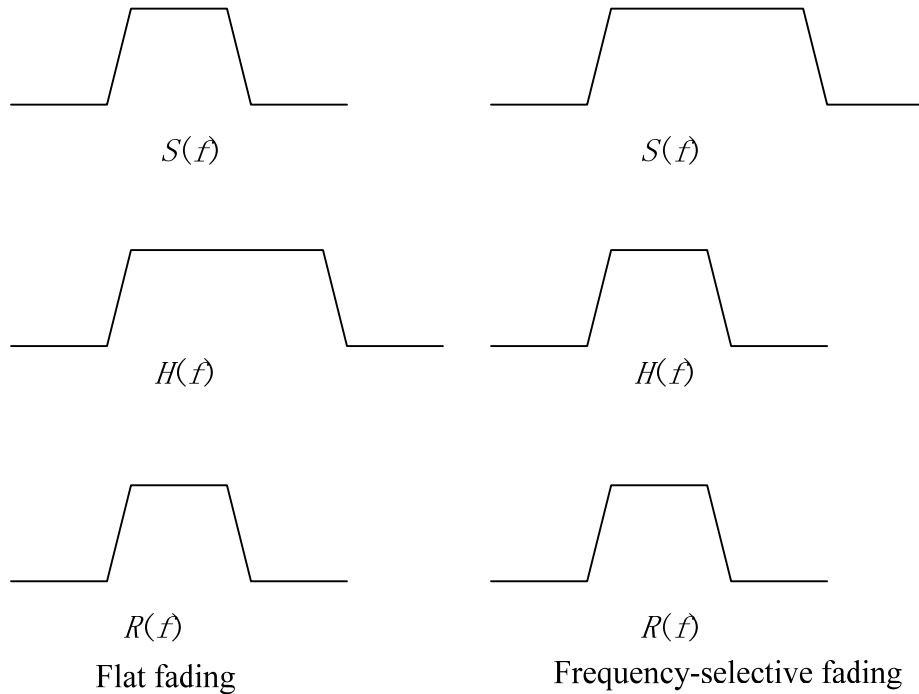
Figure 2-9 Flat Fading vs. Frequency-Selective Fading

In all, the flat or frequency-selective fading channel and the slow or fast fading channel are modeled by a linear time-varying impulse response. But the nature or practical environment of the multipath channels is impossible to keep such an ideal impulse response. Thus, statistical models are necessarily considered to explore the performance of the received signals and the most essential models are Rayleigh fading channel model, Rician fading channel model and others [31].

There are mainly two cases in a flat fading channel. If there is no LOS path between the transmitter and the receiver, it is a Rayleigh fading model. Otherwise, it is a Rician fading channel. The probability density functions of either a Rayleigh random variable or a Rician random variable are given by Equation 2.9 and Equation 2.10, respectively [31]:

$$f_{Rayleigh}(r) = \frac{r}{\sigma^2} \exp(\frac{-r^2}{2\sigma^2}), \qquad r \geq 0 \qquad (2.9)$$

$$f_{Rician}(r) = \frac{r}{\sigma^2} \exp(\frac{-(r^2 + D^2)}{2\sigma^2}) I_0(\frac{Dr}{\sigma^2}), \quad r \geq 0, D \geq 0 \qquad (2.10)$$

where r is the magnitude of the received signal, σ^2 is the average power, D indicates the peak amplitude of the LOS signal, $I(\cdot)$ is the modified Bessel function of the first kind, and $I_0(\cdot)$ is the zero-order of $I(\cdot)$. The Rician distribution will approach the Rayleigh distribution when there is no LOS path in the channel. In other words, D is very close to zero.

In addition, another quantitative description of the Rician distribution is the Rician factor, K, and it is defined as [23]

$$K = \log(\frac{D^2}{2\sigma^2}) \qquad (2.11)$$

Figure 2-10 shows the simulations of the Rician distribution when the value of K is less than zero (i.e. K is -35 dB or -15 dB in this simulation). The Rician distribution comes close to the Rayleigh distribution in this figure. This case happens frequently,

because it is very common that there is no LOS between mobile users to a base station in urban areas.

If the value of *K* is a positive number (i.e. *K* is 10 dB, 15dB or 25 dB), the simulation for the Rician distribution is shown in Figure 2-11. The Rician distribution approaches the Gaussian distribution when *K* is positive. In addition, we assume that the number of channel realization is 10,000, and the vertical axis measures the incidence for the Rayleigh or Rician distribution in both Figure 2-10 and Figure 2-11.
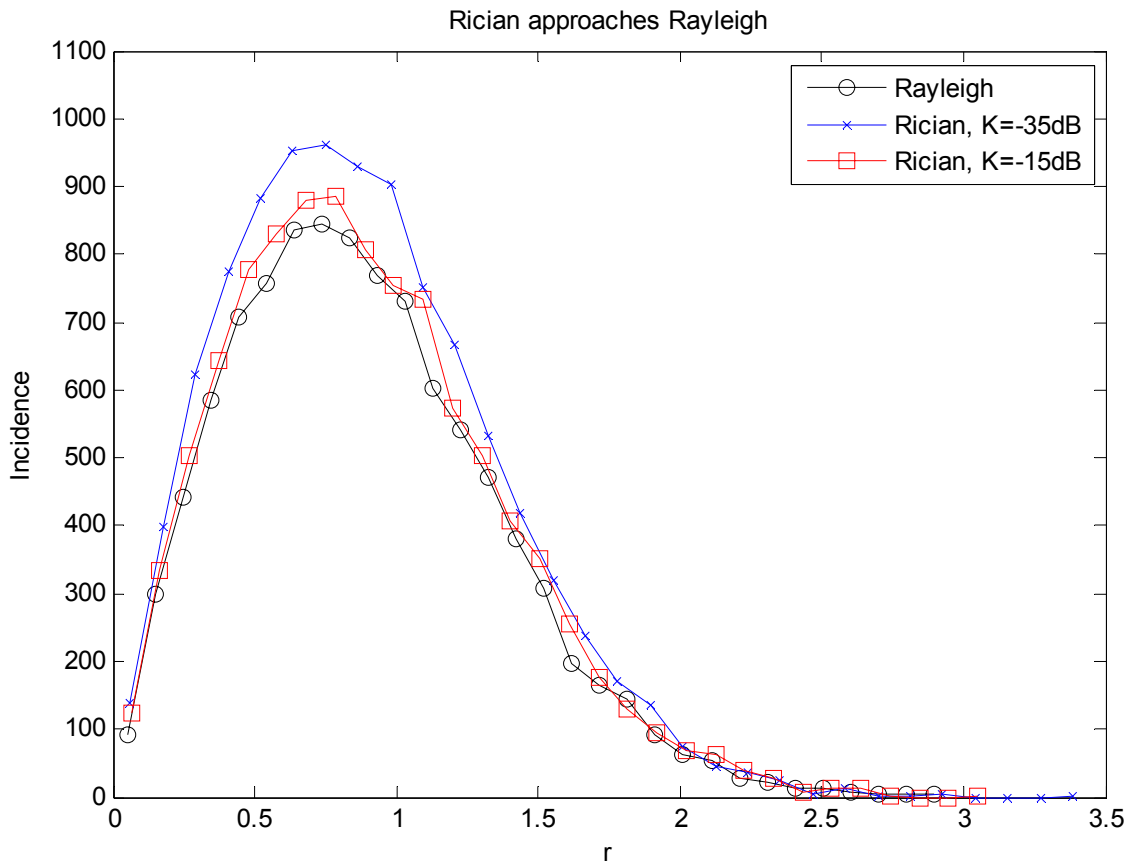
Figure 2-10 Rician Distribution with *K* < 0
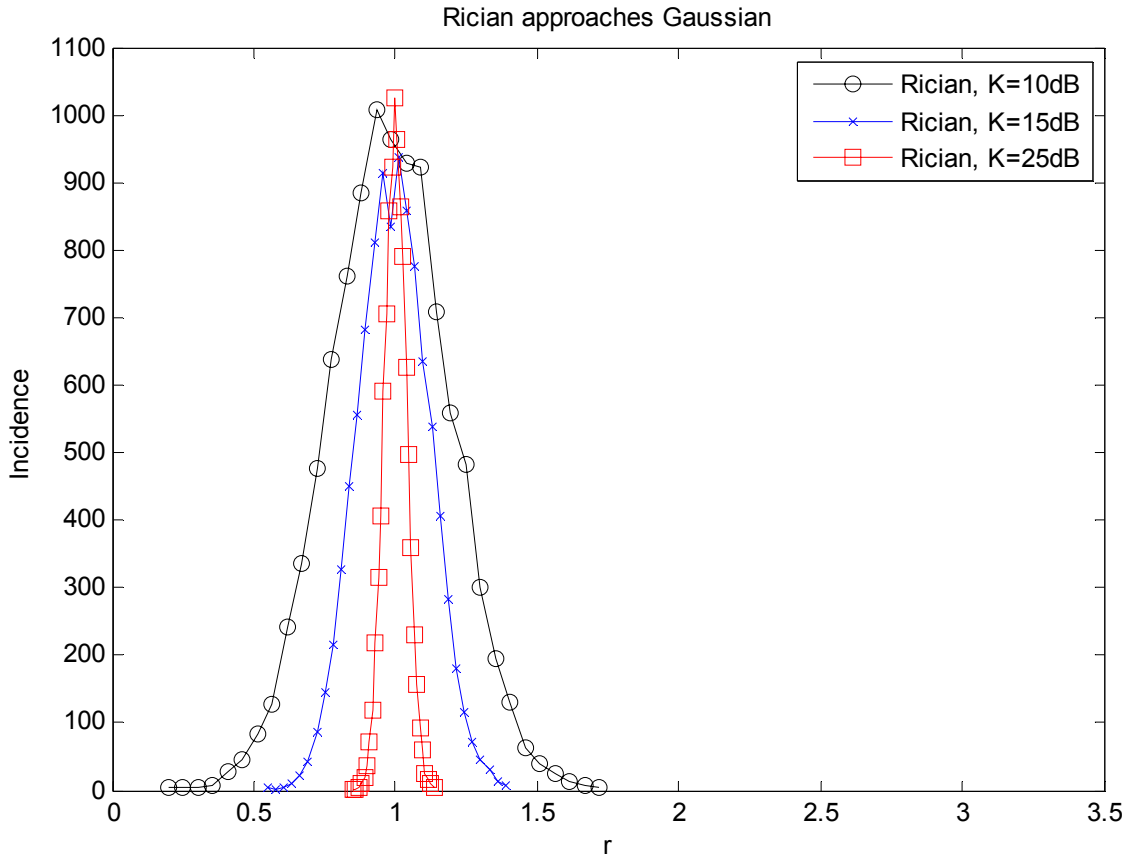
Figure 2-11 Rician Distribution with *K* > 0

2.3 MIMO Techniques

A conventional wireless system is a Single Input Single Output (SISO) antenna system that is limited by the channel capacity. Whatever modulation scenarios are chosen, there is still a physical restriction by only one single wireless channel. To increase the channel capacity, more base station, transmission power, or bandwidth will be required. Thus, an antenna array or several independent antennas can be applied in the receiver to increase the receiving diversity while the transmitter is still equipped with one antenna.

This is called Single Input Multiple Output (SIMO) system. An antenna array or several independent antennas can also be in the transmitter and the receiver is equipped with only one antenna to decrease the complexity of the receiver. This type is so-called Multiple Input Single Output (MISO) system.
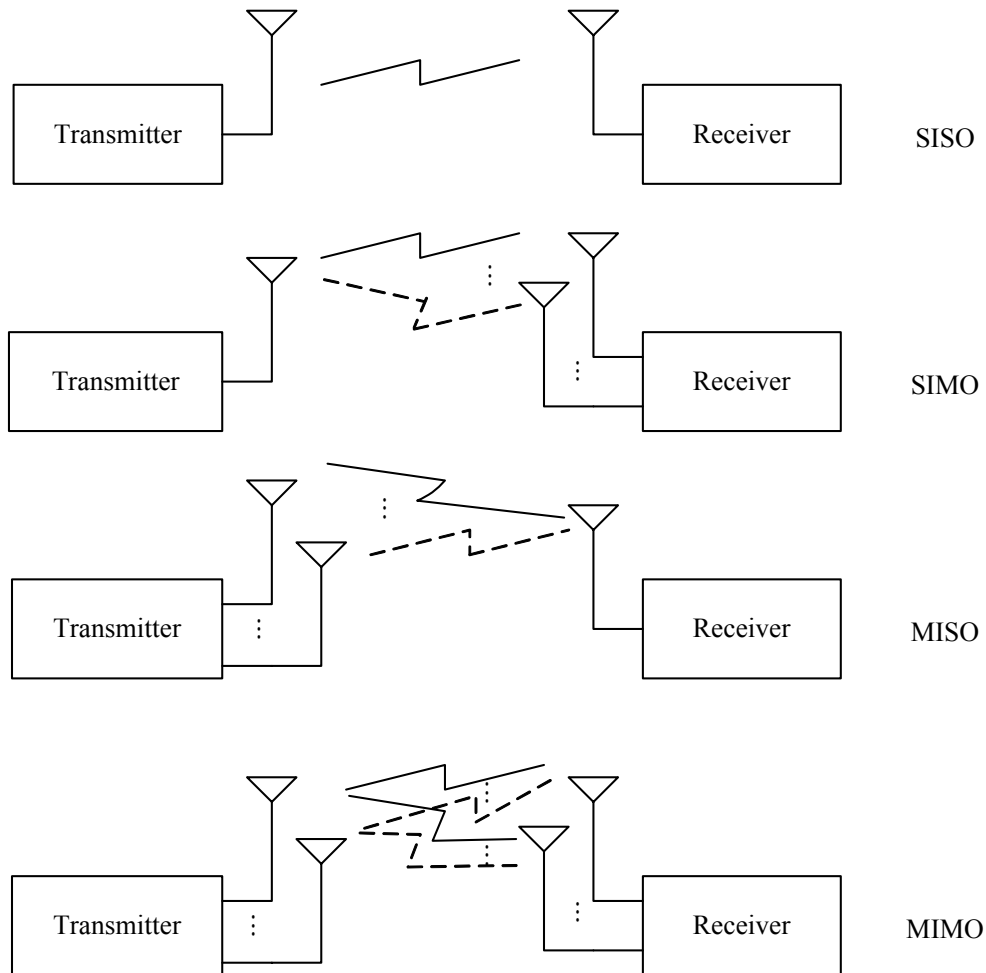
Figure 2-12 Antenna System Models

Furthermore, both the transmitter and the receiver installed an antenna array or several independent antennas are a so-called MIMO system. The MIMO techniques can not only offer a higher spectral efficiency or a higher data rate, which indicates more bits

per second per hertz of bandwidth, but also have the merit of reliability or diversity. Although the MIMO system is more complex, it is still a significant part of the modern wireless communication standards such as 4G, Worldwide Interoperability for Microwave Access (WiMAX), and IEEE 802.11n. Figure 2-12 shows these four types of antenna system models from up to down, respectively.

There are two types of MIMO systems: the closed-loop MIMO system and the open-loop MIMO system. When the receiver feeds the information about the wireless channel to the transmitter through a feedback channel, this is called the closed-loop MIMO system and Figure 2-13 illustrates it.
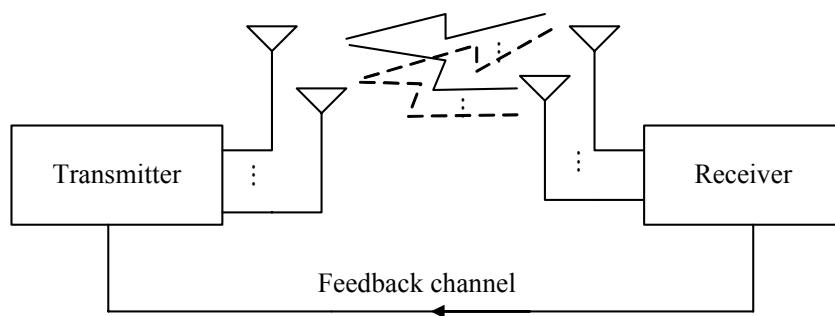
Figure 2-13 Closed-Loop MIMO System

Because the transmitters know the channel state information through the feedback channel in the closed-loop MIMO system, the transmitters can adjust the power of the paths between the transmitters and the receivers. It indicates that the transmitters do not need to send the source signals to all of the directions covered by the antenna array. Consequently, this method can dramatically save the transmission power and energy. The received signal gain is increased by the transmitted signals from different antennas; and

meanwhile, the multipath fading is reduced by the MIMO channel. The beamforming technique [32] is a type of closed-loop MIMO systems, and it can adjust the phase and the amplitude of each transmitter through the feedback channel. All of the transmitters are able to directly generate the correct phase and amplitude for each receiver.

An opposite case is that the MIMO system does not contain a feedback loop, and it cannot provide direct access to the channel state information. This type of MIMO techniques is called an open-loop MIMO system, which needs more power and energy to transmit signals through the antenna array for all of the directions. It is noticeable that the feedback channel occupies the precious wireless channel resources. In order to save the channel resources, the open-loop type is employed to the proposed SDMA-based uplink MIMO OFDM system.

Due to the obstacles between the transmitter and the receiver, and the interference from others, the power and Signal Noise Ratio (SNR) of the transmitted signals in the receiver are regularly dropped dramatically and are very small. There is normally a minimum SNR requirement at the receiver in order to detect and recover the transmitted signals. If the SNR value is less than this minimum requirement, the receiver is unable to do such a detection and recovery. Therefore, to maintain the required value of the power and SNR at the receiver is another requirement of the proposed uplink SDMA-based MIMO OFDM system.

The channel capacity is another important parameter that should be considered for the proposed uplink SDMA-based MIMO OFDM system. The amount of antennas in the transmitter and in the receiver not only influences the channel capacity but also decides

the computational complexity for multiuser detection in the receiver. Thus, a suitable choice of the amount of antennas should be considered.

The MIMO channels are not always stable and they often change randomly. If the changing procedure is an ergodic process, the channel capacity is given by [23]

$$\overline{C} = E\{C(\mathbf{H})\} = E\{ \max_{Tr(\mathbf{R}xx)=N_T} \log_2 \det(\mathbf{I}_{N_R} + \frac{\mathbf{E}_x}{N_T \mathbf{N}_0} \mathbf{H} \mathbf{R}_{xx} \mathbf{H}^H)\} \tag{2.12}$$

where $Tr(\cdot)$ is related to the squared Frobenius norm, $\mathbf{R}_{xx}$ is the autocorrelation of transmitted signal vector and equals to $E\{\mathbf{x}\mathbf{x}^H\}$, $(\cdot)^H$ is Hermitian transpose. We assume that the transmission power is the same for every transmission antenna, and then $Tr(\mathbf{R}_{xx})$ is equal to N_T. $\mathbf{E}_x$ means the energy of the transmitted signals, and $\mathbf{N}_0$ denotes the power spectral density of the additive noise.

Figure 2-14 illustrates a comparison of 2×2, 4×4 and 8×8 MIMO channel capacity. It shows that more antennas we have, more channel capacity will be generated. Although the 8×8 channel has the best channel capacity performance, the computational complexity cannot be accepted for the proposed blind multiuser detection schemes. The 2 $\times 2$ MIMO channel has 2 antennas in transmitter and 2 antennas in receiver. Since the number of antennas is limited, it is not representative for the proposed SDMA-based uplink MIMO OFDM system. As for how many of them are suitable, it is still an open question. There is no statement that the amount of antennas should be as many as possible. Thus, the 4×4 MIMO channel is selected for the proposed blind multiuser detection schemes in the proposed SDMA-based uplink MIMO OFDM system.
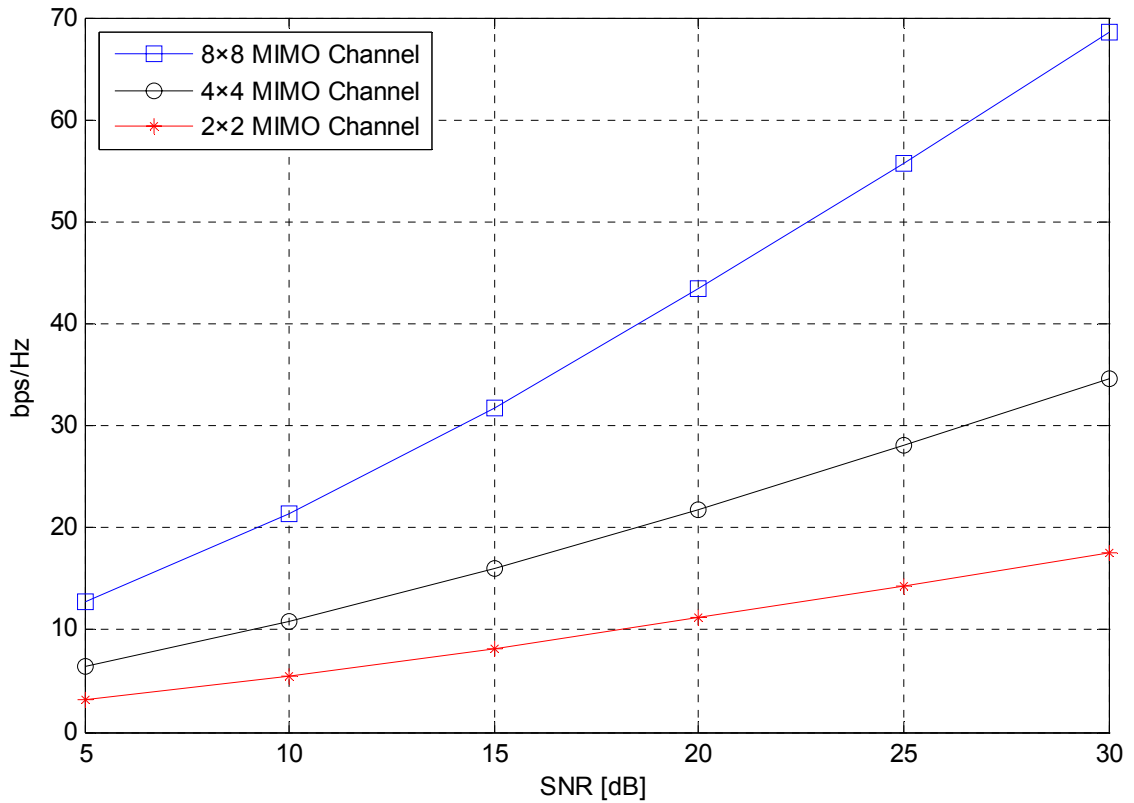
Figure 2-14 Comparison of the MIMO Channel Capacity with Different Amount of Antennas

2.4 ODFM Techniques

One of the fundamental objectives of the proposed wireless communication system is to support a high data rate and to integrate multimedia types through a unified platform. A common scenario to support this purpose is the OFDM [33], [34], which is a frequency-division multiplexing (FDM) scheme. Although the conception of OFDM can be dated back to the 1950s, high cost of implementation through analog filters is the major issue, which prevented the implementation of this scheme at that time. Fast Fourier

transform (FFT) made this implementation possible later. From then on, OFDM became more and more popular in wireless communication. Subsequently, the OFDM technique was applied in IEEE 802.11a in 1999, IEEE 802.11g in 2002, and IEEE 802.16e broadband wireless access in 2005. In recent years, this method has been taken as the key part of 3G and 4G cellular communication standard.

From a theoretical standpoint, the principal advantage of OFDM compared with single carrier schemes is the ability to divide data streams into several parallel narrowband subchannels (also called sub-carriers or subcarriers) at a low symbol rate, which means simplified channel equalization. Other advantages of the OFDM techniques include robustness against fading, low sensitivity to time synchronization errors, and so on. In addition, there are some disadvantages of OFDM systems such as sensitivity to the frequency synchronization and Doppler shift, poor power efficiency, and loss of spectrum caused by the Cyclic Prefix (CP) [35].

The orthogonal property between subcarriers is viewed as an essential part of the OFDM scheme in order to overlap frequency spectrum, and provide undisturbed channels. Compared with the OFDM scenario, the conventional frequency division multiplexing requires guard intervals between different subchannels that do not overlap with each other. Figure 2-15 shows a comparison between these two schemes. Although the realization for the conventional method is a straightforward task when the number of subcarriers is less than 64, the disadvantage is its low spectral efficiency. On the contrary, the OFDM system with more than 64 subcarriers is able to make use of the spectrum resource in high efficiency.

The OFDM scheme is not only used in the proposed SDMA-based uplink MIMO OFDM system but also has become the choice for a lot of high profile wireless systems such as WiFi, WiMax and Ultra-Wideband (UWB) [36]. The structures of the OFDM transmitter module and the OFDM receiver module are provided in this section in order to apply them to the proposed SDMA-based uplink MIMO OFDM system.
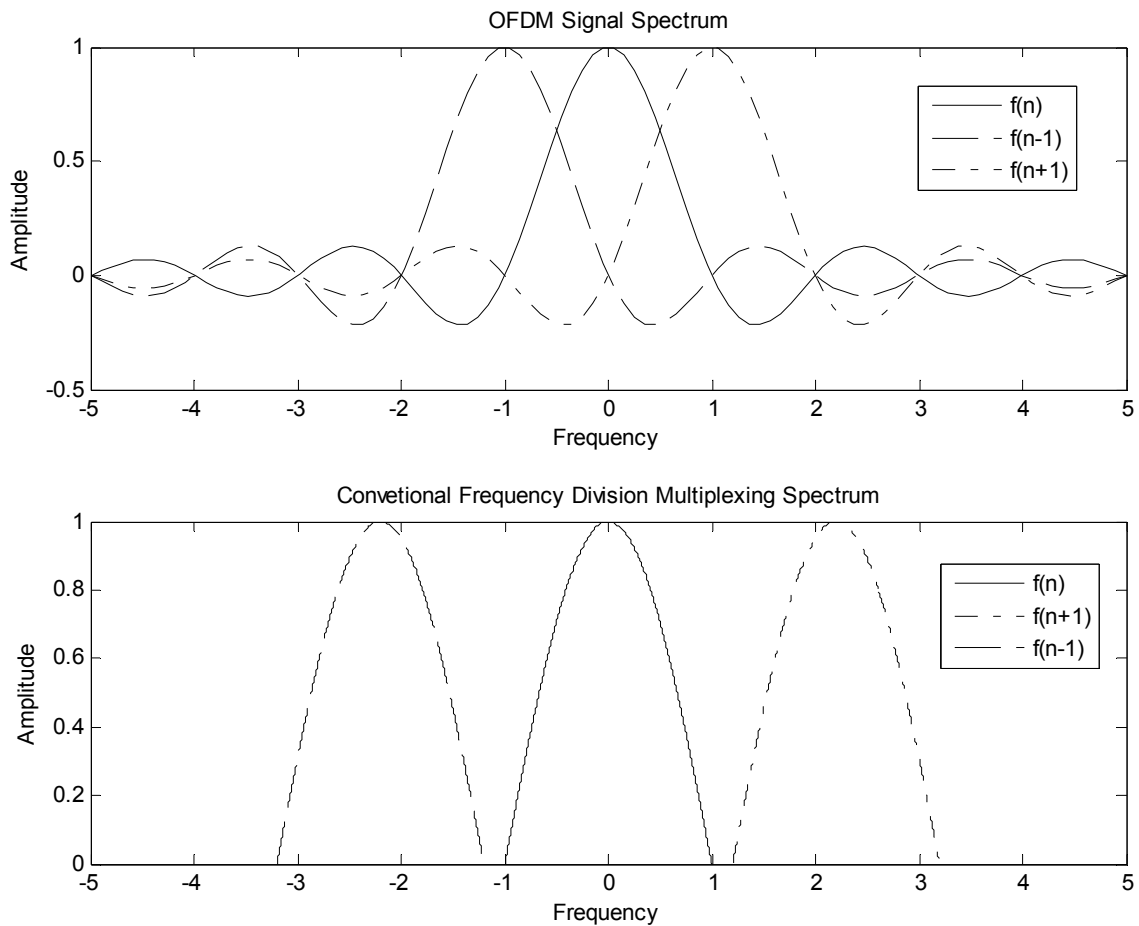
Figure 2-15 OFDM Signal Spectrum vs. Conventional FDM Signal Spectrum

If N subcarriers are used, the OFDM signal can be represented as:

$$s(t) = \sum_{n=0}^{N-1} S_n e^{\frac{j2\pi nt}{T}}, \qquad 0 \le t \le T \tag{2.13}$$

where $\{S_n\}$ is the data symbols, N is the total number of subcarriers, T is the symbol time, $1/T$ is the frequency of subcarriers, and all of subcarriers are orthogonal with each other during this symbol period T.
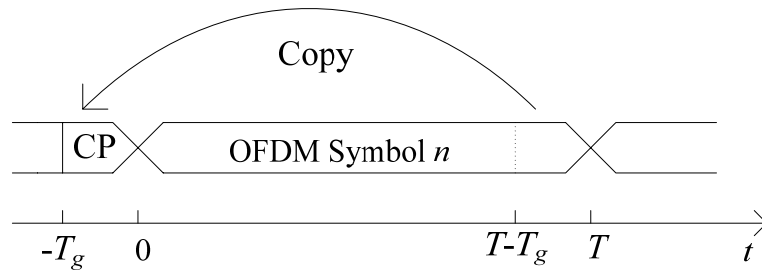
Figure 2-16 OFDM Symbols with Cyclic Prefix

If a guard interval with the length T_g is added prior to the OFDM signal, the signal in the interval $-T_g \le t < 0$ will be equal to the signal in the interval $(T-T_g) \le t < T$ to increase the robustness. The length of the guard interval should be larger than the delay of multipath channels to eliminate ISI. ISI relies on the duration of the symbol period. A shorter symbol time or/and a higher transmission data rate may bring a larger ISI. But it is quite clear that to increase this guard interval will reduce the spectrum efficiency. Thus, there is a trade-off between the guard interval and the spectrum efficiency. The design strategy is to increase the length of guard interval as much as possible with preconditions of enough spectrum efficiency and good anti-ISI ability. Figure 2-16 shows this guard interval and the arrow in this figure show this copy procedure. Then the OFDM signal with guard interval is

$$s(t) = \sum_{n=0}^{N-1} S_n e^{\frac{j2\pi nt}{T}}, \qquad -T_g \leq t \leq T \tag{2.14}$$

Assume this baseband OFDM signal is carried by a carrier frequency f_c, and then the transmitted signal can be expressed as:

$$y(t) = \mathrm{Re}\{s(t)e^{\frac{j2\pi f_c t}{T}}\} = \sum_{n=0}^{N-1} |S_n| \cos(2\pi\left(\left[f_c + \frac{k}{T}\right]t + \arg[S_n]\right) \tag{2.15}$$

where Re(·) denotes the real part of a complex value, and arg(·) stands argument on a complex value.

An inverse discrete Fourier transform (IDFT) or inverse fast Fourier transform FFT (IFFT) based OFDM transmitter module is shown in Figure 2-17. The IDFT/IFFT procedure is used to produce OFDM transmission signals. IDFT is a conventional mathematical method and IFFT is a calculation application of IDFT in a fast way. In the same way, discrete Fourier transform (DFT) and fast Fourier transform have the same relationship. For the proposed SDMA-based uplink MIMO OFDM system, it is more convenient to apply IFFT and FFT, because they can reduce the computational complexity remarkably. The following processes are deemed necessary in order to achieve the OFDM transmitter.

- Phase Shift Keying (PSK) / Quadrature Amplitude Modulation (QAM) encoder transfers the input bit sequences into Binary Phase Shift Keying (BPSK) / Quad Phase Shift Keying (QPSK) / QAM modulated symbols.

- S/P model is a series to parallel converter, which converts users' discrete-time BPSK/QPSK/QAM modulated symbols into parallel data streams.

- IDFT/IFFT module transforms the parallel data streams into N low-rate parallel sub-channels. Assume the carrier frequencies are $f_0, f_1, \ldots, f_{N-1}$. The difference in neighbor carrier frequencies is Δf. So the total bandwidth W is equal to $N\Delta f$. Thus, the symbol duration is extended by the factor of N and these N sub-carriers are orthogonal with each other.

- Cyclic Prefix, which avoids ISI at the transmitter, is added to each OFDM symbol before transmission and it is removed at the receiver.

- P/S model is a parallel-to-serial converter, which combines N modulated subcarriers to create the OFDM transmission signal.
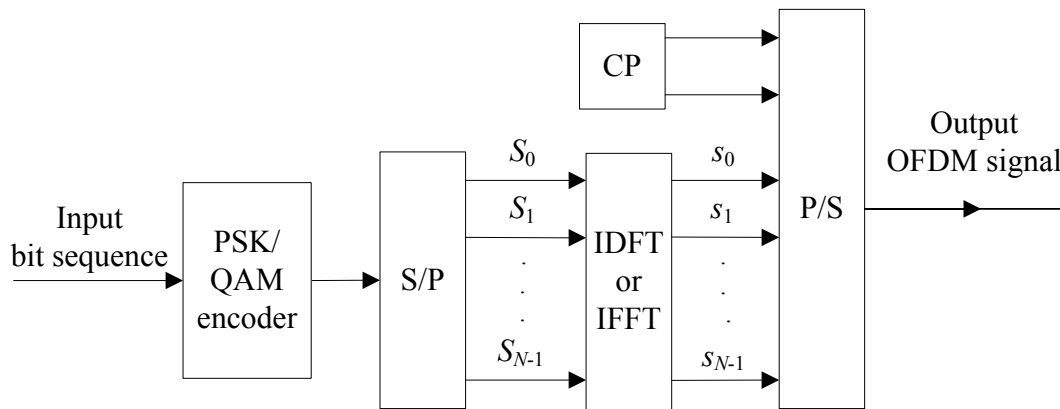
Figure 2-17 OFDM Transmitter Module

Figure 2-18 shows the structure of the OFDM receiver module. Through the serial-to-parallel converter at the receiver, the OFDM signal is demultiplexed into N sub-channels again. After remove the CP, the DFT/FFT module demodulates these OFDM symbols. The baseband BPSK/QPSK/QAM signal is then recombined through a parallel-

to-serial converter. Finally, the output bit sequence is generated by the PSK/QAM decoder module. Although the DFT/FFT modulation increase the implementation complexity compared with a conventional serial model, the *N* times lower symbol rate is less sensitive to ISI than the conventional serial system. Therefore, the channel equalization will be avoided in this case.
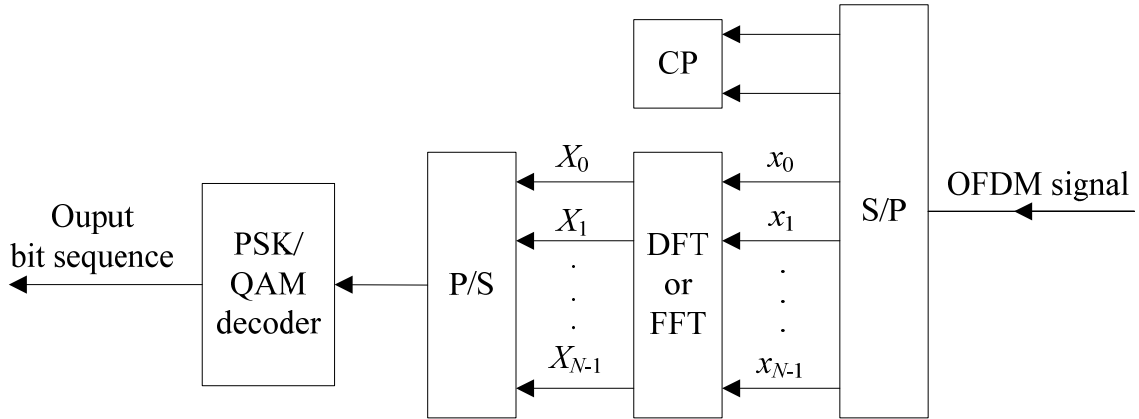
Figure 2-18 OFDM Receiver Module

The BER performance of the OFDM scheme can be theoretically described by the following two equations for AWGN and Rayleigh fading channels, respectively [37]. The Rician channel is not given here, because it is similar to an AWGN or Rayleigh fading channel, according to the simulation from Figures 2-10 and 2-11.

$$P_e\_AWGN = \frac{2(M-1)}{M\log_2 M}Q(\sqrt{\frac{6E_b}{N_0}\cdot\frac{\log_2 M}{M^2-1}}) \tag{2.16}$$

$$P_e\_Rayleigh = \frac{M-1}{M\log_2 M}(1-\sqrt{\frac{3(E_b/N_0)\log_2 M/(M^2-1)}{3(E_b/N_0)\log_2 M/(M^2-1)+1}}) \tag{2.17}$$

where *M* indicates the modulation order, and *M* is 2, 4, 8, 16, 32, 64 for BPSK, QPSK, 8-QAM, 16-QAM, 32-QAM and 64-QAM, respectively. $Q(\cdot)$ is the standard *Q*-function defined by

$$Q(x) = \frac{1}{\sqrt{2\pi}} \int_x^{\infty} e^{-t^2/2} dt \qquad (2.18)$$
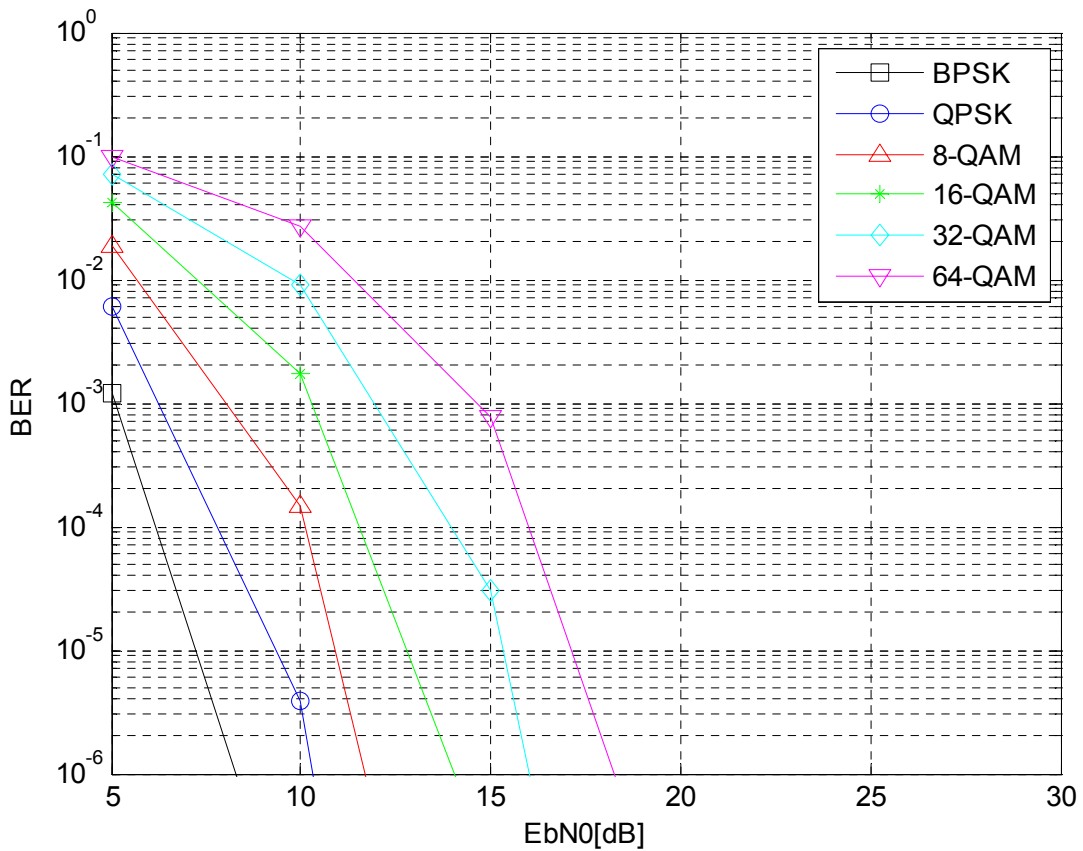
Figure 2-19 BER Performance of the BPSK/QPSK/QAM Modulations in the AWGN Channel

According to Equations 2.16 and 2.17, the BER performance of BPSK, QPSK and QAM modulations in an AWGN channel or a Rayleigh fading channel is simulated, and Figures 2-19 and 2-20 show their performances. BPSK, QPSK, 8-QAM, 16-QAM, 32-

QAM and 64-QAM have different transmission rate, e.g. 1, 2, 3, 4, 5, and 6 bits per symbol, respectively. Generally, the faster the transmission rate is, the more attractive the result is. However, the simulation results show that with the increment of the transmission rate, the BER performance becomes worse. One of goals in this dissertation aims to identify the best BER performance. Based on the simulation results, the BPSK modulation possesses the best performance, so it is selected for the proposed SDMA-based uplink MIMO OFDM system.
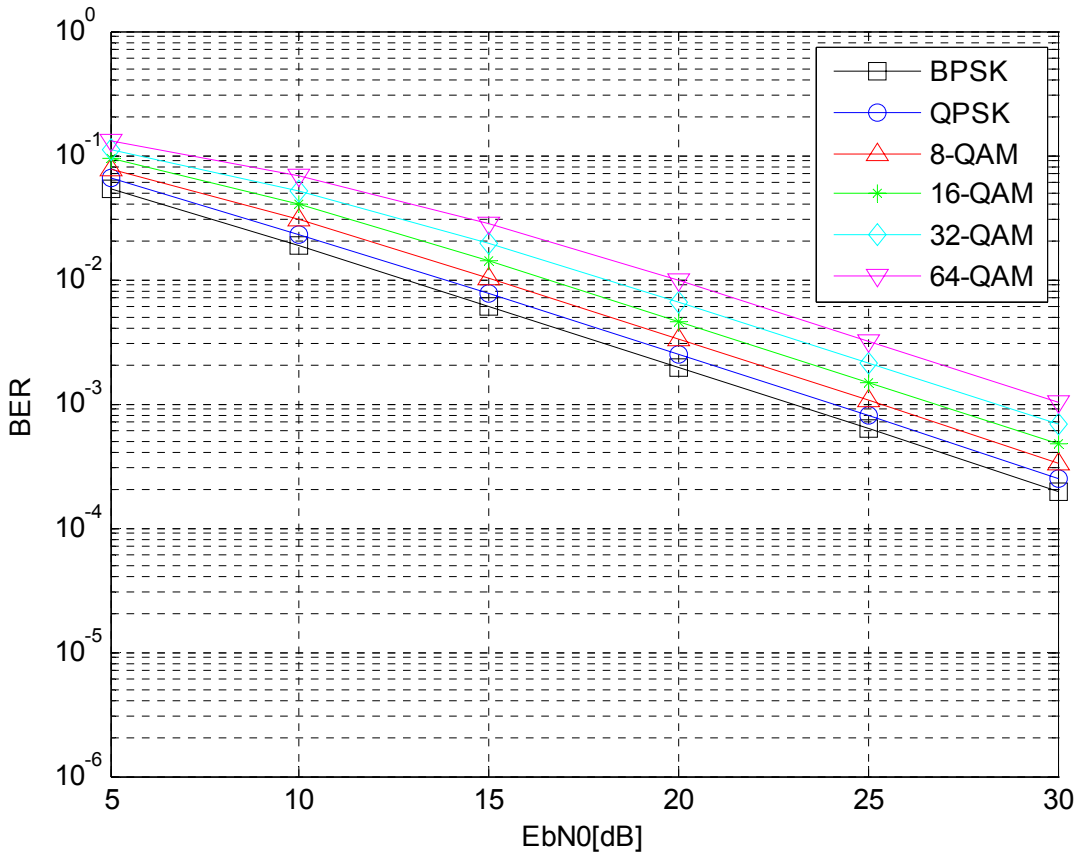
Figure 2-20 BER Performance of the BPSK/QPSK/QAM Modulations in the Rayleigh Fading Channel

Baseband OFDM signals with the BPSK modulation are shown in Figure 2-21, Figure 2-22 and Figure 2-23. The oversampling factor and the number of subchannels are set to 8 and 4, respectively. In fact, the experimental and meaningful amount of subchannels should be at least 64. Figure 2-24 illustrates the OFDM baseband signals when the number of subchannels is 64. In order to give us a straightforward and clear vision of the track of the mixed procedure, only 4 channels are chosen in Figures 2-21, 22, 23 to illustrate the processes. Figure 2-21 shows the real part of 4 subchannel signals and the sum of them, while Figure 2-22 demonstrates the imaginary part. The OFDM signals in the time domain when N is 4 and 64 are illustrated in Figure 2-23 and Figure 2-24, respectively.
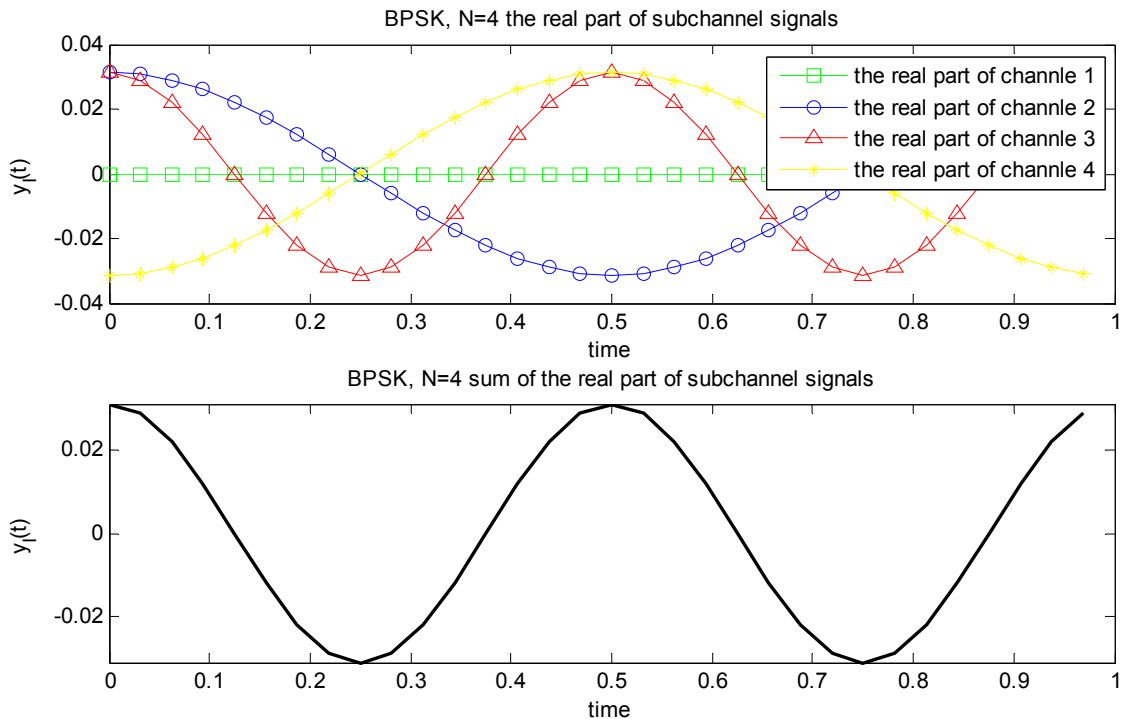
Figure 2-21 Real Part of OFDM Signals with the BPSK Modulation and $N = 4$
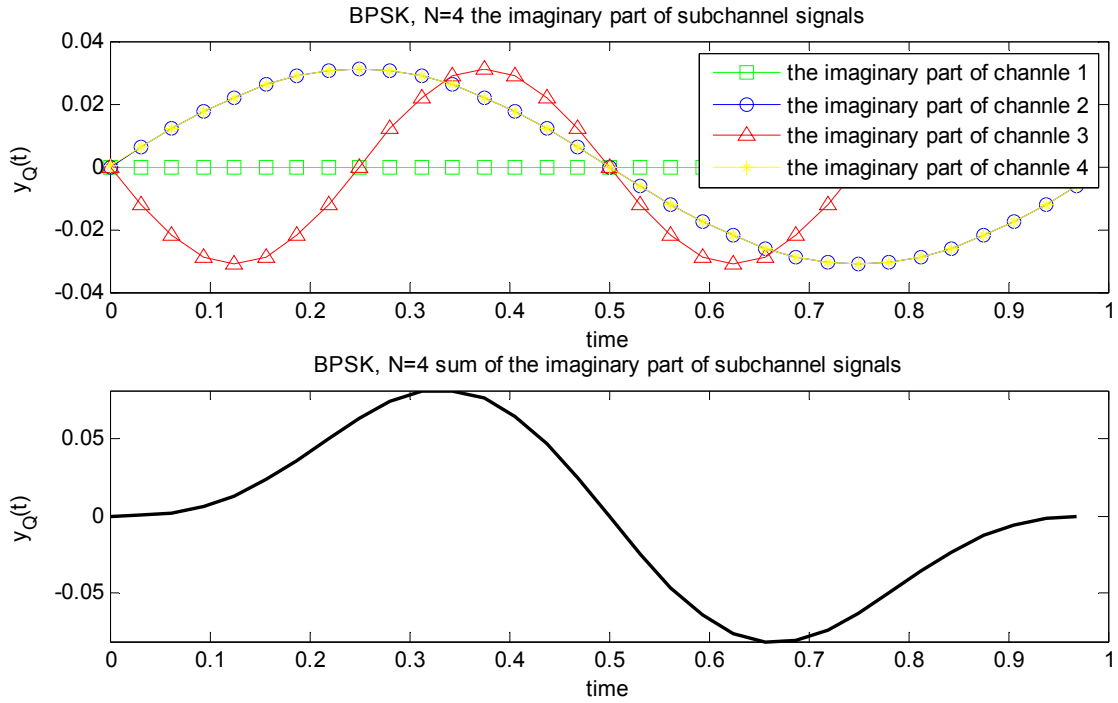
Figure 2-22 Imaginary Part of OFDM Signals with the BPSK Modulation and *N* = 4
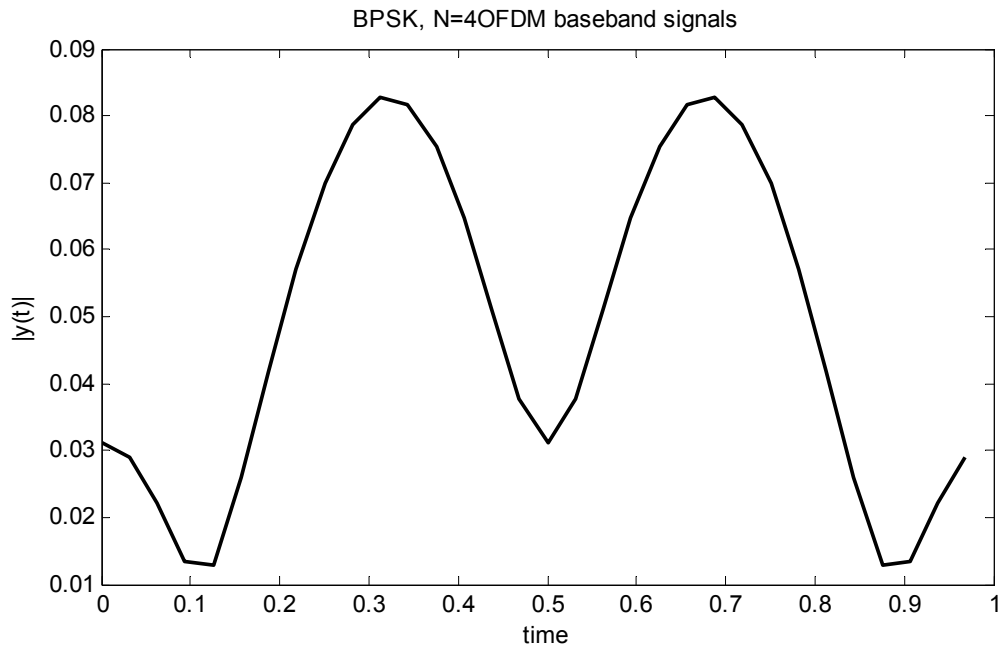
Figure 2-23 OFDM Baseband Signals with the BPSK Modulation and *N* = 4
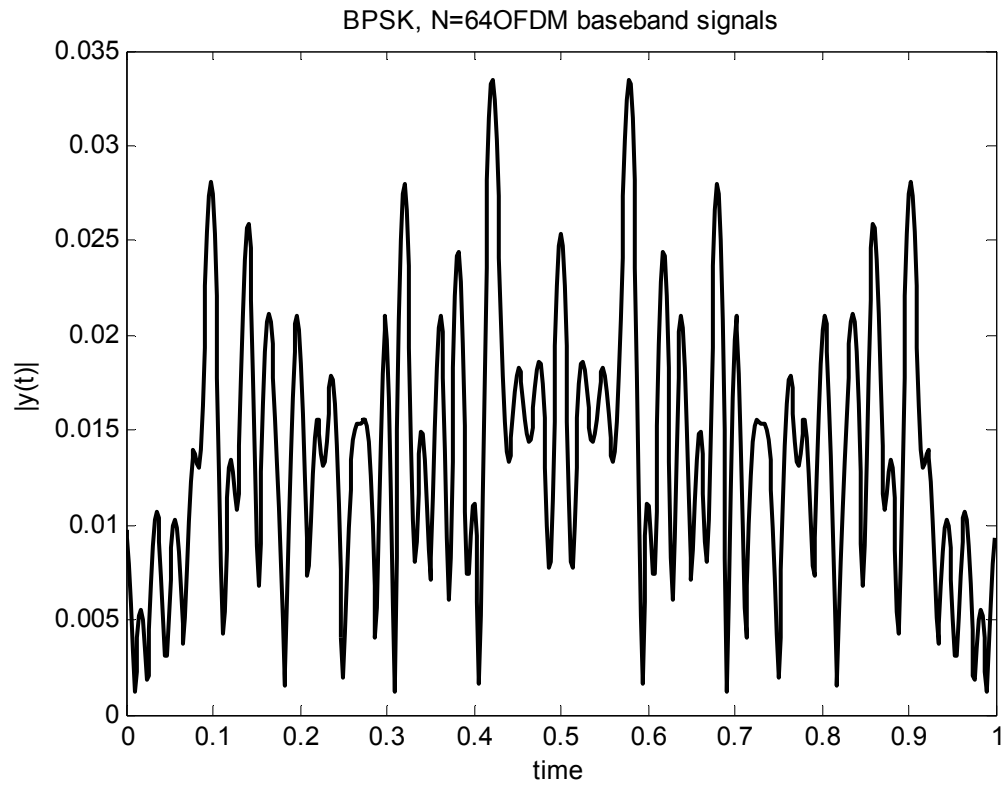
Figure 2-24 OFDM Baseband Signals with the BPSK Modulation and *N* = 64

CHAPTER 3

BLIND SIGNAL SEPARATION TECHNIQUES

This chapter presents a signal-processing scheme, which is called ICA [3-8], aimed at separating mixed independent source signals only through observed output signals without information about input signals. B. Ans, J. Hérault and J.C. Jutten introduced the ICA theory in the 1980s [38]. Then, BSS techniques by ICA were developed quickly and they have been a very active frontier for researchers in recent years. BSS techniques have a wide range of applications in communications [39-41], biomedical signal processing [42-46], audio source separation [47-52], image processing [53-58] and so on. Furthermore, BSS techniques can be applied to the proposed SDMA-based uplink MIMO OFDM system to save the expensive channel resources, compared with the conventional multiuser detection schemes. A group of complex FastICA algorithms is analyzed and simulated in this chapter, and a suitable one is obtained for three proposed blind multiuser detection schemes.

3.1 Blind Signal Separation Theory

The rigorous definition of ICA is

$$\mathbf{x} = \mathbf{Hs} \tag{3.1}$$

where $\mathbf{x}$ is the observed mixed random column vector with elements $x_1, x_2, \ldots, x_n$ and $\mathbf{s}$ is the original random column vector with elements $s_1, s_2, \ldots, s_m,$ which are called

independent components. The full column rank matrix $\mathbf{H}$ with elements H_{ij} means an unknown mixed procedure.

All elements of $\mathbf{H}$ and $\mathbf{s}$ are assumed to have zero mean. The elements s_i should obey non-Guassian distributions. The noise elements are omitted here and the number of observed elements is the same as that of original independent components for description simplicity. That means n is equal to m. This statistical model means how the observed data $\mathbf{x}$ are generated by a process of mixed $\mathbf{s}$. We assume that the separation matrix for mixed real source signals is $\mathbf{W}$, and the separation matrix for mixed complex source signals is $\mathbf{W}^H$. Our goal is to process mixed complex source signals with BSS in the SDMA-based uplink MIMO OFDM system, so $\mathbf{W}^H$ is selected here. The separation of mixed complex source signals can be described as

$$\mathbf{s} = \mathbf{W}^H \mathbf{x} \tag{3.2}$$

where $(\cdot)^H$ is the Hermitian transpose.
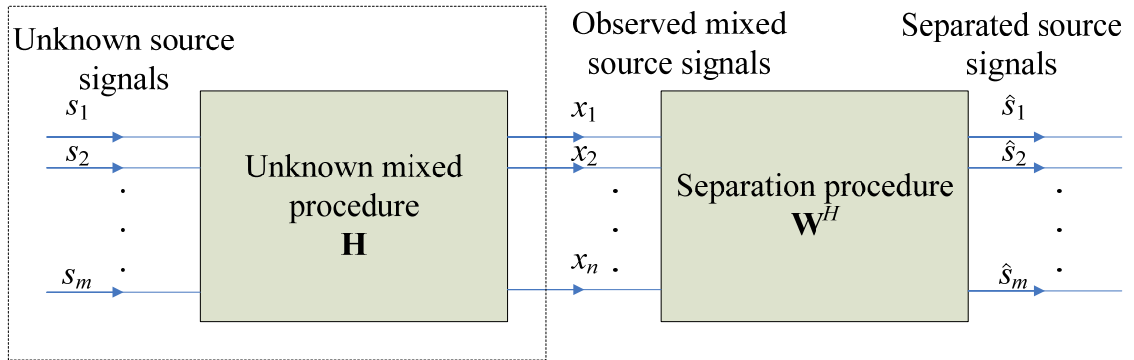
Figure 3-1 Model for BSS by ICA

Now the question focuses on how to find the separation matrix $\mathbf{W}^H$. Based on the statistically independent property of source signals, which have to be from different physical processes (e.g., different mobile users), ICA can be used to separate the mixed complex signals. The model for BSS by ICA is shown in Figure 3.1.
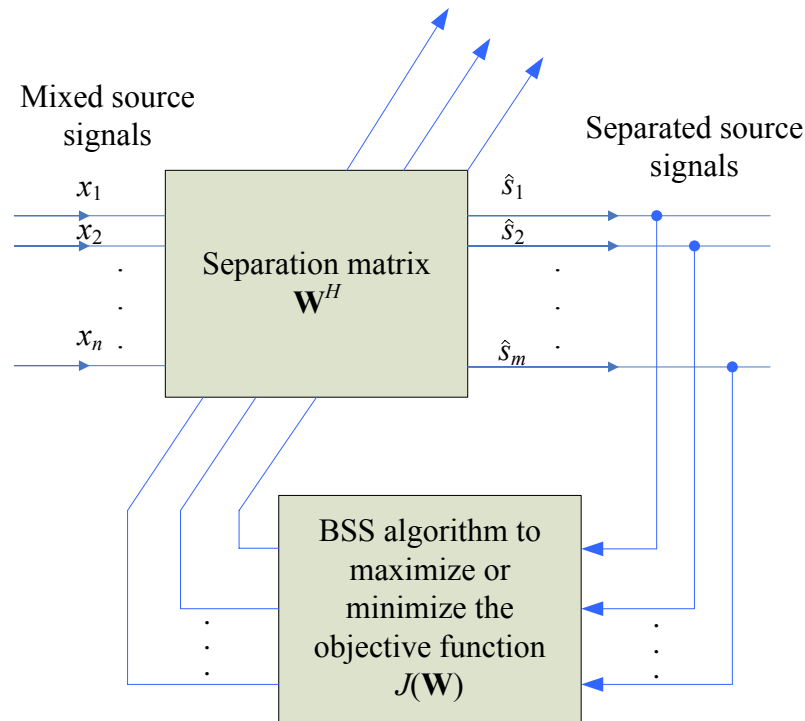
Figure 3-2 Separation Procedure by BSS

The separation process primarily includes two parts: (1) setting up an objective function and (2) tracking its optimization to implement the approximation. Figure 3-2 shows the schematic diagram of this process. It is impossible to obtain the optimized separation $\mathbf{W}^H$ directly with unknown mixture and source signals. Therefore, an initial guess of the separation matrix $\mathbf{W}^H$ with the objective function $J(\mathbf{W})$ is given to the BSS algorithms first. To obtain an optimized separation matrix $\mathbf{W}^H$, the following step is to

adjust the objective function $J(\mathbf{W})$ which is normally maximized or minimized. Different BSS algorithms have their own strategies for the optimization. The updated separation matrix $\mathbf{W}^H$ tries to let their separated independent elements approach the source signals as close as possible. Finally, an optimized matrix $\mathbf{W}^H$ is obtained for the separation.

3.2 ICA Classifications

In [12], it is noticeable that the ICA model for MIMO OFDM systems is an instantaneous linear mixture of each subcarrier, which is a basic requirement that allows the application of ICA to blind multiuser detection in MIMO OFDM systems. The recent research works include two classifications, which are second-order statistics (SOS) and higher-order statistics (HOS). A subspace approach, which is a kind of SOS methods, has been proposed by [9] in MIMO systems. But this scheme requires additional feedback information of transmission channel. Since HOS blind signal separations can produce a better BER performance, the existing HOS algorithms will be employed in this research work. Three vital HOS blind signal separation algorithms, Nature Gradient [14], [59], [60], Joint Approximate Diagonalization of Eigenmatrices (JADE) [12], [61] and FastICA [5], [13], [62], will be focused on.

3.2.1 Nature Gradient Algorithm

The authors in [14] choose nature gradient algorithm for MIMO OFDM systems because it has a hardware-friendly iterative processing structure. The nature gradient algorithm is proposed by [59] for real-valued signals. The complex-valued nature

gradient algorithm is given by [60] and it is capable of being applied to MIMO systems. The separation matrix is given by the following steps

1) Organize the output according to the frequency bin index in which the mixed source signals can be treated as a set of instantaneous mixture.

2) Set up the Nature Gradient learning rule at every frequency bin index. The complex version of this rule is given by

$$\Delta \mathbf{W} \propto [\mathbf{I} - f(\mathbf{y})\mathbf{y}^H]\mathbf{W} \tag{3.3}$$

where $\mathbf{y} = \mathbf{W}\mathbf{x}$, $f(\cdot)$ is a non-linear sigmoid function in the complex domain. The important point is how to choose an appropriate sigmoid function in the complex domain. The conventional sigmoid functions show poor performance due to their singularities in the complex domain. Therefore, a proper choice of the sigmoid function to fulfill all complex activation function requirements is made, which is defined as [60]

$$f(y_i) = \tanh[Re(y_i)] + j*\tanh[Im(y_i)] \tag{3.4}$$

3) Generate the whole separation through Equation (3.2) at every frequency bin index. Although to do the separation at each frequency bin index will increase the amount of separations, the separation by Nature Gradient remains the same complexity and convergence properties at every frequency bin index. In addition, all of frequency bins are orthogonal with each other, and every separation is

independent. Thus, the computational performance can be improved, compared with the separation without using frequency bins.

4) Identify the scaling and permutation for each user. The drawback of Nature Gradient at every bin index is the ambiguity of scaling and permutation for each user. A useful solution is to calculate the correlation in different frequency bin to remove the uncertainty [14]. After this step, the source signals can be recovered.

3.2.2 JADE Algorithm

The authors in [12] employ JADE [61] to MIMO systems because the JADE algorithm is a "parameter free" blind receiver and this algorithm is able to make data-sequences shorter compared with other BSS algorithms. The procedure to apply JADE algorithm is divided into the following steps:

1) To decrease the complexity of the mixed signals, the received signals need to be whitened from the Eigenvalue Decomposition of the covariance matrix of the received signal. A random whitened vector $\mathbf{z}$ has the following property

$$E\{\mathbf{z}\mathbf{z}^H\} = \mathbf{I} \tag{3.5}$$

where $\mathbf{I}$ is the unit matrix. This step is related to second order statistics, and the BSS problem is significantly simplified by this whiten step.

2) The unit variance soft stream is obtained by

$$\mathbf{s} = \mathbf{V}^H\mathbf{z} \tag{3.6}$$

where $\mathbf{V}$ is found by minimizing the orthogonal contrast function $\Phi_{\text{JADE}}[\cdot]$, which is a 4th order approximation of a mutual information based contrast function.

$$\mathbf{V} = \arg\min_{\mathbf{V}} \phi_{\text{JADE}}[\mathbf{s}] \tag{3.7}$$

3) Generate the whole separation through Equation (3.6). For an MIMO OFDM system, this stream estimation can be employed to every subcarrier.

4) Identify the scaling and permutation for each user. Because most of BSS methods have a similar scaling and permutation indeterminacy, this step has to be added to obtain the source signals.

3.2.3 FastICA Algorithm

Among existing HOS algorithms, the complex FastICA algorithm [62] is adopted for the proposed SDMA-based uplink MIMO OFDM system because of its fast convergence, less computation complexity, and good BER performance. The related real-valued algorithm is first proposed by [5] and this algorithm is extended to complex-valued signals [62], which can be employed in MIMO OFDM systems.

The members of the family of the complex FastICA algorithms are differentiated by both algorithmic methods and different contrast functions. The algorithmic methods mainly include two ways that are the symmetric approach and the deflation approach. The former can update the separation matrix simultaneously and separate the independent sources at the same time. On the other hand, the latter can only update the columns of separation matrix individually and find one independent source at a time. Although it is

an attractive feature of the complex FastICA family to recover only one or some of the source signals if the exact number of independent components is not identified, we will only consider symmetric approach in order to have a better convergence speed to separate all of the source signals at the same time.

Before using the complex FastICA to estimate the original signals, the received signals in every subcarrier should be whitened. It means the observed vector **x** is linearly transformed and a new whitened vector is obtained. The whitening process is less complicated than any ICA algorithms. This standard procedure can reduce the number of parameters to be estimated and solve half of the problem of ICA [5]. The whitening process can be worked out by Principal Component Analysis (PCA) [6]. Equation 3.5 is a useful example to do the whitening process.

According to [62], the contrast functions are minimized or maximized by modifying the separation matrix **W** for every **H**. The contrast function adopted in this research is

$$J_G(\mathbf{w}) = E\{G(\left|\mathbf{w}^H \mathbf{x}\right|^2)\}$$
(3.8)

where G is a smooth even function, E is the expectation, **w** is an n-dimensional complex weight vector, and $E\{|\mathbf{w}^H\mathbf{x}|^2\}=1$. The members of complex FastICA algorithms depend on the diverse G functions, three choices of G functions are:

$$G_1(y) = \sqrt{a_1 + y} \qquad a_1 \approx 0.1$$
(3.9)

$$G_2(y) = \log(a_2 + y) \qquad a_2 \approx 0.1 \tag{3.10}$$

$$G_3(y) = \frac{1}{2}y^2 \tag{3.11}$$

Here y is a complex-valued random variable, denoted as $y = u + iv$. And u and v are real-valued random variables.

The G function mainly determines two aspects in the complex FastICA algorithm, which are the BER performance and the computational complexity. A complicated $G(\cdot)$ function means the contrast function $J_G(\cdot)$ is complicated as well, which is able to give a better BER performance but show a worse computational complexity in comparison with a simple $G(\cdot)$ function when estimating source signals. It is straightforward that the G_1 and G_2 functions are more complicated than the G_3 function.

Table 3-1 Elements of the random complex mixed matrix H

0.6880 + 0.2808i	0.7443 + 0.8011i	0.3774 + 0.2584i	0.8930 + 0.4045i	0.8218 + 0.5355i
0.6420 + 0.4613i	0.0433 + 0.6797i	0.8511 + 0.0132i	0.6142 + 0.5300i	0.0941 + 0.6180i
0.5852 + 0.7155i	0.7037 + 0.3266i	0.9258 + 0.6988i	0.0569 + 0.1501i	0.0802 + 0.9172i
0.4133 + 0.9909i	0.9719 + 0.7312i	0.2718 + 0.5297i	0.5791 + 0.1940i	0.8348 + 0.4662i
0.5437 + 0.0504i	0.9747 + 0.8843i	0.1669 + 0.2096i	0.3790 + 0.2666i	0.0288 + 0.5857i

A MATLAB simulation for these three $G(\cdot)$ functions is shown in Figure 3-3 to determine which $G(\cdot)$ function has the best BER performance. We assume that there are

five source signals and the length of each is set to 50,000 bits. The distributions of the five source signals considered in this simulation include Binomial distribution, Gamma distribution, Poisson distribution, Hyper-geometric distribution and Beta distribution. These complex source signals are mixed by a random complex matrix **H** whose elements are shown in Table 3-1.
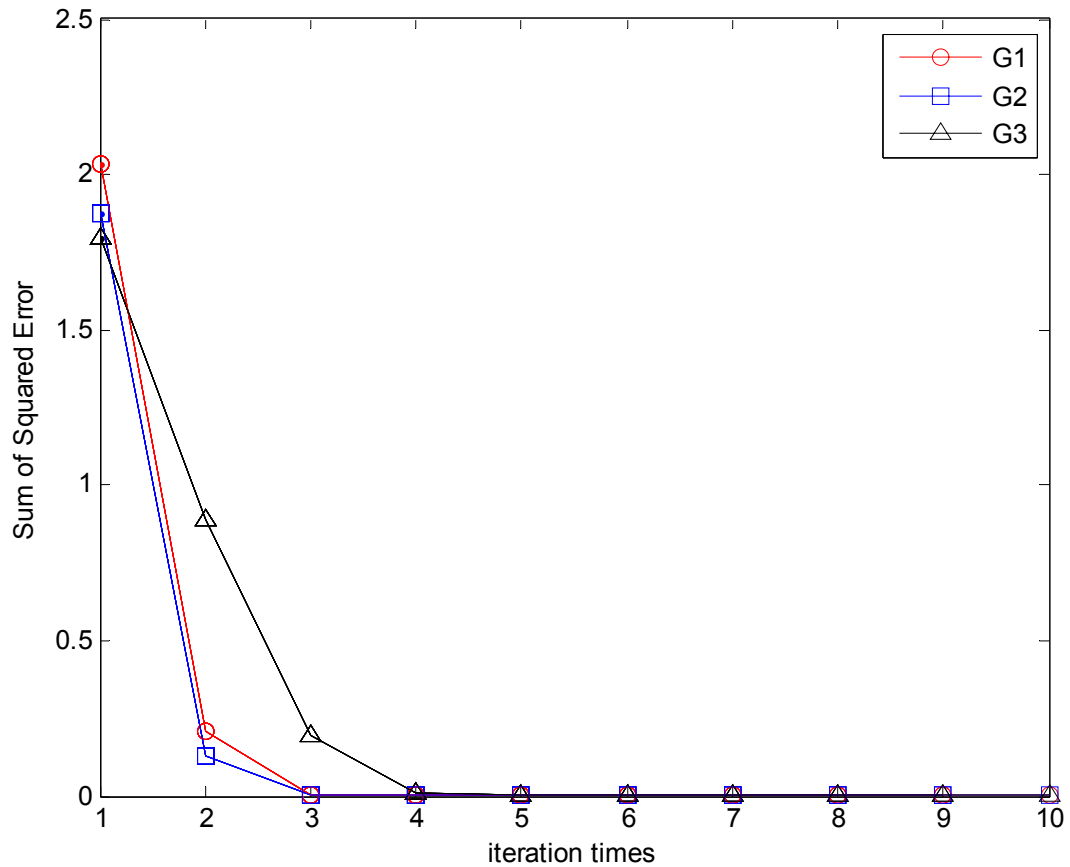
Figure 3-3 A Comparison of G_1, G_2, G_3 Functions

From Figure 3-3, it is noticeable that G_2 needs to run 3 iterations to converge. G_3 requires about 4 iterations while G_1 necessitates 3 iterations. So we can say that all of the

$G(\cdot)$ functions take similar number of iterations for convergence, also G_2 has the best Sum of Square Errors (SSE) performance, which is equivalent to the best BER performance. Therefore, the G_2 function is selected for the complex FastICA algorithm that will be applied to the proposed blind multiuser detection schemes.

The iteration matrices, $\mathbf{w}^+$ and $\mathbf{w}_{new}$, are given by [62]

$$\mathbf{w}^+ = E\{\mathbf{x}(\mathbf{x}(\mathbf{w}^H\mathbf{x})^* g(|\mathbf{w}^H\mathbf{x}|^2)\} - E\{g(|\mathbf{w}^H\mathbf{x}|^2) + |\mathbf{w}^H\mathbf{x}|^2 g^{'}(|\mathbf{w}^H\mathbf{x}|^2)\}\mathbf{w} \qquad (3.12)$$

$$\mathbf{w}_{new} = \frac{\mathbf{w}^+}{\|\mathbf{w}^+\|} \qquad (3.13)$$

where $(\cdot)^+$ is the pseudo-inverse, $(\cdot)^*$ is the complex conjugation, $g(\cdot)$ is the derivative of $G(\cdot)$, $g'(\cdot)$ is the derivative of $g(\cdot)$, and $\|\cdot\|$ is the Euclidean norm. The separation matrix for one source signal can be extended to the whole separation matrix $\mathbf{W}$ for all of l source signals by

$$\mathbf{W} = (\mathbf{w}_1, \ \mathbf{w}_2, \ \ldots, \ \mathbf{w}_l) \qquad (3.14)$$

The final step for the complex FastICA algorithm is to solve the phase/scaling and permutation indeterminacy. In [13], a Phase-Locked Loop (PLL) is performed for each sub-stream to solve the indeterminacy. The permutation and scaling problem can be handled by a statistical correlation method [14]. The phase ambiguity of complex signals is given by [63]

$$a_j s_j = (v_j a_j)(\frac{s_j}{v_j}), \qquad |v_j| = 1, \ v_j \in \mathbb{C} \qquad\qquad (3.15)$$

where v_j is the unknown phase for each s_j, and $\mathbb{C}$ is the complex space. If the distribution of s_j only relies on the modulus of s_j, the variable v_j will not change the distribution of s_j. Thus, the phase of complex signals is undetermined.
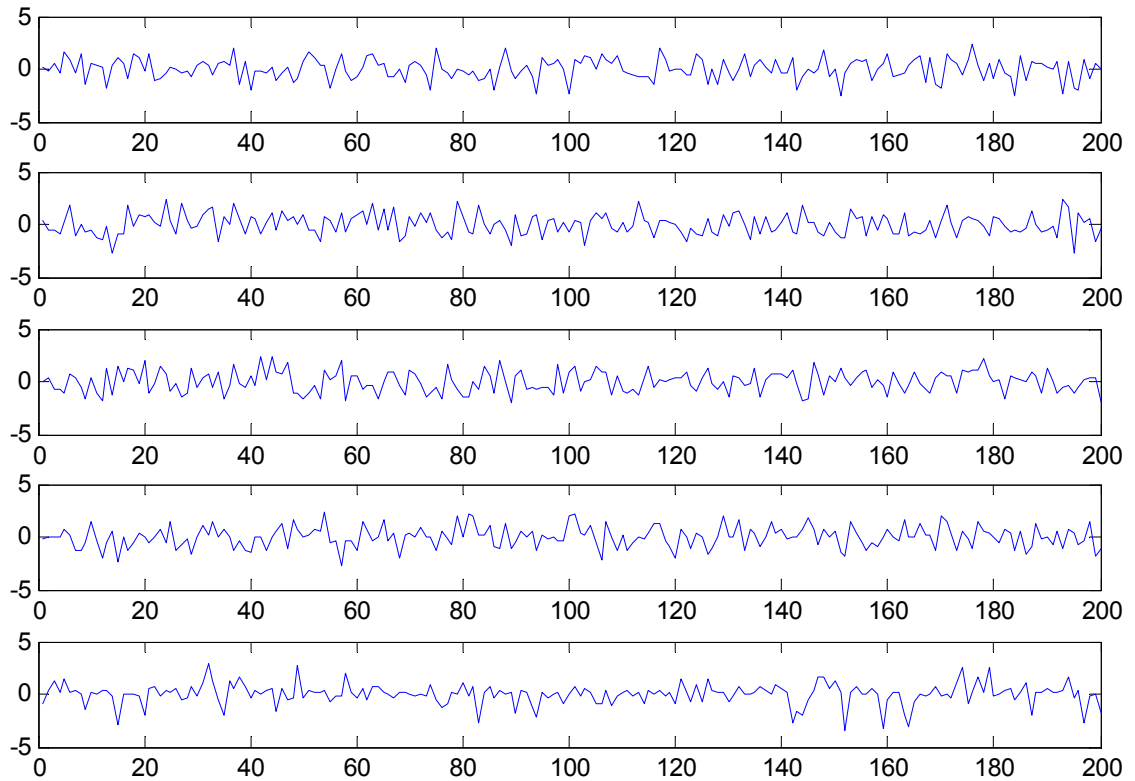
Figure 3-4 Real Parts of Five Complex Source Signals with Binomial Distribution, Gamma Distribution, Poisson Distribution, Hyper-geometric Distribution and Beta Distribution

To simulate the separated signals and track the phase/scaling and permutation indeterminacy, we selected five complex source signals, which are uncomplicated to differentiate them. The real parts of these five complex source signals include: sine wave,

square wave, funny curve, saw-tooth, and impulsive noise. Here, we do not select the same five source signals considered in the simulation as shown in Figure 3-3. Because the source signals with Binomial distribution, Gamma distribution, Poisson distribution, Hyper-geometric distribution and Beta distribution are hard to be distinguished with each other. Figure 3-4 shows 200 data for the real parts of each of the source signals from top to bottom, and they look similar to each other. Thus, we choose another set of five source signals with 200 data for the real parts which can be distinguished without difficulty, shown in Figure 3-5 from top to bottom.
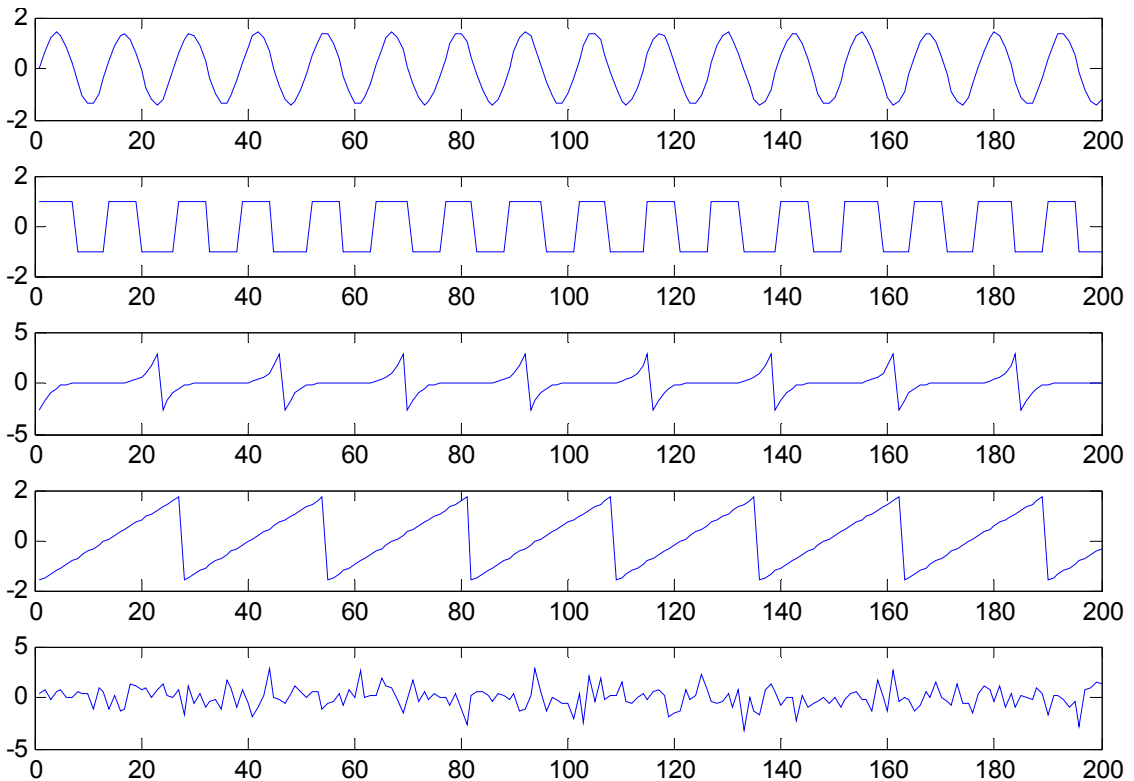
Figure 3-5 Real Parts of Five Complex Source Signals with Sine Wave, Square Wave, Funny Curve, Saw-tooth, and Impulsive Noise
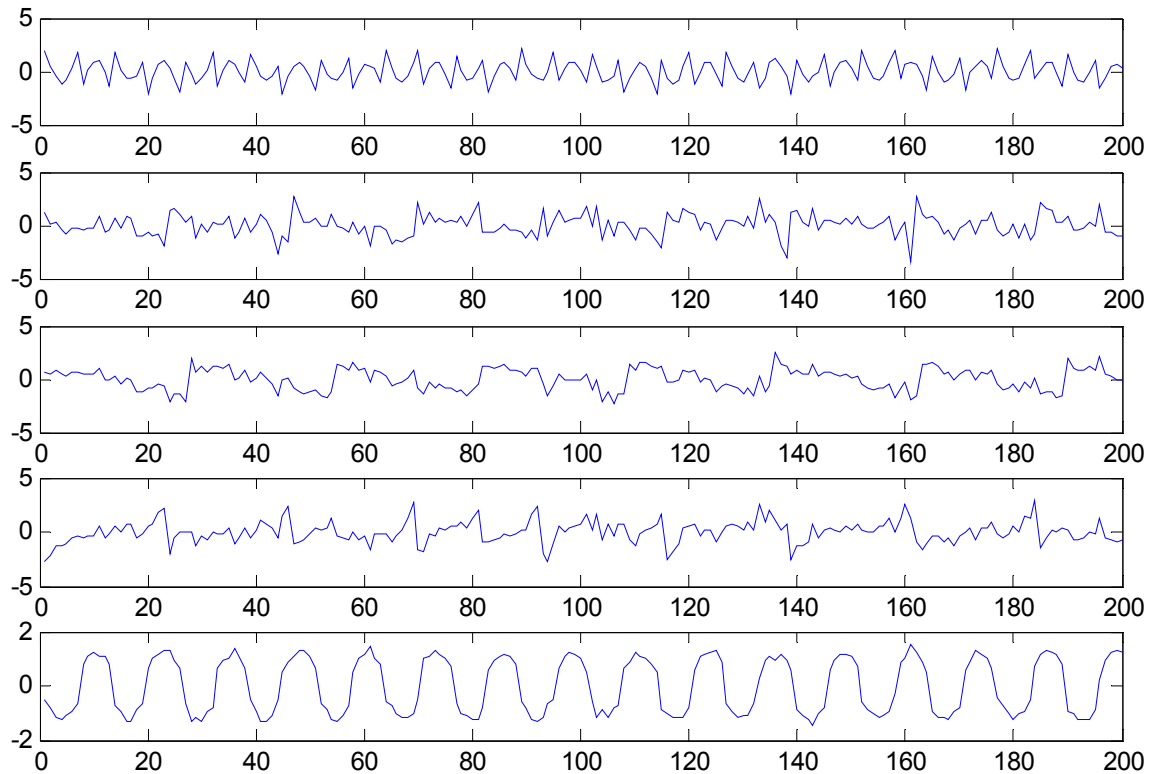
Figure 3-6 Whitened Signals for the Source Signals Shown in Figure 3-5

According to the simulation from Figure 3-3, G_2 function is chosen for the complex FastICA algorithm because of its best BER performance. We apply the complex FastICA algorithm with the G_2 function to five mixed source signals which are shown in Figure 3-5. We assume the order of these five source signals from top to bottom is sine wave, square wave, funny curve, saw-tooth, and impulsive noise. The whitened signals are shown in Figure 3-6. The new whitened signals are obtained by PCA, and the target of this procedure is to reduce the number of parameters to be estimated by FastICA and half of the problem of ICA is solved by this step.
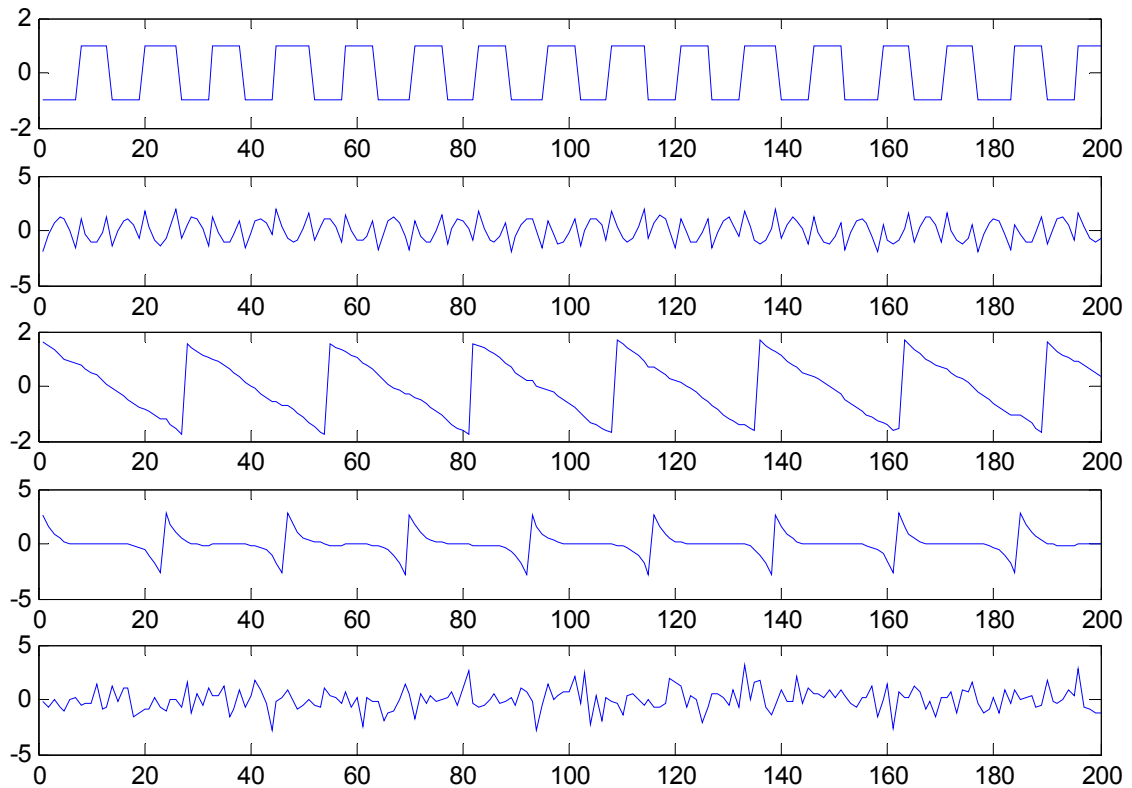
Figure 3-7 Separated Signals for the Real Parts of Five Complex Source Signals with Sine Wave, Square Wave, Funny Curve, Saw-tooth, and Impulsive Noise

After applying the complex FastICA algorithm, the separated source signals for the real parts of those five complex signals are illustrated in Figure 3-7. From this figure, we can find the new order of those five signals is square wave, sine wave, saw-tooth, funny curve, and impulsive noise. Compared with Figure 3-5, the permutation indeterminacy is observed. It is clear that BSS techniques miss the permutation information and the reordering step should be added. In addition, the phase indeterminacy for both saw-tooth and funny curve are also shown in Figure 3-7. In comparison with their original signals, the separated signals are opposite in phase. Thus, this is another

54

issue that needs to be considered. At last, those five separated signals have acceptable separation quality in this simulation.

In general, the step-by-step of this algorithm is summarized as follows:

1) The whitening procedure by PCA [6] is performed to reduce the number of parameters to be estimated.

2) The one-unit algorithm updated matrices for the separation matrix **w** are Equations (3.12) and (3.13). The one-unit algorithm can be extended to the whole separation matrix **W** by Equation (3.14).

3) The estimation of the source signals can be found by Equation (3.2).

4) Identify the phase offset and permutation indeterminacy for each user.

CHAPTER 4

BLIND MULTIUSR DETECTION SCHEMES

This chapter proposes three blind schemes for signal detection in the SDMA-based uplink MIMO OFDM system. These schemes include BSS-only, BSS-MMSE and BSS-MBER for the SDMA-based uplink MIMO OFDM system. From the theoretical point of view, these blind multiuser detection schemes are analyzed and compared with each other for the best BER performance, the best computational efficiency, or a compromise between the BER performance and the computational complexity.

4.1 BSS-only Scheme

At the receiver of an MIMO OFDM system, the mixed signals are always delayed by transmission through multiple paths. Since the mixed signals cannot arrival at the receiver at the same time, the observation is a convolutive mixture of source signals because of the delays. To find a solution for the separation of the convolutive mixture is complicated because the separation process requests memory for the mixture. Therefore, an attractive solution is to transform the convolutive mixture into the instantaneous mixture, which can be applied by the BSS algorithms directly. Depending on the DFT/FFT module from the OFDM receiver, the convolutive mixture can be switched into the instantaneous mixtures. Therefore, the complicated separation procedure for the convolutive mixture can be broken down into a simple, linear, and instantaneous separation at each subcarrier. Overall, it is a basic requirement that allows the application of ICA to the blind multiuser detection in the SDMA-based uplink MIMO OFDM system.

Among the existing HOS ICA algorithms, the complex FastICA algorithm will be adopted.

Figure 4-1 shows the proposed BSS-only structure for the SDMA-based uplink MIMO OFDM system. The geographically separated l independent mobile users send different l source signals through l independent antennas. In other words, each mobile user is equipped with only one monopolized antenna which can guarantee users' signals are mutually independent. The OFDM transmitter modules transform the source signals into the OFDM signals. The AWGN is added to the SDMA MIMO channel to represent the channel noise. After being received by the p-element antenna array at the base station, removed CP, and applied the DFT modules, the complex FastICA modules are applied to separate the mixed source signals for each subcarrier. Finally, the reordering module solves the permutation problem which is caused by BSS. The details of the OFDM transmitter module and the receiver module are illustrated in Chapter 2, Figures 2-14 and 2-15, respectively.
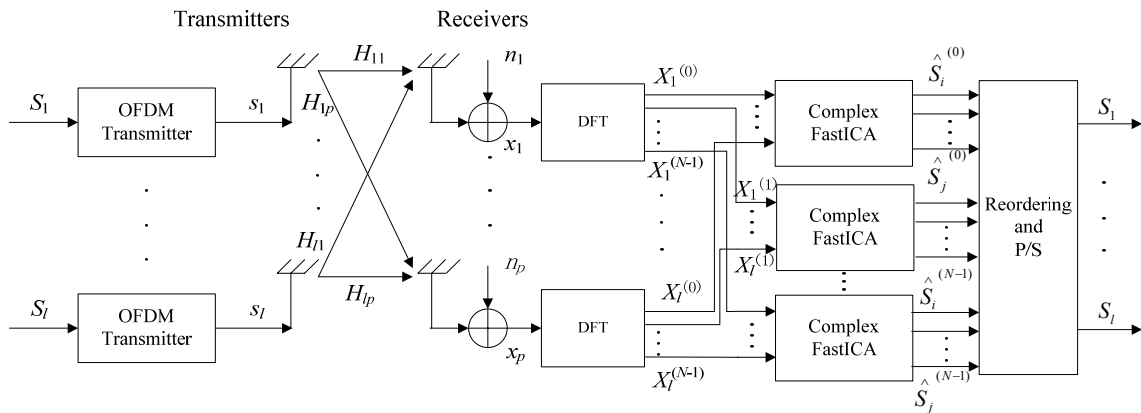
Figure 4-1 BSS-only Scheme for the SDMA-based Uplink MIMO OFDM System

Prewhitening of mixed signals by PCA i.e. the real and imaginary parts of x_i are uncorrelated and their variances are equal

Random initial non-linear contrast function

$$J_G(\mathbf{w}) = E\{G(\left|\mathbf{w}^H\mathbf{x}\right|^2)\}$$

Choose G function as:

$$G_2(y) = \log(a_2 + y),\ a_2 \approx 0.1$$

Maximize

$$\sum_{i=1}^{l} J_G(\mathbf{w}_i)$$

N

Updating by

$$\mathbf{w}^+ = E\{\mathbf{x}(\mathbf{x}(\mathbf{w}^H\mathbf{x})^* g(\left|\mathbf{w}^H\mathbf{x}\right|^2)\}^2$$
$$- E\{g(\left|\mathbf{w}^H\mathbf{x}\right| + \left|\mathbf{w}^H\mathbf{x}\right|^2 g^{'}(\left|\mathbf{w}^H\mathbf{x}\right|^2)\}\,\mathbf{w}$$

$$\mathbf{w}_{new} = \frac{\mathbf{w}^+}{\left\|\mathbf{w}^+\right\|}$$

Y

Seperate the source signals by

$$\mathbf{s} = \mathbf{W}^H\mathbf{x}$$
$$\mathbf{W} = (\mathbf{w}_1, \mathbf{w}_2, \ldots, \mathbf{w}_l)$$

Reordering

Apply BPSK decoder to get source signals $\hat{S}_i$
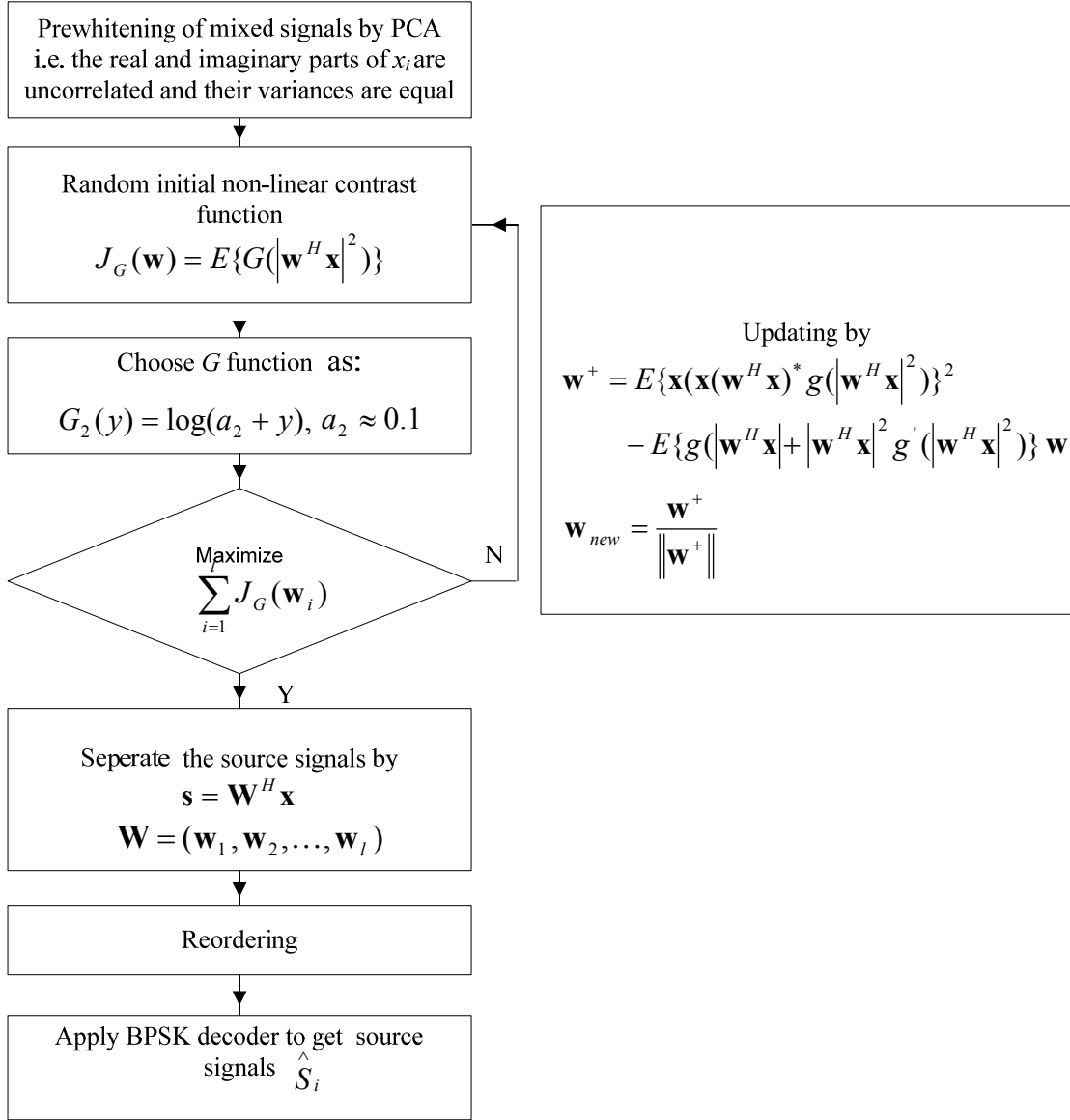
Figure 4-2 Flowchart of the BSS-only Scheme for the SDMA-based Uplink MIMO OFDM System

Some important assumptions need be noticed here. The transmitted signals are stationary, statistically independent, non-Gaussian, and zero mean. The AWGN noises have zero mean and a variance of σ_n^2. The channel transfer function is stationary and has complex Gaussian distribution. All of l independent transmitted OFDM streams are of the

same energy. These assumptions are suitable for many applications in wireless communications.

It is worth noting that the received signals need to be whitened before using the complex FastICA algorithm to estimate the source signals. The contrast function used here is the G_2 function in Equation 3.8 because the G_2 function shows the best BER performance, according to the simulation shown in Figure 3-3. The one-unit updated matrix is decided by Equations 3.12 and 3.13, and can be extended to the whole separation by Equation 3.14. The flowchart of the BSS-only scheme for the SDMA-based uplink MIMO OFDM system in the subcarrier k (k is omitted for the sake of notational convenience) is illustrated in Figure 4-2.

Due to the permutation and scaling ambiguity of the BSS methods, the reordering step and rescaling step have to be applied after employing the complex FastICA algorithm at each subcarrier. After the complex FastICA Module, the estimated source signals for the subcarrier k is described by

$$\hat{\mathbf{S}}^{(k)} = \mathbf{W}^{H(k)}\mathbf{X}^{(k)} \tag{4.1}$$

where $\hat{\mathbf{S}}^{(k)}$ is the estimated vector of the source vector $\mathbf{S}^{(k)}$. Because this blind reconstruction is only from the knowledge of the mixtures, the permutation and scaling are missed. The full estimation $\mathbf{Y}^{(k)}$ at the subcarrier k is given by

$$\mathbf{Y}^{(k)} = \mathbf{S}^{(k)} = \mathbf{P}^{(k)}\mathbf{D}^{(k)}\hat{\mathbf{S}}^{(k)} \tag{4.2}$$

where the matrix $\mathbf{P}^{(k)}$ denotes the unknown permutation at the subcarrier k, and the matrix $\mathbf{D}^{(k)}$ stands for the unknown scaling at the subcarrier k. Since we assume that each stream from l antennas has the same energy, the scaling problem is not considered here. Therefore, the main question is how to find the permutation matrix $\mathbf{P}^{(k)}$.

To solve this problem, we first assume that the ordering of every subcarrier is the same. If not, the correct OFDM signals cannot be reconstructed, mathematically, i.e.

$$\mathbf{P}^{(0)} = \mathbf{P}^{(1)} = \mathbf{P}^{(2)} = \mathbf{P}^{(N-1)} \tag{4.3}$$

According to reference [64], we assume that $\mathbf{P}^{(k)}$ is referred as a local permutation for subcarriers. The global permutation $\mathbf{P}$ can be solved by a higher signal layer or by coding.

Most of the current methods to find the permutation matrix $\mathbf{P}^{(k)}$ are based on the calculation of correlation [14], [64]. The proposed method also depends on the correlation and has the schematic diagram shown in Figure 4.3. The framework is to calculate the cross-correlation between neighborhood subcarriers. The initial calculation can be started from any subcarriers. For example, we can calculate the subcarrier 0 with the frequency f_0 and the subcarrier 1 with the frequency f_1 first. The cross-correlation of the separated signals in the subcarriers 0 and 1 has the following property:

$$\begin{aligned} E[\hat{S}_i^{(0)} \hat{S}_j^{*(1)}] &= 0 \\ E[\hat{S}_i^{(0)} \hat{S}_i^{*(1)}] &\neq 0 \end{aligned} \quad , \quad i \neq j \tag{4.4}$$

where 0 and 1 are the index of subcarriers, and i and j are different users. After the calculation of all of the cross-correlations between all neighborhood subcarriers, the user

i's signals can be found. The dash arrows in Figure 4-3 are joined with each other for the signal from the same source. In addition, the signals connected with each other by the solid arrows show that they belong to different sources. Based on this strategy, all of *l* sources can be found. The subscripts {···, *i*, *j*, *a*, *c*, ···}, {···, *e*, *d*, *i*, *a*, ···}, {···, *j*, *i*, *c*, *d*, ···} ∈ {1, 2, ···, *l*} in Figure 4-3 are in a random separation order by the complex FastICA modules.
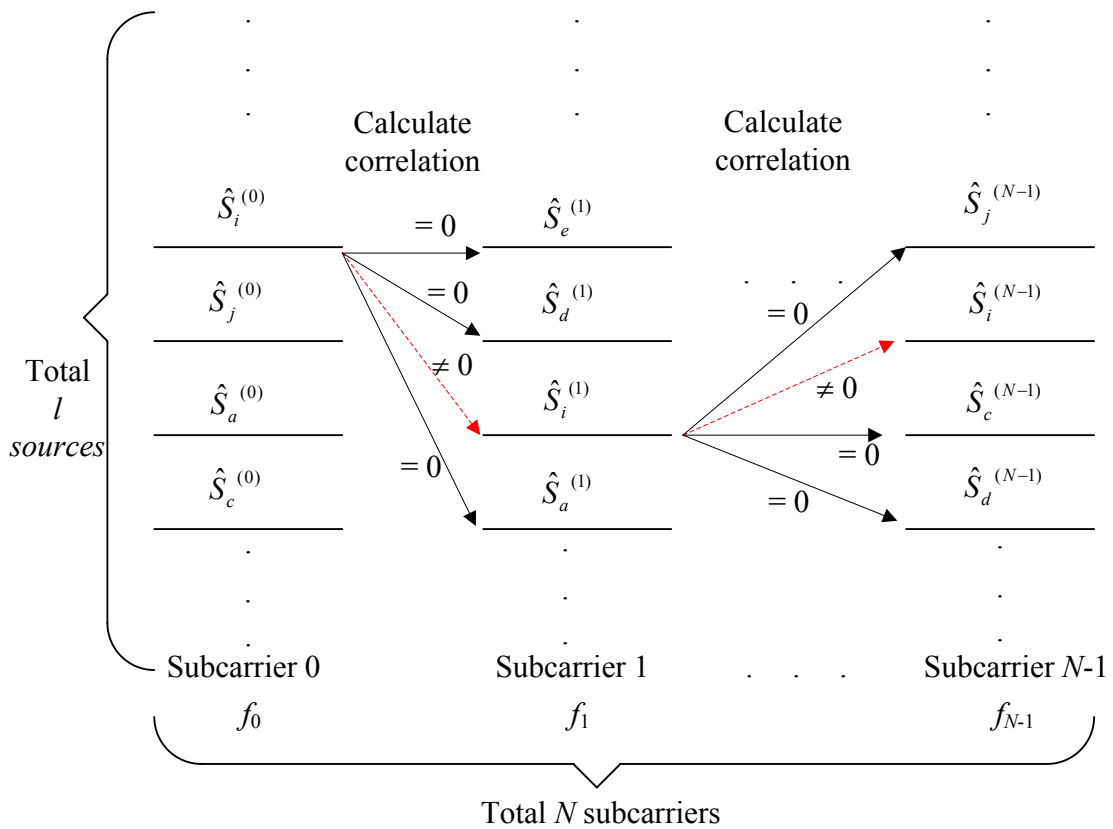
Figure 4-3 Schematic Diagram of How to Calculate the Correlation for the Permutation

One of the disadvantages of the BSS-only method is its high computational cost. The total numbers of the cross-correlation calculated by the BSS-only scheme is given by

$$N_{cross-correlation} = [\frac{l(l+1)}{2} - 1](N-1) \qquad (4.5)$$

where l is the total number of sources. N is the total number of subcarriers. The amount of calculations for the cross-correlation is illustrated in Table 4-1. The number of antennas is set to 2, 4, or 8, respectively. In addition, 64 or 128 subcarriers are considered. It is obvious that the BSS-only scheme brings more than one thousand calculation tasks to solve the permutation problems when the number of antennas is larger than 4 and there are more than 128 subcarriers. Thus, the amount of subcarriers should be equal or less than 64 and the antenna number should be less than 4 for the purpose of less computational complexity.

Table 4-1 Total number of the calculations for the cross-correlation

Number of antennas l	Number of subcarriers N	Amount of the calculations for the cross-correlation
2	64	126
4	64	567
4	128	1143
8	128	4480

4.2 BSS-MMSE Scheme

In order to take the advantages from the BSS-only scheme and at the same time to eliminate its computational complexity in the calculation of the cross-correlation, the

BSS algorithm combined with the MMSE structure, which is referred to as the BSS-MMSE scheme, is proposed in this section.

The BSS-MMSE method has a lower computational complexity through applying a BSS algorithm for only one subcarrier. And then the MMSE separation modules are employed for all of the remaining adjacent subcarriers. Therefore, the BSS-MMSE scheme is free from the permutation and gains indeterminacy by choosing the separating coefficients. Since this approach can separate and recover all of the sources with the same permutation and gain, the computation is efficient.
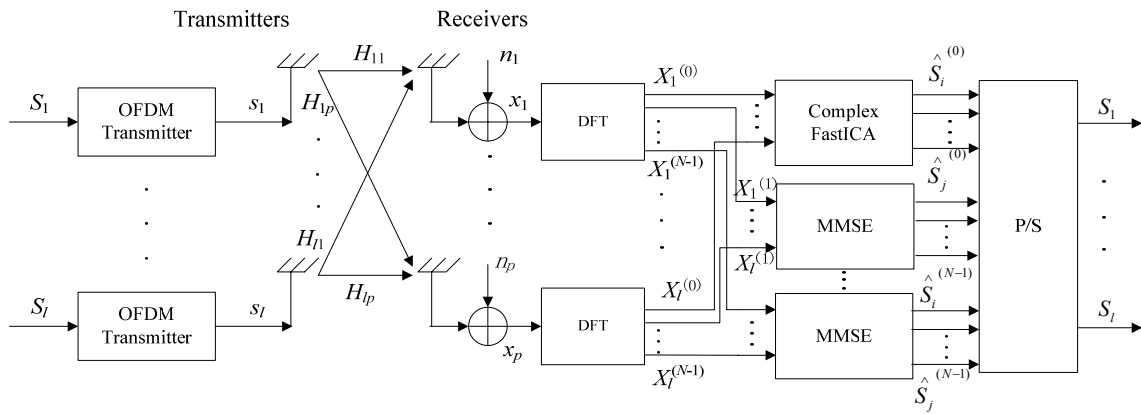
Figure 4-4 BSS-MMSE Scheme for the SDMA-based Uplink MIMO OFDM System

The proposed BSS-MMSE structure for the SDMA-based uplink MIMO OFDM system is illustrated in Figure 4-4. Compared with the BSS-only method as shown in Figure 4-1, the new structure only keeps one complex FastICA module in any arbitrary subcarrier (i.e., a complex FastICA module for subcarrier 0 in Figure 4-4). And then MMSE modules replace all of the other N-1 complex FastICA modules. The complex FastICA module separates the mixture of sources at the subcarrier 0, and the adjacent

MMSE module takes this separation output as the reference to separate the mixed sources with the same ordering at the adjacent subcarrier 1. The output of the subcarrier 1 is now used as the reference for separation with the same ordering at the subcarrier 2. This separation process is continued until the last separation is completed at the subcarrier N-1. Thus, there is no permutation problem in the proposed BSS-MMSE scheme.

Figure 4-5 represents the schematic diagram for the proposed BSS-MMSE method. Assume there are N subcarriers and l sources. A complex FastICA module is employed at the subcarrier r, and this module calculates the separation matrix $\mathbf{W}^{(r)}$. Assume the random separation ordering by the complex FastICA module at the subcarrier r is $\{\cdots, a, c, i, j, \cdots\} \in \{1, 2, \cdots, l\}$ in Figure 4-5. The output of this complex FastICA module is given by

$$\hat{\mathbf{Y}}^{(r)} = \hat{\mathbf{S}}^{(r)} = \cdots + \hat{S}_a^{(r)} + \hat{S}_c^{(r)} + \hat{S}_i^{(r)} + \hat{S}_j^{(r)} + \cdots \tag{4.6}$$

where r is an arbitrary subcarrier and belongs to N. For ease of discussion, a simple and convenient way is to let r equal to 0 as shown in Figure 4-4. The next step is to apply the MMSE module to neighborhood subcarriers (i.e., subcarriers r-1 and r+1) where the separation holds the same ordering as the separation in the subcarrier r in Figure 4-5. As the curved arrows show in Figure 4-5, the similar process can be applied to the MMSE module for the subcarriers r-2 and r+2, respectively.

The solution for the MMSE scheme is shown in Figure 4-6. Applying a weight matrix $\mathbf{W}^{(k)}$, we define

$$\hat{\mathbf{S}}^{(k)} = \boldsymbol{\gamma}^{(k)(r)}\mathbf{W}^{(k)}\hat{\mathbf{X}}^{(r)} \tag{4.7}$$

where $k = r - 1$ or $k = r + 1$, $\mathbf{W}^{(k)}$ denotes the MMSE estimation in the subcarrier k, and $\boldsymbol{\gamma}^{(k)(r)}$ is the inverted diagonal matrix for $\mathbf{P}^{(k)(r)}$, which ensures the same permutation and gain in all subcarriers.
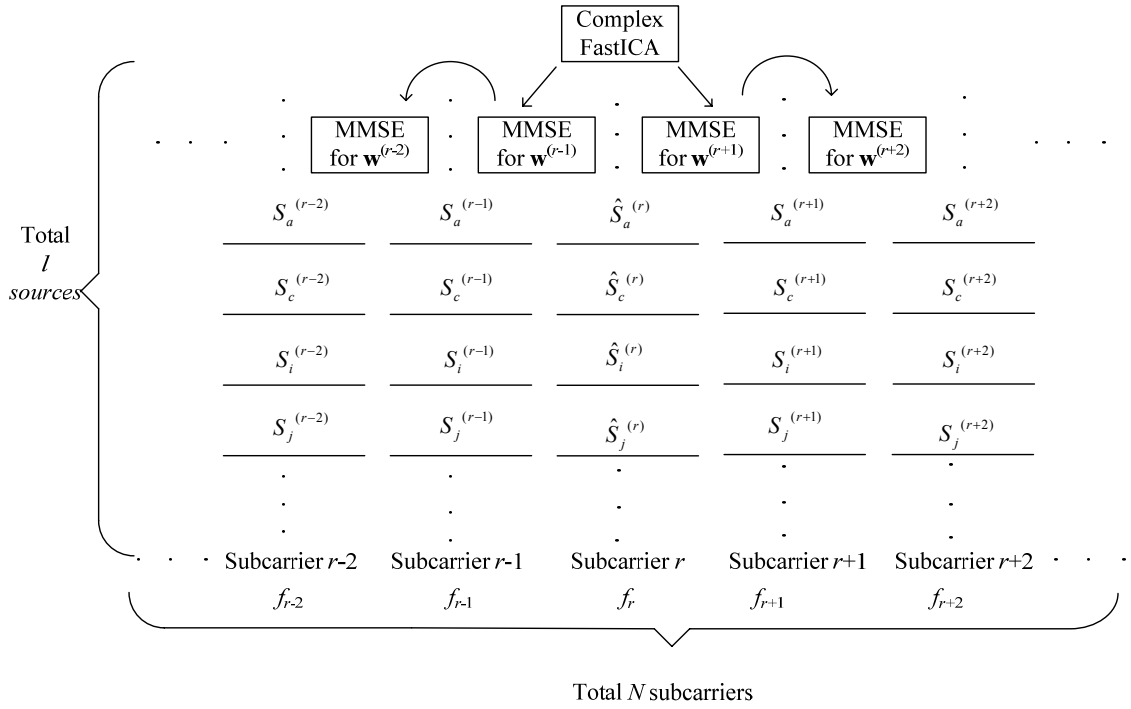
Figure 4-5 Schematic Diagram of the BSS-MMSE Method

The MMSE error vector in the subcarrier k is defined by

$$\mathbf{e}^{(k)} = \mathbf{S}^{(k)} - \hat{\mathbf{S}}^{(k)} \tag{4.8}$$

Applying the most popular multiuser detection strategy (i.e., the Mean Square Error (MSE) criterion [65], [66]), the cost function in the subcarrier k is defined as

$$J(\hat{\mathbf{H}}) = E\{\|\mathbf{e}^{(k)}\|^2\} = E\{\|\mathbf{S}^{(k)} - \hat{\mathbf{S}}^{(k)}\|^2\} \tag{4.9}$$
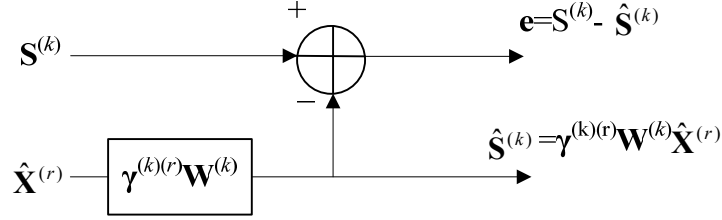
Figure 4-6 Schematic Diagram of the MMSE Estimation

The question now is how to find an estimation of $\hat{\mathbf{S}}^{(k)}$ in terms of $\mathbf{W}^{(k)}$ to minimize this cost function. The orthogonal property claims that the error vector $\mathbf{e}^{(k)}$ in the subcarrier k is orthogonal to $\hat{\mathbf{X}}^{(r)}$ in the subcarrier r as follows:

$$
\begin{aligned}
E\{\mathbf{e}^{(k)}\hat{\mathbf{X}}^{H(r)}\} &= E\{(\mathbf{S}^{(k)} - \hat{\mathbf{S}}^{(k)})\hat{\mathbf{X}}^{H(r)}\} \\
&= E\{(\mathbf{S}^{(k)} - \gamma^{(k)(r)}\mathbf{W}^{(k)}\hat{\mathbf{X}}^{(r)})\hat{\mathbf{X}}^{H(r)}\} \\
&= E\{\mathbf{S}^{(k)}\hat{\mathbf{X}}^{H(r)}\} - \gamma^{(k)(r)}\mathbf{W}^{(k)}E\{\hat{\mathbf{X}}^{(r)}\hat{\mathbf{X}}^{H(r)}\} \\
&= \mathbf{R}_{\mathbf{S}^{(r)},\hat{\mathbf{X}}^{(r)}} - \gamma^{(k)(r)}\mathbf{W}^{(k)}\mathbf{R}_{\hat{\mathbf{X}}^{(r)},\hat{\mathbf{X}}^{(r)}} = 0
\end{aligned}
\tag{4.10}
$$

where $\mathbf{R}_{\mathbf{S}^{(r)},\hat{\mathbf{X}}^{(r)}}$ is the cross-correlation matrix between $\mathbf{S}^{(k)}$ and $\hat{\mathbf{X}}^{(r)}$, and $\mathbf{R}_{\hat{\mathbf{X}}^{(r)},\hat{\mathbf{X}}^{(r)}}$ is the autocorrelation matrix of $\hat{\mathbf{Y}}^{(r)}$. Solving Equation 4.10 for the MMSE matrix $\mathbf{W}^{(k)}$, which is referred to as $\mathbf{W}_{\mathrm{MMSE}}^{(k)}$, we obtain

$$\mathbf{W}_{\mathrm{MMSE}}^{(k)} = \gamma^{-1(k)(r)}\mathbf{R}_{\mathbf{S}^{(k)},\hat{\mathbf{X}}^{(r)}}\mathbf{R}^{-1}{}_{\hat{\mathbf{X}}^{(r)},\hat{\mathbf{X}}^{(r)}} \tag{4.11}$$

Recall that $\gamma^{(k)(r)}$ is the inverted matrix of $\mathbf{P}^{(k)(r)}$, and it is defined by

$$\gamma^{(k)(r)} = \mathbf{P}^{-1(k)(r)} \tag{4.12}$$

where $\mathbf{P}^{(k)(r)}$ is defined by the cross-correlation property in Equation 4.4, and is given by

$$\mathbf{P}^{(k)(r)} = \begin{bmatrix} \dfrac{E[S_1^{*(k)} S_1^{H(r)}]}{E[|S_1^{(r)}|^2]} & 0 & \cdots & 0 \\ 0 & \dfrac{E[S_2^{*(k)} S_2^{*(r)}]}{E[|S_2^{(r)}|^2]} & \cdots & 0 \\ \vdots & \vdots & \ddots & \vdots \\ 0 & 0 & \cdots & \dfrac{E[S_l^{*(k)} S_l^{*(r)}]}{E[|S_l^{(r)}|^2]} \end{bmatrix} \tag{4.13}$$

Finally, the separation for the subcarrier k can be solved by the following equation:

$$\hat{\mathbf{S}}^{(k)} = \mathbf{W}_{\text{MMSE}}^{H(k)} \mathbf{X}^{(k)} \tag{4.14}$$

Now, the output of Equation 4.14 is the reference for the adjacent subcarriers $r - 2$ or $r + 2$. After doing this process for all of the subcarriers, the estimation of the sources is achieved.

4.3 BSS-MBER Scheme

Although the MMSE detection is a most popular strategy, it cannot promise to accomplish the minimum BER. A better strategy is to minimize the error probability or the bit error rate directly instead of the mean squared error. The authors in [25] [26] [67-69] show several MBER schemes to realize this objective for the minimum BER.

However, in order to achieve an excellent BER performance by using above-mentioned methods, the receiver of MIMO OFDM systems requires the knowledge of the channel transfer function **H** or the channel impulse responses (CSI). In other words, closed-loop MIMO systems have to be chosen, which are described in Chapter 2. For the purpose of avoiding sending those users' information from the mobile user to the base station and simultaneously achieving the best BER performance, a BSS based MBER scheme, referred to as BSS-MBER, is proposed in this section.

The BSS-MBER scheme is to apply a BSS algorithm to predict the channel matrix **H** first, and then the current available MBER algorithms are employed to the system. Because the BER performed by the BSS-only scheme cannot guarantee the minimum BER, a MBER module is added to generate and update the separation matrix $\mathbf{W}_{\text{MBER}}^{(k)}$ in the subcarrier k for a better BER performance. The proposed BSS-MBER receiver for the subcarrier k in the SDMA-based MIMO OFDM system is shown in Figure 4-7. After the DFT/FFT modules at the receiver, the mixed signals in the subcarrier k go through the complex FastICA module to recover the channel status $\hat{\mathbf{H}}^{(k)}$, which is given by

$$\hat{\mathbf{H}}^{(k)} = [\cdots, \hat{H}_i^{(k)}, \cdots, \hat{H}_j^{(k)}, \cdots] \in [\hat{H}_1^{(k)}, \hat{H}_2^{(k)}, \cdots, \hat{H}_l^{(k)}] \tag{4.15}$$

On the basis of the cross-correlation property in Equation (4.4), the reordering module is able to remove the permutation problem by using the complex FastICA algorithm. The updated channel status is

$$\hat{\mathbf{H}}^{(k)} = [\hat{H}_1^{(k)}, \hat{H}_2^{(k)}, \cdots, \hat{H}_l^{(k)}] \tag{4.16}$$

With the predicted channel transfer function by the complex FastICA model in the subcarrier k, a conventional MBER algorithm can be applied to the proposed systems to pursuit the minimum BER. Compared with the BSS-only method, the proposed BSS-MBER scheme inserts an extra linear MBER module, which consequentially increases the computational complexity in each subcarrier. But the attractive advantage is its better BER performance, which is one of the major goals of this research. In other words, the BER performance is improved through the increment of the computational complexity. With the development of the hardware in the base station, this computational increment can be reduced by powerful hardware.
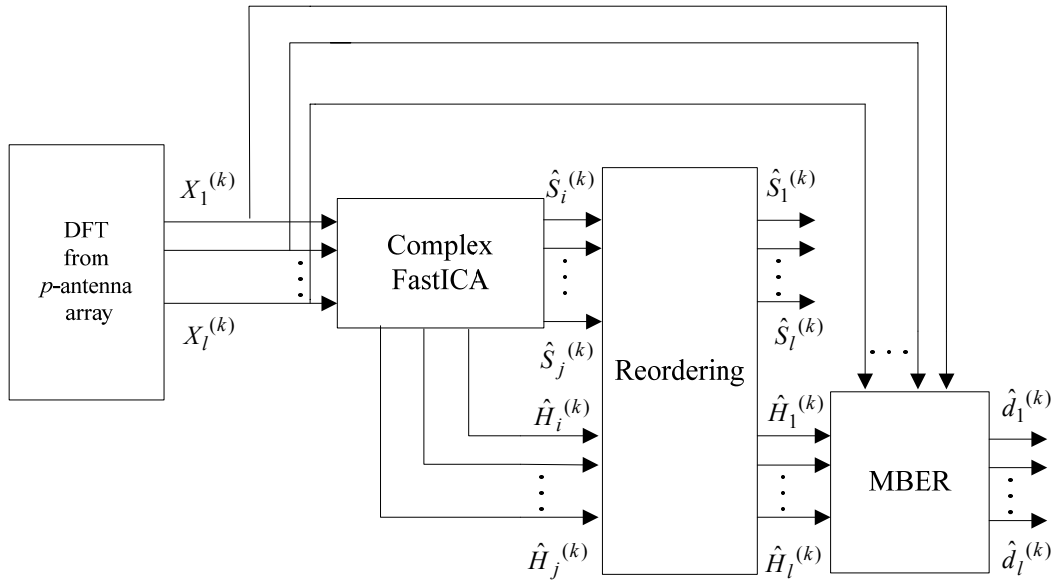
Figure 4-7 BSS-MBER Scheme for the Subcarrier k in the SDMA-based Uplink MIMO OFDM System

If we consider Figure 4-7 as a BSS-MBER module, the overall framework for the proposed BSS-MBER structure for the SDMA-based uplink MIMO OFDM system is illustrated in Figure 4-8. The BSS-MBER module is added to every subcarrier. Thus, the computational increment is added to all of the subcarriers.

Recall from Figures 2-16 and 2-17 in Chapter 2, we know that the BPSK modulation is the best choice for the BER performance. Thus, the number of bit per symbol is 1, and the bit error rate equals to the symbol error rate (SER) in the proposed SDMA-based MIMO OFDM system. Therefore, after the symbol error rate is calculated, we also have the bit error rate, which can be expressed as

$$BER = SER \qquad\qquad (4.17)$$
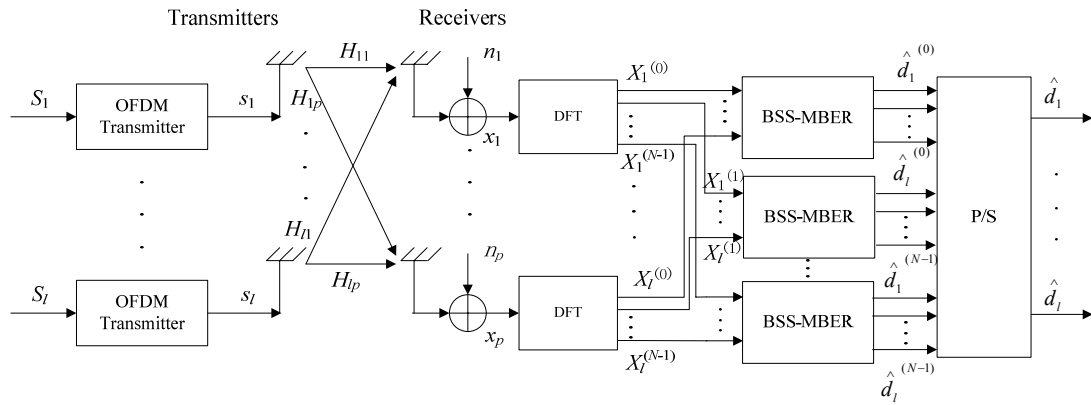
Figure 4-8 BSS-MBER Structure for the SDMA-based Uplink MIMO OFDM System

It is obvious that to seek the minimum P_{BER} is equivalent to search the minimum BER. Based on the past experience, to find the minimum P_{BER} is usually easier than to find the BER directly. Equation 4.17 can also be written as

$$P_{BER} = P_{SER} \tag{4.18}$$

where P_{BER} is the bit error probability, and P_{SER} is the symbol error probability.

After the BPSK decoder module, the estimated symbols $\hat{S}_i^{(k)}$ are transferred to the estimated data signals $\hat{d}_i^{(k)} \in \{+1, -1\}$. Thus, the estimated data signals at the user i $\in \{1, 2, \cdots, l\}$ in the subcarrier k can be expressed as

$$\hat{d}_i^{(k)} = \text{sgn}(\text{Re}(\mathbf{w}_i^{H(k)} \mathbf{V}^{(k)})) \tag{4.19}$$

where $\text{sgn}(\cdot)$ is the Sign function. Then the users' signal vector in the subcarrier k is defined by

$$\mathbf{V}^{(k)} = \mathbf{H}^{(k)} \mathbf{d}^{(k)} + \mathbf{n}^{(k)} \tag{4.20}$$

According to Equation 4.20, a noise free signal vector $\overline{\mathbf{V}}^{(k)}$ in the subcarrier k is expressed by

$$\overline{\mathbf{V}}^{(k)} = \mathbf{H}^{(k)} \mathbf{d}^{(k)} \tag{4.21}$$

The goal of the MBER scheme is to find a suitable $\mathbf{w}_i^{H(k)}$, which can minimize the probability $P_{BER}^{(k)}$. According to the P_{BER} definition given in reference [67] for the Direct-Sequence Code Division Multiple Access (DS-CDMA) system, $P_{BER}^{(k)}$ at user i $\in \{1, 2, \cdots, l\}$ in the subcarrier k for the proposed SDMA-based uplink MIMO OFDM system can be defined by

$$P_{BERi}^{(k)} = \Pr[\text{sgn}(d_i^{(k)})\text{Re}(\mathbf{w}_i^{H^{(k)}}\mathbf{V}^{(k)}) < 0]$$

$$= E[\Pr[\text{sgn}(d_i^{(k)})\text{Re}(\mathbf{w}_i^{H^{(k)}}\mathbf{H}^{(k)}\mathbf{d}^{(k)}) + \text{sgn}(d_i^{(k)})\text{Re}(\mathbf{w}_i^{H^{(k)}}\mathbf{n}^{(k)}) < 0 \,|\, \text{Re}(\mathbf{d}^{(k)})]] \quad (4.22)$$

$$= E[Q(\frac{\text{Re}(\mathbf{w}_i^{H^{(k)}}\mathbf{H}^{(k)}\mathbf{d}^{(k)})\text{sgn}(d_i^{(k)})}{\sqrt{\mathbf{w}_i^{H^{(k)}}\mathbf{w}_i^{(k)}}\sigma_n})]$$

where the expectations are over $N_d = 2^l$ binary bit vectors $\mathbf{d}^{(k)}$ in the subcarrier k, $Q(\cdot)$ is the standard Q-function, $d_i^{(j)}\, j \in \{1, 2, \cdots, 2^l\}$ is the user i's transmitted bit, σ_n is the standard deviation for the variance of the noise σ_n^2. Combined with the definition for the noise free signal vector $\overline{\mathbf{V}}^{(k)}$ in Equation 4.21, Equation 4.22 can be expressed as

$$P_{BERi}^{(k)} = E[Q(\frac{\text{Re}(\mathbf{w}_i^{H^{(k)}}\overline{\mathbf{V}}^{(k)})\text{sgn}(d_i^{(k)})}{\sqrt{\mathbf{w}_i^{H^{(k)}}\mathbf{w}_i^{(k)}}\sigma_n})] = \frac{\sum_{j=1}^{N_d^{(k)}}Q(\frac{\text{Re}(\mathbf{w}_i^{H^{(k)}}\overline{\mathbf{V}}_j^{(k)})\text{sgn}(d_i^{(k)})}{\sqrt{\mathbf{w}_i^{H^{(k)}}\mathbf{w}_i^{(k)}}\sigma_n})}{N_d^{(k)}} \quad (4.23)$$

From Equation 4.23, it is obvious that the minimum value of $P_{BERi}^{(k)}$ only depends on the direction of $\mathbf{w}_i^{H^{(k)}}/\sqrt{\mathbf{w}_i^{H^{(k)}}\mathbf{w}_i^{(k)}}$ calculated by $\mathbf{w}_i^{(k)}$ in the subcarrier k. However, the solution of this complex and irregular cost function is not unique. If $\mathbf{w}_i^{(k)}$ can minimize $P_{BERi}^{(k)}$, then $\alpha\mathbf{w}_i^{(k)}$ can also minimize $P_{BERi}^{(k)}$ in the subcarrier k. Here α is an arbitrary positive constant.

By setting the gradient of Equation 4.23 to zero, this equation will have the minimum value. We define

$$\nabla_{\mathbf{w}_i^{(k)}} P_{BERi}^{(k)} = \nabla_{\mathbf{w}_i^{(k)}} \left(\frac{\sum_{j=1}^{N_d^{(k)}} Q\left(\frac{\mathrm{Re}(\mathbf{w}_i^{H(k)} \overline{\mathbf{V}}_j^{(k)}) \mathrm{sgn}(d_i^{(k)})}{\sqrt{\mathbf{w}_i^{H(k)} \mathbf{w}_i^{(k)}} \sigma_n} \right)}{N_d^{(k)}} \right) \tag{4.24}$$

$$= \frac{-1}{\sqrt{2\pi}\sigma_n} E\left[\exp\left(\frac{-(\mathbf{w}_i^{H(k)} \overline{\mathbf{V}}^{(k)})^2}{2\mathbf{w}_i^{H(k)} \mathbf{w}_i^{(k)} \sigma_n^2} \right) \frac{\mathbf{w}_i^{H(k)} \mathbf{w}_i^{(k)} \overline{\mathbf{V}}^{(k)} - \mathbf{w}_i^{H(k)} \overline{\mathbf{V}}^{(k)} \mathbf{w}_i^{(k)}}{\sqrt{\mathbf{w}_i^{H(k)} \mathbf{w}_i^{(k)}}^3} \mathrm{sgn}(d_i^{(k)}) \right] = 0$$

In addition, we define the function $f(\mathbf{w}_i^{(k)})$ by:

$$f(\mathbf{w}_i^{(k)}) = E\left[\exp\left(\frac{-(\mathbf{w}_i^{H(k)} \overline{\mathbf{V}}^{(k)})^2}{2\mathbf{w}_i^{H(k)} \mathbf{w}_i^{(k)} \sigma_n^2} \right) \overline{\mathbf{V}}^{(k)} \right] = \frac{\sum_{j=1}^{N_d^{(k)}} e^{-\xi_j^2/2}}{N_d^{(k)}} \mathbf{V}_j^{(k)} \tag{4.25}$$

where $\xi = \dfrac{\mathbf{w}_i^{H(k)} \overline{\mathbf{V}}^{(k)}}{\sqrt{\mathbf{w}_i^{H(k)} \mathbf{w}_i^{(k)}} \sigma_n}$ for a simplified formula of the function $f(\mathbf{w}_i^{(k)})$.

At last, the proposed MBER algorithm in the subcarrier k is defined by

$$\mathbf{w}_{inew}^{(k)} = \mathbf{w}_i^{(k)} + \mu f(\mathbf{w}_i^{(k)}) \tag{4.26}$$

where μ is a step size with a small positive value. A necessary assumption is that $\mathbf{w}_i^{(k)}$ minimizes $P_{BERi}^{(k)}$, when $P_{BERi}^{(k)} \leq 2^{-l}$.

Figure 4-9 shows the flowchart of the MBER detection for the subcarrier k. Equation 4.25 is iterated after starting the MBER algorithm. When it converges, i.e. $P_{BERi}^{(k)} \leq 2^{-l}$, $\mathbf{w}_i^{(k)}$ will be the separation matrix for user i in the subcarrier k. Otherwise, the process is repeated until Equation 4.25 converges. When all l users' data are found,

the separation for the subcarrier k is completed. This separation procedure has to be done for all of N subcarriers. The calculation process is relatively complicated. However, the BSS-MBER scheme improves the BER performance.

Use $P_{BER\,i}^{(k)}$ as the objective function

Start MBER

Convergence? No

Iterate
$$\mathbf{w}_{inew}^{(k)} = \mathbf{w}_i^{(k)} + \mu f(\mathbf{w}_i^{(k)})$$

Convergence? Yes

Finish MBER

Iteration again

Separated users' signals by $\mathbf{w}_i^{(k)}$
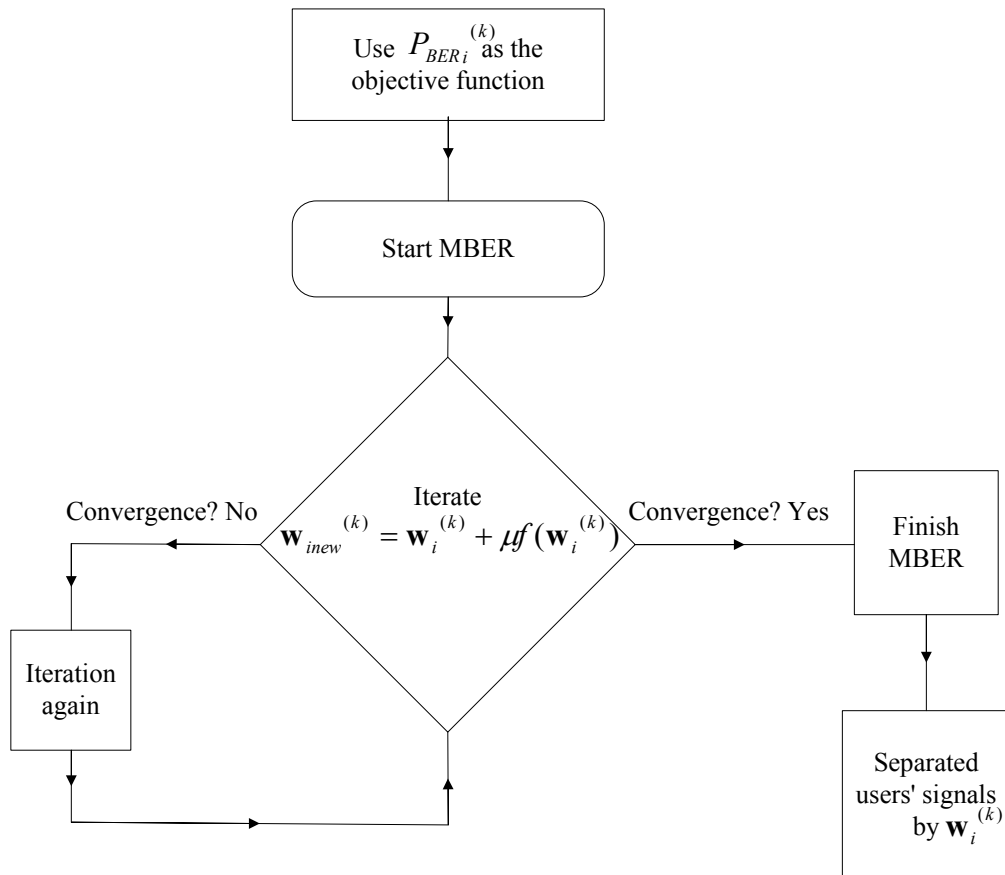
Figure 4-9 Flowchart for the MBER Detection in the Subcarrier k

CHAPTER 5

SIMULATION AND PERFORMANCE ANALYSIS

This chapter presents, analyzes, and compares the MATLAB simulation results for the three proposed schemes in Chapter 4. The BER performance is provided in the context of different simulation conditions and parameters for the SDMA-based uplink MIMO OFDM system. In addition, the computational complexity for each method is assessed.

5.1 Simulation Environment

The simulation programs are run on a computer equipped with Windows XP and Intel Core2 2 GHz CPU with 2GB memory. The software version of the MATLAB is R2008a.

We assume the parameters of OFDM for the SDMA-based MIMO OFDM system are the same for every user in the transmitter. To demonstrate the performance of the proposed systems and to consider the complexity of the systems, the parameters of both 802.11n [2], [70], [71] standard and 802.11a [72], [73] standard are taken into account. Table 5.1 shows the major parameters for the proposed SDMA-based uplink MIMO OFDM system. Recalling the discussion about the FFT size in Chapter 2, the value of the FFT size should be equal to or larger than 64 to make use of the high spectral efficiency of OFDM techniques. The bandwidth, f_0, and Cyclic Prefix size is selected based on 802.11n and 802.11a standard. The BSPK modulation is chosen because of its best BER

performance. One frame contains 100 symbols and the amount of frames or symbols for each subcarrier is varied in order to show how the frame or symbol size influences the BER performance. According to the analysis about the amount of antennas in Figure 2-14 in Chapter 2, 4 mobile users are equipped with 4 independent antennas in the transmitters, and the receiver is employed with a 4-element antenna array in the SDMA-based uplink MIMO OFDM system.

Table 5-1 Main parameters for the proposed SDMA-based uplink MIMO OFDM system

Main parameters	Specifications
FFT Size N_{FFT}	64
Bandwidth	20 MHz
f_0	312.5 KHz
Cyclic Prefix size	$N_{FFT}/4$
PSK/QAM type	BPSK
Symbols per subcarrier	1,000/5,000/10,000
Frame size	100 symbols
MIMO Channels	4×4

The AWGN with zero mean and a variance of σ_n^2 is added for each element of the antenna array to simulate the noise in the receiver. In reference [23], it confirms that an unstable time-varying wireless fading channel can be converted into a stable AWGN-like

channel without important instantaneous fading. Thus, only the AWGN channel for MIMO systems is simulated in this research. We also assume that the frequency channel transfer functions **H** is stationary and the complex Gaussian distributed processes of **H** are set to zero-mean. Another assumption is that the received OFDM signals are synchronized in the receivers and no synchronization issues need to be considered in the simulation.

5.2 BER Performance Analysis

We assume that the transmission channel is stable and independent for the period of each frame. All of the simulation results are averaged for the selected frame sizes. The SNR range is from 5 dB to 30dB.

The BER performance of three proposed schemes is shown in Figure 5-1. The value of the OFDM frame size is 50 in this simulation. The received mixed signals are under the interference by AWGN in the testing SDMA-based uplink MIMO OFDM environment. When AWGN increases, the separation matrix $\mathbf{W}^H$ by any of these schemes will begin to be far from their mixing matrix **H**, so the separation quality of the BER performance tends to become poor at a smaller SNR. According to the designed SDMA-based uplink MIMO OFDM testing environment, both BSS-only and BSS-MBER achieve acceptable BER performance within the SNR range between 5 dB to 30 dB. But the BER performance from the BSS-MMSE scheme is average at all SNR values. The reason is that the symbol error by the BSS-MMSE scheme is passed from one subcarrier to its neighboring subcarrier, and this error cannot be dismissed. In addition, Figure 7-1

shows that the BSS-MBER scheme has the best BER performance at different SNR values, compared with the other two schemes. Furthermore, the BER performance for the BSS-only scheme gives the second best BER performance. A large performance gap takes place among these schemes when the values of SNR are more than 20 dB.
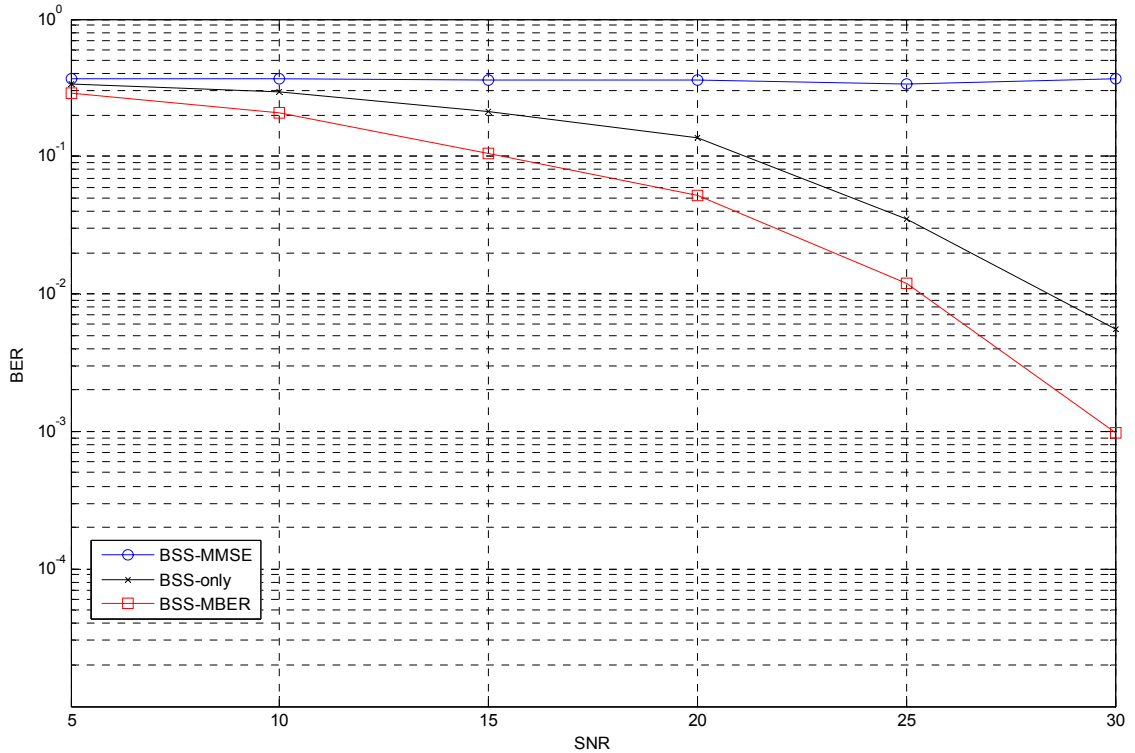
Figure 5-1 BER Performance for Three Proposed Schemes in the Uplink SDMA-based MIMO OFDM System

For a quantitative analysis for the BER vs. SNR performance of the three proposed schemes in the SDMA-based MIMO OFDM systems, Table 5-2 shows the improvement percentage of the BER performance according to Figure 5-1. When the SNR range is from 5 dB to 30 dB, according to Table 5-2's data, there are about 18.92%

relative BER improvements on average for the BSS-only method compared with the

BSS-MMSE method. At the same time, there are about 24.85% relative BER

improvements on average for the BSS-MBER scheme in comparison of the BSS-MMSE

method. In addition, the BSS-MBER scheme obtains the best BER performance by

5.93% on average in contrast with the BSS-only method.

Table 5-2 Relative BER improvement

SNR(dB)	5	10	15	20	25	30
Relative improvement BSS-only compared with BSS-MMSE	3.03%	7.11%	14.95%	21.93%	30.51%	35.98%
Relative improvement BSS-MBER compared with BSS-MMSE	7.58%	15.92%	25.78%	30.56%	32.83%	36.46%

Table 5-3 Comparison among three proposed schemes in terms of the error probability for a variety of frame sizes at SNR = 25 dB

Schemes	Frame sizes		
	10	50	100
BSS-only without reordering module	0.6542	0.6480	0.7435
BSS-only	5.68×10^{-2}	3.52×10^{-2}	1.32×10^{-2}
BSS-MMSE	0.3725	0.3403	0.2812
BSS-MBER	3.35×10^{-2}	1.20×10^{-2}	0.86×10^{-2}

Error probability for a variety of frame sizes at SNR = 25 dB
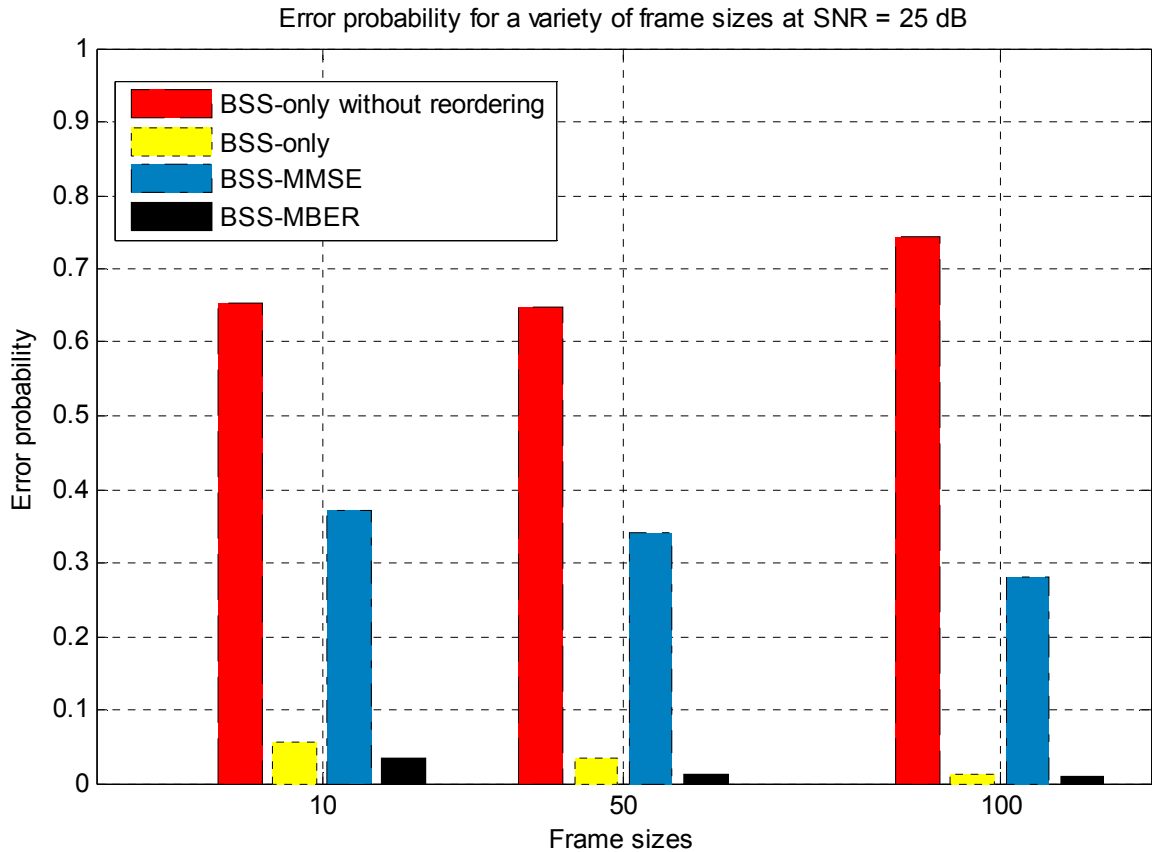
Figure 5-2 Error Probability for a Variety of Frame Sizes at SNR = 25 dB for Three Proposed Schemes

Table 5-3 and Figure 5-2 illustrate the BER performance of three proposed schemes, which is influenced by various frame sizes when SNR is 25dB. The BSS-only scheme without the reordering modules is also included in this table to compare with our schemes. This table reveals how important the reordering modules are for the BSS-only scheme and the BSS-MBER scheme under different symbol sizes, especially when the size is relatively large. Such an obvious difference of error probability between the BSS-only scheme and the BSS-only scheme without the reordering modules shows that the permutation problems must be handled properly in order to not lose the BER

performance. In addition, another fact from this simulation is that the BER performance for three proposed methods will be improved with the increment of the frame sizes. The reason is because of statistical properties of BSS techniques. They require a large number of received symbols to separate the mixed signals. However, the advantage of BSS techniques is that we do not need to know the channel status or the channel impulse responses that normally waste expensive transmission resources. Because the trend of the BER performance with various frame sizes is similar at other SNR values, they are not shown here. In all, this table validates the merits of the three proposed schemes and their low error probability. The BSS-MBER scheme takes the best BER performance. The BSS-only scheme is in the second best position, and the BSS-MMSE scheme ranks the third best.

5.3 Computational Complexity Analysis

Table 5-4 shows the analysis of the computational complexity for three proposed blind multiuser schemes in the SDMA-based uplink MIMO OFDM system. The main load of computations for the proposed schemes generally comes from the FastICA module, the reordering module, the MMSE module and/or the MBER module. All of them are the main terms to contribute to the overall computational complexity and there is no uncomplicated term among those modules. From this table, it is easy to conclude that the computational complexity level from highest to lowest is the BSS-MBER scheme, the BSS-only scheme, and the BSS-MMSE scheme, respectively.

Table 5-4 Analytical computational complexity among three proposed schemes

Computational Modules	Schemes		
	BSS-only	BSS-MMSE	BSS-MBER
FastICA Module	N×[Equations 3.8, 3.10, 3.12-14]	1×[Equations 3.8, 3.10, 3.12-14]	N×[Equations 3.8, 3.10, 3.12-14]
Reordering	N×[Equations 4.4, 4.5]	0	N×[Equations 4.4, 4.5]
MMSE Module	0	$(N$-1)×[Equations 4.7-4.14]	0
MBER Module	0	0	N×[Equations 4.19-4.26]

Table 5-5 Comparison among three proposed schemes in terms of the running time for a variety of frame sizes at SNR = 15 dB

Schemes	Running time with different frame sizes (Seconds)		
	10	50	100
BSS-only	0.67	2.03	3.86
BSS-MMSE	0.042	0.18	0.32
BSS-MBER	0.83	3.95	6.97

The computational complexity for the three proposed schemes is measured by the running time in MATLAB. The processing time for the three proposed methods is shown in Table 5-5 and Figure 5-3. It is easy to notice that the BSS-MMSE scheme has the best computational efficiency for all frame sizes when SNR is 15 dB. It is only 8.87% of the

running time compared with the BSS-only scheme, and 4.56% of the running time compared with the BSS-MBER scheme, when the frame size is 50. The computational complexity of the BSS-MBER scheme is about two times larger than the BSS-only method. The reason comes from the MBER modules in which the iteration takes too much running time.
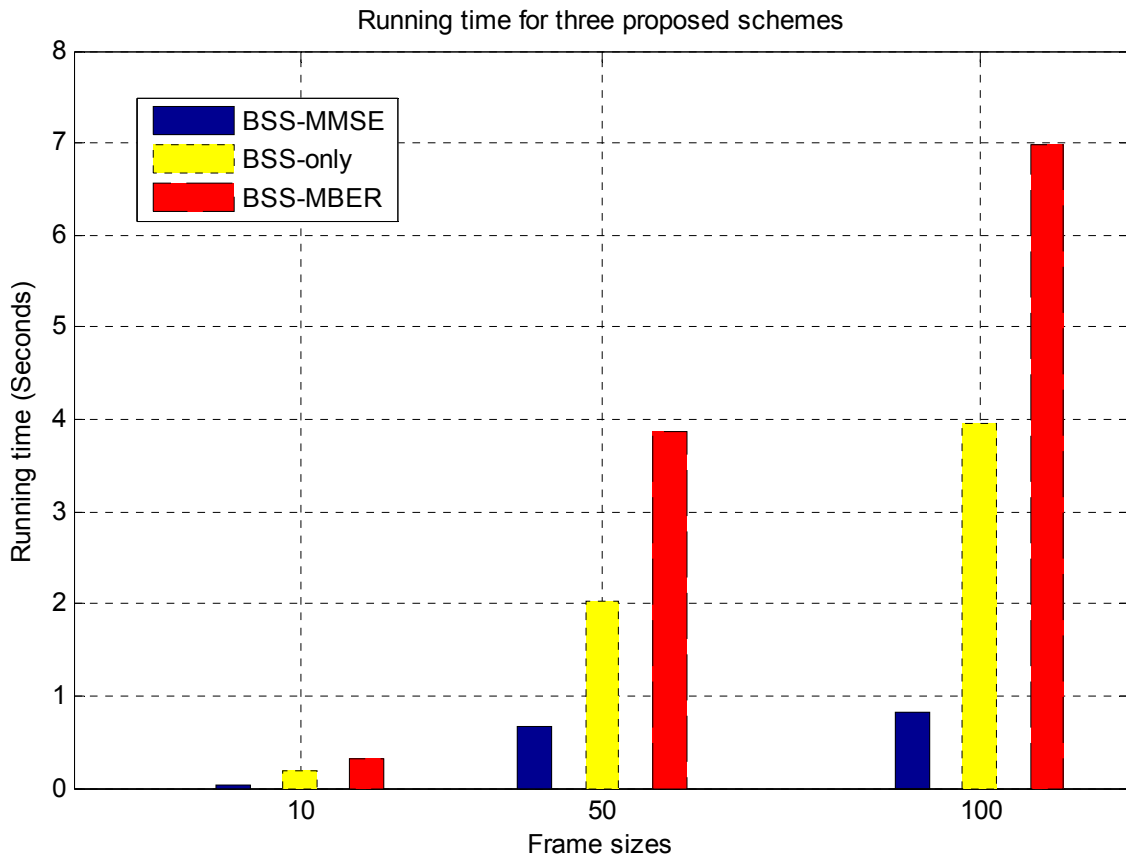
Figure 5-3 Running Time for a Variety of Frame Sizes at SNR = 15 dB for the Three Proposed Schemes

Thus, we can choose a suitable scheme from those proposed schemes with various purposes. For a fast running speed and less computational complexity, the BSS-MMSE

scheme can be chosen. For the best BER performance, the BSS-MBER method should be selected. For a compromise between the running speed and the BER performance, the BSS-only method is the best choice.

CHAPTER 6

CONCLUSIONS

The achievements of this dissertation include: (a) obtaining an efficient channel utilization by BSS techniques; (b) realizing blind multiuser detection for uplink MIMO OFDM systems by SDMA techniques; (c) getting the best BER performance by the proposed BSS-MBER scheme; (d) having the merit of low computational complexity by the proposed BSS-MMSE scheme; and (e) maintaining the balance between the BER performance and computational complexity by the proposed BSS-only method.

To display the performance of all proposed scenarios, a simulation environment is built by MATLAB to simulate and verify the BER performance and the computational complexity in various conditions of the proposed SDMA-based uplink MIMO OFDM system. Such simulations also offer useful suggestions for various purposes of applications.

6.1 Major Outcomes

The primary contribution of this dissertation is the development of three blind multiuser detection approaches for the proposed SDMA-based MIMO OFDM system to save expensive channel resources, and realize multiuser detection in the uplink MIMO OFDM system from mobile devices to a base station.

The outcomes of the three proposed schemes are summarized in the following facts:

- The three proposed blind multiuser detection schemes have higher channel utilization and they are able to save the channel resources, compared with the conventional detection schemes in MIMO OFDM systems.

- Compared with space-time coding or spatial multiplexing MIMO OFDM systems, the proposed SDMA-based MIMO OFDM system is suitable for the uplink communication from mobile users to the base station.

- The BSS-MBER scheme takes the best BER performance by 5.93% on average in comparison with the BSS-only method, and 24.85% on average in comparison with the BSS-MMSE method.

- The BSS-MMSE method is the fastest. According to our MATLAB simulation, it only takes less than 1 second running time to obtain separation results, compared with about 2 seconds running time by the BSS-only method, or about 4 seconds running time by the BSS-MBER method.

- The BSS-only scenario takes a compromise between the BER performance and the computational complexity.

- In the proposed SDMA-based MIMO OFDM system, three proposed schemes increase the computational complexity only in the base station, not in mobile devices, whereas this increment of the computational complexity is easy to be overcome by current hardware in base stations.

- All proposed schemes are operated in N parallel subcarriers, and these schemes have high parallel computing efficiency and save a long running time in the proposed SDMA-based MIMO OFDM system.

6.2 Prospective Research Endeavors

There are several issues that will be studied and investigated in the future for the three proposed schemes in the SDMA-based uplink MIMO OFDM system:

- This research assumes that the source signals are linearly mixed, and the proposed schemes solve the problem of the linear mixture. The research may be extended to the non-linear mixture.

- The permutation problem is solved by calculating the cross-correlation between neighboring subcarriers. However, when there are more users and more subcarriers, the computational complexity increases substantially. In this research, if the number of users is larger than 4 and the number of subcarriers is more than 64, the amount of calculations for the cross-correlation will be increased from several hundred to more than one thousand. This issue needs to be studied further.

- This research assumes that the amplitudes of mixed signals are the same for every antenna element in the receiver. The further research may extend to the unknown scaling of amplitudes at different antenna elements.

- To develop the proposed schemes in a hardware system is probable in the future. Although this is still an open question for BSS techniques in practical applications, the authors in [74-76] implement BSS algorithms on Field Programmable Gate Array (FPGA) or Taxis Instrument's Digital Signal Processing (DSP) devices. Thus, it is possible to develop a hardware system for our proposed schemes in the future.

6.3 Summary

In this dissertation, the blind multiuser detection in MIMO OFDM systems is studied. To exactly recover users' signals in a MIMO-OFDM system, the conventional solution is to retransmit the channel state information that incurs low channel efficiency. However, the three proposed blind multiuser detection schemes are valuable solutions with higher channel utilization. In addition, the SDMA technique is employed to achieve the uplink MIMO OFDM system from mobile devices to a base station. Furthermore, those proposed scenarios focus on diverse goals: the BSS-MMSE scheme has the merit of low computational complexity; the BSS-MBER possesses the best BER performance; and the BSS-only method, a compromised method, maintains the balance between the BER performance and computational complexity.

In order to verify the performance of the three proposed methods, a SDMA-based uplink MIMO OFDM system is established by MATLAB. Compared with the BSS-MMSE method, 24.85% relative BER improvements on average by the BSS-MBER scheme are obtained, when the frame size is 50. If the BSS-only scheme is applied in the simulation environment, our simulation shows that there are about 18.92% relative BER improvements on average in contrast with the BSS-MMSE method, when the frame size is 50.

As for the computational complexity, the running times in accordance with our MATLAB simulation for BSS-MMSE, BSS-only and BSS-MBER are less than 1 second, about 2 seconds and about 4 seconds, respectively, when the frame size is 50. From the

engineering perspective, it is very important and necessary to propose those schemes with the consideration of various goals in MIMO OFDM systems, and to conduct such a significant performance analysis in this field.

LIST OF REFERENCES

1   M. Jiang and L. Hanzo, "Multiuser MIMO-OFDM for next-generation wireless systems," Proceedings of the IEEE Vol.95, No.7, pp.1430-1469, July 2007.

2   Wi-Fi CERTIFIED 802.11n, "Draft 2.0: Longer-Range, Faster-Throughput, Multimedia-Grade Wi-Fi Networks," IEEE 802.11n Draft, June 2007.

3   J. Ma, Y. Niu and H. Chen, "Blind signal separation," National Defense Industry Press, China, 2006.

4   F. Zhang, B.Zhang and X. Zhang, "Operation and Application of Blind Signal," Xidian University Press, Xi'an, China, 2006.

5   A. Hyvärinen, J. Karhunen and E. Oja, "Independent component analysis," Wiley-Interscience, 2001.

6   P. Comon, "Independent Component Analysis-A New Concept?," Signal Processing, Vol. 36, pp.287-314, 1994.

7   J. V. Stone, "Independent Component Analysis, A Tutorial Introduction," MIT Press, Cambridge, Massachusetts, USA, 2004.

8   P. Comon and C. Jutten, "Handbook of Blind Source Separation, Independent Component Analysis and Applications," Elsevier Press, Burlington, Massachusetts, USA, 2010.

9   C. Tu and B. Champagne, "Subspace blind MIMO-OFDM channel estimation with short averaging periods: performance analysis," 2008 IEEE Wireless Communications and Networking Conference, pp.24-29, March 31 - April 3, 2008.

10   T. Abrudan, M. Sirbu and V. Koivunen, "Blind multi-user receiver for MIMO-OFDM systems," the 4th IEEE Workshop on Signal Processing Advances in Wireless Communications, pp.363-367, June 2003.

11   A. L. F. de Almeida, G. Favier, C. C. Cavalcante, and J. C. M. Mota, "Tensor-Based Space-Time Multiplexing Codes for MIMO-OFDM Systems with Blind Detection," the 17th Annual IEEE International Symposium on Personal, Indoor and Mobile Radio Communications, pp.1-5, September 2006.

12   L. Sarperi, X. Zhu, A. K. Nandi, "Blind OFDM receiver based on independent component analysis for Multiple-Input Multiple-Output systems," IEEE transactions on Wireless Communications, Vol.6, pp.4079-4089, November 2007.

13   S. R. Curnew and J. Ilow, "Blind signal separation in MIMO OFDM systems using ICA and fractional sampling," ISSSE'07 International symposium on Signals, Systems and Electronics, pp.67-70, July 30–August 2, 2007.

14   B. Guo, H. Lin and K. Yamashita, "Blind signal recovery in multiuser MIMO-OFDM System," the 47th IEEE international Midwest symposium on circuits and systems, vol.2, pp.637-640, July 2004.

15   M. Jankiraman, "Space-Time codes and MIMO systems," Artech House, Boston and London, 2004.

16   B. Vucetic and J. Yuan, "Space-Time coding," Wiley, England, 2003.

17   L. Zheng and D. N. C. Tse, "Diversity and multiplexing: a fundamental tradeoff in multiple-antenna channels," IEEE Transactions on Information Theory, Vol. 49, No. 5, pp. 1073-1096, May 2003.

18   A. Gorokhov, D.A. Gore and A.J. Paulraj, "Receive Antenna Selection for MIMO Spatial Multiplexing: Theory and Algorithms," IEEE transactions on Signal Processing, Vol.51, No.11, pp.2796-2807, November 2003.

19   H. Lee, S. Park and I. Lee, "Orthogonalized Spatial Multiplexing for MIMO Systems," IEEE 64th Vehicular Technology Conference, pp.1-5, Montreal, Canada, September 2006.

20   J. An, H. Park and S. Kim, "Performance of Spatial Multiplexing MIMO Receivers in Frequency Selective Rayleigh Fading Channels," 2009 International Waveform Diversity and Design Conference, pp.94-97, Kissimmee, Florida, February 2009.

21   H. M. Karkhanechi and B.C. Levy, "Spatial Multiplexing and Diversity Gain in OFDM-based MIMO Systems," 2003 IEEE Topical Conference on Wireless Communication Technology, pp.299-301, Honolulu, United States, October 2003.

22   J.C. Roh and B.D. Rao, "Design and Analysis of MIMO Spatial Multiplexing Systems with Quantized Feedback," IEEE Transactions on Signal Processing, Vol.54, No.8, pp.2874-2886, August 2006.

23   Y. S. Cho, J. Kim, W. Y. Yang and C. G. Kang, "MIMO-OFDM Wireless Communications with Matlab," John Wiley & Sons (Asia) Pte Ltd, 2010.

24   M. Cooper and M. Goldburg, "Intelligent antennas: spatial division multiple access," ArrayComm: Annual Review of Communications, pp.999-1002, 1996.

25   M.Y. Alias, S.Chen and L.Haozo, "Genetic algorithm assistant minimum bit error rate multiuser detection in multiple antenna aided OFDM," Vehicular Technology Conference, VTC2004-Fall, 2004 IEEE 60th, Vol.1, pp.548-552, September 2004.

26   M.Y. Alias, S.Chen and L.Haozo, "Multiple-antenna-aided OFDM employing genetic-algorithm-assisted Minimum bit error rate multiuser detection," IEEE transactions on vehicular technology, Vlo.54, No.5, pp.1173-1721, September 2005.

27   D. Tse and P. Viswanath, "Fundamentals of wireless communication," Cambridge University Press, New York, 2005.

28   L. Hanzo, Y. Akhtman, L. Wang and M. Jang, "MIMO-OFDM for LTE, WiFi and WiMax Coherent Versus Non-coherent and Cooperative Turbo-transceivers," Jonn Wiley & Sons Ltd, UK, 2011.

29   IEEE Computer Society, "Part 11: Wireless LAN Medium Access Control (MAC) and Physical Layer (PHY) Specifications, Amendment 5: Enhancement for Higher Throughput," IEEE candidate standard 820.11n, 2009. http://standards.ieee.org/getieee802/download/802.11n-2009.pdf

30   Wi-Fi CERTIFIED 820.11n, "Longer-Range, Faster-Throughput, Multimedia-Grade Wi-Fi Networks," http://www.wifi.org/register.php?file=wp_WiFi_CERTIFIED_n_Industry.pdf, September 2009.

31   H. Jafarkhani, "Space-Time Coding, Theory and Practice," Cambridge University Press, New York, 2005.

32   B. D. V. Veen and K. M. Buckley, "Beamforming: A versatile approach to spatial filtering," IEEE ASSP Magazine, pp.4–24, April 1988.

33   S. B. Weinstein and P.M. Ebert, "Data Transmission by Frequency-Division Multiplexing Using the Discrete Fourier Transform," IEEE Transactions on Communication Technology, Vol. Com-19, No. 5, pp.628-634, October 1971.

34   L. J. Cimini, JR., "Analysis and Simulation of a Digital Mobile Channel Using Orthogonal Frequency Division Multiplexing," IEEE Transactions on Communications, Vol. Com-33, No. 7, pp.665-675, July 1985.

35   Wikipedia, "http://en.wikipedia.org/wiki/OFDM," March 2011.

36   H. Liu and G. Li, "OFDM-Based Broadband Wireless Networks Design and Optimization," John Wiley & Sons, Inc., Hoboken, New Jersey, 2005.

37   J. G. Proakis and M. Salehi, "Digital Communications," McGraw-Hill, New York, January 2008.

38   B. Ans, J. Hérault, and C. Jutten, "Adaptive Neural Architectures: Detection of Primitives," Proceedings of COGNITIVA'85, pp.593-597, Paris, France, 1985.

39   P. Chevalier, L. Albera, A. Ferréol and P. Comon, "Comparative Performance Analysis of Eight Blind Source Separation Methods on Radio Communications Signals," Proceedings of 2004 IEEE International Joint Conference on Neural Networks, pp.273-278, Budapest, July 2004.

40   A. Orozco-Lugo, M. Lara, D. MClernon and H. Muro-Lemus, "Multiple Packet Reception in Wireless Ad Hoc Networks Using Polynomial Phase-modulating Sequences," IEEE Transactions on Signal Process, Vol. 51, pp.2093-2110, 2003.

41   P. Jallon, A. Chevreuil and P. Loubaton, "Separation of Digital Communication Mixtures with the CMA: Case of Unknown Symbol Rates," Signal Processing, Vol. 90, pp. 2633-2647. 2010.

42   V.D. Calhoun, T. Adali, L.K. Hansen, J. Larsen and J.J. Pekar, "ICA of Functional MRI Data: An Overview," Fourth International Symposium on Independent Component Analysis and Blind Signal Separation, pp.909-914, Nara, Japan, April 2003.

43   R. Vigario and E. Oja, "BSS and ICA in Neuroinformatics: From Current Practices to Open Challenges," IEEE Reviews in Biomedical Engineering, Vol.1, pp.50-61, 2008.

44   L. Albera, A. Ferréol, D. Cosandier-Rimélé, I. Merlet and F. Wendling, "Brain Source Localization Using a Fourth-order Deflation Scheme," IEEE Transactions on Biomedical Engineering, Vol. 55, pp.281-288, 2008.

45   H. Taigang, G. Glifford and L. Tarassenko, "Application of Independent Component Analysis in Removing Artefacts from the Electrocardiogram," Neural Computing and Applications, Vol.15, pp.105-116, 2006.

46   S. Hu, M. Stead and G.A. Worrell, "Automatic Identification and Removal of Scalp reference Signal for Intracranial EEGs Based on Independent Component Analysis," IEEE transactions on Biomedical Engineering, Vol.54, pp.1560-1572, 2007.

47   S. Makino, T.-W. Lee and H. Sawada, "Blind Speech Separation," Springer, Dordrecht, the Netherlands, 2007.

48   E. Vincent, R. Gribonval and C. Févotte, "Performance Measurement in Blind Audio Source Separation," IEEE Transactions on Audio, Speech and Language processing, Vol.14, No.4, pp.1462-1469, 2006.

49   D. Smith, J. Lukasiak, and I.S. Burnett, "An Analysis of the Limitations of Blind Signal Separation Applications with Speech," Signal Processing, Vol. 86, pp.353-359, 2006.

50   N. Mitianoudis, and M.E. Davies, "Audio Source Separation of Convolutive Mixtures," IEEE Transactions on Speech and Audio Processing, Vol.11, No.5, pp.489-497, 2003.

51   O. Yilmaz and S.T. Rickard, "Blind Separation of Speech Mixtures via Time-frequency Masking," IEEE Transactions on Signal Processing, Vol.52, No.7, pp.1830-1847, 2004.

52   C. Prabhu, S. Pradeep, R. Baskaran and C. Chellappan, "Convolutive Blind Speech Separation in a Room Using Cross Spectral Density Matrix," 2010 IEEE International Conference on Computational Intelligence and Computing Research, pp.1-4, Coimbatore, India, December 2010.

53   S. Haykin and B. Kosko, "Intelligent Signal Processing," Wiley-IEEE Press, 2001.

54   A. Hyvärinen, P.O. Hoyer, "Emergence of Phase and Shift Invariant Features by Decomposition of natural Images into Independent Feature Subspaces," Neural Computation, Vol.12, No.7, pp.1705-1720, 2000.

55   A.K. Moorthy and A.C. Bovik, "Blind Image Quality Assessment: From Natural Scene Statistics to Perceptual Quality," IEEE Transactions on Image Processing, Vol. 20, No.12, pp.3350-3364, December 2011.

56   G. Xu and E. Tang, "Blind Deconvolution for Image Restoration Based on Text Characteristic," 2011 International Conference on Control, Automation and Systems Engineering, pp.1-3, Singapore, July 2011.

57   T.E. Bishop, R. Molina and J.R. Hopgood, "Nonstationary Blind Image Restoration Using Variational Methods," 2007 International Conference on Image Processing, Vol. I, pp.125-128, San Antonio, Texas, USA, September 2007.

58   D. Chao and P. Guo, "Blind Image Restoration Based on Wavelet Analysis," Proceedings of the Fourth international Conference on machine Learning and Cybernetics, Vol.8, pp.4977-4982, Guangzhou, China, August 2005.

59   S. Amari, A. Cichocki and H. H. Yang, "A New Learning Algorithm for Blind Signal Separation," Advances in Neural Information Processing Systems, Vol.8, pp.757-763, 1996.

60   P. Smaragdis, "Blind Separation of Convolved Mixtures in the Frequency Domain," Neurocomputing, Vol.22, pp.21-34, 1998.

61   J. F. Cardoso and A. Souloumiac, "Blind Beamforming for Non-Gaussian Signals," IEE proceedings-F, Vol.140, No.6, pp.362-370, December 1993.

62   E. Bingham and A. Hyvärinen, "ICA of complex valued signals: a fast and robust deflationary algorithm," IEEE Proc. of the international joint conference on neural networks, vol.3, pp.357-362, July 2000.

63   E. Bingham and A. Hyvärinen, "A Fast Fixed-point Algorithm for Independent Component Analysis of Complex-valued Signals," International Journal of Neural Systems, Vol.10, No.1, pp.1-8, 2000.

64   D. Obradovic, N. Madhu, A. Szabo and C. S. Wong, "Independent Component Analysis for Semi-Blind Signal Separation in MIMO Frequency Selective Communication Channels," Proceedings of the International Joint Conference on Neural Networks, Vol.1 pp.53-58, July 2004.

65   A. Dapena, D. Iglesia and C. J. Escudero, "An MSE-Based Method to Avoid Permutation/Gain Indeterminacy in Frequency-Domain Blind Source Separation," Circuits System Signal Process Vol. 29, pp.403-417, 2010.

66   Wikipedia, "http://en.wikipedia.org/wiki/Minimum_mean-square_error," October 2011.

67   C. C. Yeh, R. Lopes, and J. Barry, "Approximate minimum bit-error rate multiuser detection," in Proc. IEEE Globe communication Conference, pp.3590-3595, 1998.

68   D. Gesbert, "Robust linear MIMO receivers: a minimum error-rate approach," IEEE Transactions on signal processing, Vol.51, No.11, pp.2863-2871, November 2003.

69   L. Xu, S. Tan, S. Chen, L. Hanzo, "Iterative minimum bit error rate multiuser detection in multiple antenna aided OFDM," 2006 IEEE wireless communications and networking conference, vlo.3, pp.1603-1607, April 2006.

70   P. Belanger, "802.11n Delivers Better Range," http://www.wi-fiplanet.com/tutorials/article.php/3680781/80211n-Delivers-Better-Range.htm, May 31, 2007.

71   E. Perahia and R. Stacey, "Next Generation Wireless LANs: Throughput, Robustness, and Reliability in 802.11n" Cambridge University Press, September 22, 2008.

72   IEEE 802.11a, "Part 11: Wireless LAN Medium Access Control (MAC) and Physical Layer (PHY) Specifications: High-speed Physical Layer in the 5GHz Band," supplement to IEEE 802.11 Standard, September 1999.

73   Wikipedia, "http://en.wikipedia.org/wiki/IEEE_802.11a-1999," January 12, 2012.

74   J. Peter, J. D. Laar, E. Haberts, P. Lokkart, and P. Sommen, "Adaptive Blind Audio Signal Separation System Using a TI DSP," http://home. tiscali.nl/ehabets /files/A_BLASS_TI.pdf, April 2010.

75   M. Hori and M. Ueda, "FPGA Implementation of a Blind Source Separation System based on Stochastic Computing," 2008 IEEE Conference on Soft Computing in Industrial Applications, pp.182-187, Muroran, Japan, June 2008.

76   K. Shyu, M. Lee, Y. Wu and P. Lee, "Implementation of Pipelined FastICA on FPGA for Real-Time Blind Source Separation," IEEE Transactions on Neural Networks, Vol.19, pp.958-970, June 2008.

VITA

YU DU

Education

04/2012 – 01/2008   Florida International University (FIU), Miami, Florida, USA
Doctoral Candidate in Electrical Engineering
Graduate Fellowship, FIU, (04/2012-04/2011)
Graduate Assistantship, FIU, (04/2011-01/2008)

04/2007 – 09/2004   Florida International University (FIU), Miami, Florida, USA
Master of Science in Electrical Engineering

06/2004 – 09/2000   Wuhan University of Technology, Wuhan, China
Bachelor of Electronic Science and Technology

Main Publications

1. Yu Du, Nansong Wu and Kang Yen "Blind Signal Separation Techniques on Different types of MIMO Systems – An Overview" on the International Journal of Research and Reviews in Computer Science (IJRRCS) for Vol. 1, No. 3, April 2011

2. Yu Du, Kang Yen, Yechang Fang and Nansong Wu, "Blind Multiuser Detection in SDMA-aided MIMO OFDM Systems by FastICA Algorithm" on the International Journal of Computer Science and Information Security (IJCSIS), Vol. 8, No. 5, pp1-5, August 2010

3. Yu Du, Hongbing Xiao, Chunyu Bai and Kang Yen "A Four-order PLL Design for High-Voltage Converter in Airbag Electronic Safety" on the 2011 Research in Applied Computation Symposium (ACM RACS 2011), Miami, Florida, November 2011

4. Yu Du, Kang Yen and Nansong Wu "A new scenario for the receiver of MIMO OFDM systems" on the 75th Annual Meeting of the Florida Academy of Sciences, Melbourne, Florida, March 2011

5. Yu Du, Yechang Fang, Nansong Wu and Kang Yen "Performance Analysis for Complex FastICA Algorithms in MIMO OFDM Systems" on the Second International Conference on Future Computer and Communication, Volume 2, pp782-786, Wuhan, China, May 2010

6. Yu Du, Nansong Wu, Yechang Fang, Kang Yen, "A comparison of different contrast functions of FastICA algorithm in a MIMO OFDM system" on the 74th Annual Meeting of the Florida Academy of Sciences, Fort Pierce, Florida, March 2010

7. Nansong Wu and Yu Du "A survey of WiMAX security" on the 75th Annual Meeting of the Florida Academy of Sciences, Melbourne, Florida, March 2011

8. Nansong Wu, Yechang Fang, Yu Du, Kang Yen, "Multiuser scheduling schemes for MIMO-OFDM systems" on the 74th Annual Meeting of the Florida Academy of Sciences, Fort Pierce, Florida, March 2010

9. Yechang Fang, Nansong Wu, Yu Du and Kang Yen, "A Queue Management Algorithm Based on Network Processors " on the Proc. of the 8th Int'l Conf. on Information and Management Sciences, Kunming, China, July 2009